Thermal Stability of the Polyesters PCL and PLGA during Melt Electrowriting

Dissertation zur Erlangung des naturwissenschaftlichen Doktorgrades der Julius-Maximilians-Universität Würzburg

vorgelegt von

Christoph Böhm

aus Schwebheim

Aschaffenburg 2022

Thermal Stability of the Polyesters PCL and PLGA during Melt Electrowriting

Dissertation zur Erlangung des naturwissenschaftlichen Doktorgrades der

Julius-Maximilians-Universität Würzburg

vorgelegt von

Christoph Böhm

aus Schwebheim

Aschaffenburg, 2022

Eingereicht bei der Fakultät für Chemie und Pharmazie am

_____

Gutachter der schriftlichen Arbeit

1. Gutachter: _____

2. Gutachter: _____

Prüfer des öffentlichen Promotionskolloquiums

1. Prüfer: _____

2. Prüfer: _____

3. Prüfer: _____

Datum des öffentlichen Promotionskolloquiums

_____

Doktorurkunde ausgestellt am

_____

This work was conducted from November 2016 till March 2021 at the Department for Functional Materials in Medicine and Dentistry, University Hospital of Würzburg, Würzburg, Germany under the supervision of Prof. Dr. rer. nat. Jürgen Groll.

"Not all who wander are lost."

– J. R. R. Tolkien (1892 – 1973)

LIST OF PUBLICATION

As first author

1) Böhm, C., Stahlhut, P., Weichhold, J., Hrynevich, A., Teßmar, J., Dalton, P. D., The Multiweek Thermal Stability of Medical-Grade Poly(ε-caprolactone) During Melt Electrowriting. *Small* 2021, 2104193.

2) Böhm, C., Tandon, B., Hrynevich, A., Teßmar, J., Dalton, P. D., Processing of poly(lactic-co-glycolic acid) microfibers via melt electrowriting. *Macromol. Chem. Phys.*, 2022, 223, 2100417.

As co-author:

3) Ryma, M., Tylek, T., Liebscher, J., Blum, C., Fernandez, R., Böhm, C., Kastenmüller, W., Gasteiger, G., Groll, J., Translation of Collagen Ultrastructure to Biomaterial Fabrication for Material-Independent but Highly Efficient Topographic Immunomodulation. *Adv. Mater.* 2021, 33, 2101228.

TABLE OF CONTENTS

Abbreviation and Symbol Index

Abbreviation	Description
µm	Micrometer
2D	two-dimensional
3D	three-dimensional
3DP	inkjet printing
AM	additive manufacturing
ATEC	acetyl triethyl citrate
CAD	computer-aided design
$CDCl_3$	deuterated chloroform
CLIP	continues liquid interface production
CO_2	carbon dioxide
CTS	critical translation speed
d	Day
DSC	differential scanning calorimetry
e.g.	exempli gratia (for example)
EHD	Electrohydrodynamic
et al.	et alii (and others)
FDM	fused deposition modelling
FTIR	Fourier transformed infrared spectrometry
G	Gauge
g	Gram
G'	storage modulus
G''	loss modulus
GC-MS	gas chromatography coupled with mass spectrometry
GMP	good manufacturing practice
GPC	gel permeation chromatography
h	Hour
H_20	Water
HCl	hydrochloric acid
He	Helium
HV	high voltage
Hz	Hertz = 1 s^{-1}
i.e.	id est (that is)
ICP-MS	inductively coupled plasma mass spectrometry
J	Joule
kDa	kilodalton
kV	Kilovolt
LOM	Laminated object manufacturing
M	Molar
m	Meter
mA	Milliampere
MeOH	Methanol
MES	melt electrospinning
MEW	melt electrowriting
mg	Milligram

Abbreviation	Description
min	Minute
mL	Milliliter
mm	Millimeter
mmol	Millimole
M_n	number average molecular weight
MPa	Megapascal
MS	mass spectrometry
M_w	weight average molecular weight
NMR	nuclear magnetic resonance
PCL	Poly-ε-caprolactone
PCL_{Ac}	PCL end capped with acetyl ground
PGA	poly(glycolic acid)
PLA	poly(lactic acid)
PLA-PEG-PLA	poly(lactide-block-ethylene glycol-block-lactide)
PLGA	poly(lactic-*co*-glycolic acid)
PS	Polystyrene
PTFE	Polytetrafluoroethylene
Pyr-PCL	pyrene-modified PCL
Pyr-PCL_{Ac}	pyrene-modified PCL end capped with acetyl ground
Pyr-PCL_W	pyrene-modified PCL washed with hydrochloric acid
RI	refractive index
ROP	ring-opening polymerization
rpm	rounds per minute
s	Second
SEM	scanning electron microscopy
SES	solution electrospinning
SLA	Stereolithography
SLM	selective laser melting
SLS	selective laser sintering
TERM	tissue engineering and regenerative medicine
T_g	glass transition temperature
TGA	thermogravimetric analysis
T_m	melting temperature
TN_{ozzle}	nozzle temperature
TS_{yringe}	syringe temperature
TVA	thermal volatilization analysis
USA	United States of America
UV	Ultraviolet
v_{fix}	fixed collector speed
WHO	World Health Organization
XRD	X-ray diffraction

Symbol	Description
%	Percent
°	Degree
°C	degree Celsius
Å	ångström = 10^{-10} m
m	Multiplett
ppm	parts per million
t	Triplett
wt-%	weight percent
λ	Wavelength
σ	Young's modulus

Chapter 1

INTRODUCTION AND MOTIVATION OF THE THESIS

According to the World Health Organization (WHO) seven of the top ten causes of death were noncommunicable diseases such as ischaemic heart disease, trachea, bronchus or lung cancers and Alzheimer's disease [1]. Often the last resort treatment for many of these diseases is the removal of damaged/tumor tissue and healing of the remaining tissue. Another last resort is the entire exchange of the organ through transplantation. There are, of course several, consequences from each last resort treatment. For transplantation, several issues need to be addressed starting with the discrepancy between the need for organs and donors, that fulfills the physiological criteria of the patient. Technological advances in autonomous driving and disruption due to the COVID-19 pandemic will reduce the availability of healthy organs [2], making alternatives a necessity.

The field of tissue engineering and regenerative medicine (TERM) has promised to solve many issues connected to these noncommunicable diseases for several decades. TERM aims to enhance the self-healing of the body by providing patient-specific scaffolds in combination with own precursor cells. The big scope of this approach even intends to grow entire organs ready for implantation made from patient's own cells. As this is a very complicated challenge to be tackled, TERM is comprised of a combination of "*different disciplinary approaches, including stem cell biology, functional scaffold materials, nanotechnology and the most recent additive manufacturing*" [3]. Additive manufacturing (AM) techniques provide a platform to fabricate scaffolds that can be used in TERM approaches. One of these techniques is melt electrowriting (MEW), which is a high-resolution AM technology, firstly conceptualized by Brown *et al.* in 2011 [4]. It enabled fiber-based scaffold production that produced fibers with diameters in the lower micrometer range that could be precisely arranged in different shapes. Even though, it is a decade since its first description, MEW is still developing as a technology and requires further better know-how as well as the efficacy of this technique to make scaffolds for TERM.

This thesis aims to shed more light on the material side of this technique, which includes long-term printing capability and thermal degradation investigations on the gold-standard material poly(ε-caprolactone) (PCL) as well as establishing an entirely new material in the form of poly(lactic-*co*-glycolic acid) (PLGA).

Chapter 2 outlines the state of knowledge of the topics in this thesis, including a historical outline of the development of different AM techniques. This is followed by the introduction of MEW, discussing its development as well as its structure and operation. Since the material aspect of an AM technique must fulfill certain criteria, these requirements are addressed by better understanding the current gold-standard of MEW, PCL. This thesis adds PLGA to the material portfolio of processable fibers and its physical properties and literature about the melt processing are provided. Since MEW uses polymer melts that require prolonged heating, it is important to investigate how materials might alter when maintained at high temperatures. Therefore, thermal degradation research performed with PCL and PLGA is discussed.

PCL is the most-used polymer for MEW. However, despite users are experiencing this polymer as very resilient towards the processing conditions, no comprehensive investigation on its printing stability has yet been conducted. Chapter 3 addresses this question on how a PCL MEW jet behaves by observing it for a heating time span of 25 d. Additionally, a look into changes of the physical properties of the printed constructs is given.

Based on Chapter 3, more insight into the chemistry of thermal degradation is warranted. Instead of an accelerated thermal degradation study as is common in literature, Chapter 4 focuses on chemical mechanisms taking place under actual printing conditions and how they contribute to the rheological behavior of the PCL melt.

Chapter 5 introduces a new polymer into the MEW-processing material portfolio, PLGA. In addition to printing neat PLGA, this polymer is combined with a plasticizer to reduce thermal degradation by decreasing the processing temperature to extend the time window for printability.

Chapter 6 draws together the research performed in this thesis with a discussion and conclusion, putting forward suggestions on future perspectives.

To conclude, Chapter 7 summarizes the research in this thesis in both English and German.

Chapter 2

THEORETICAL BACKGROUND AND STATE-OF-KNOWLEDGE

2.1 Additive manufacturing

AM is a general term for a fabrication approach that builds objects layer-by-layer. More traditional approaches include either formative or subtractive manufacturing, which deforms or takes away material from an initial object, respectively. For example, subtractive manufacturing starts with a bigger piece of material and excess is removed with cutting, chiseling, or grinding to generate objects. The following pages will take a closer look into the history and the working principle of AM.

2.1.1 Historical outline

AM was established in the 1980s and added to the established manufacturing processes that can be classified in the following categories: subtractive, joining, dividing and transformative (**Figure 1**) (adapted from [5]).

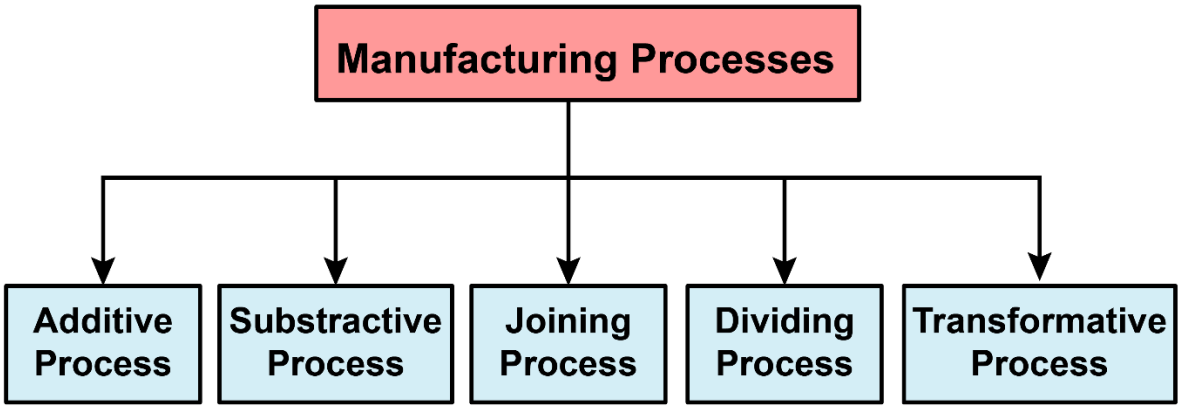

Figure 1. Categories of manufacturing processes.

2.1.1.1 Stereolithography

AM as an official fabrication process began with the development of stereolithography (SLA) by Charles W. Hull in 1986 [6]. This technique uses a photo-sensible resin that can be cured by ultraviolet (UV) light. This technique was further improved over the last three decades with four distinct step-changes in manufacturing [7]. The first step-change is a laser scanning approach invented by Hull as already mentioned. The second step-change used a digital micromirror device to speed up the production rate by crosslinking an entire surface layer at once. In 2015 the third breakthrough arose, firstly reported by Tumbleston *et al.* called continues liquid interface production (CLIP), which

again greatly sped up the fabrication process [8], leading to successful companies such as Carbon3D. The most recent development in resin-based AM technologies was volumetric stereolithography by Shusteff *et al.* in 2017 upgrading the material that can be crosslinked at once from two-dimensional (2D) to three-dimensional (3D) [9]. An illustration of stereolithography is shown in **Figure 2**.

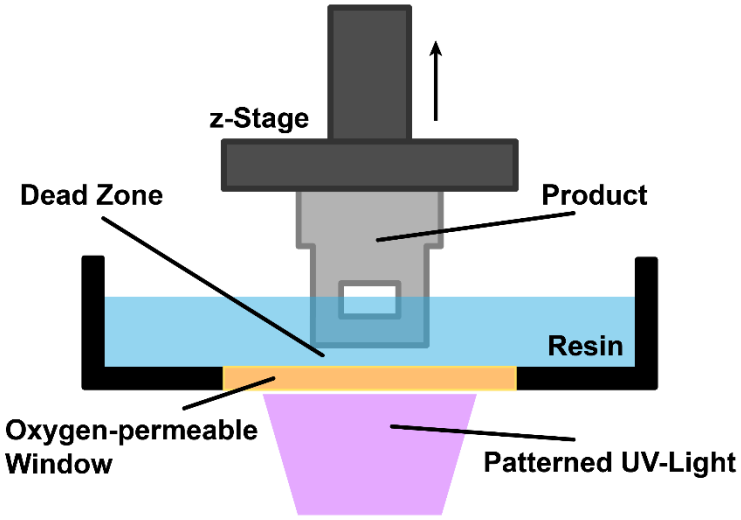

Figure 2. Illustration of stereolithography.

2.1.1.2 Fused Deposition Modeling

In 1991 another AM technique was commercialized in form of fused deposition modeling (FDM) [10]. FDM was a new concept using polymer melts to generate structures in a fiber-based approach. FDM was patented by Crump in 1988, who founded Stratasys Cooperation one year later [11]. The technique is based on melt extrusion using a feedstock filament that is delivered to a heated liquefier by electric motors. Controllable x-, y- and z-axis allow for a controlled deposition to produce complex structures [11]. Research surrounding FDM was mainly focused on understanding process design and interlayer interaction to better predict the FDM part strength [12-15] and on establishing different materials and new applications [16-21]. In general, FDM is probably the most known AM method in public also already being widely used by private customers. **Figure 3** shows an illustration of fused deposition modeling.

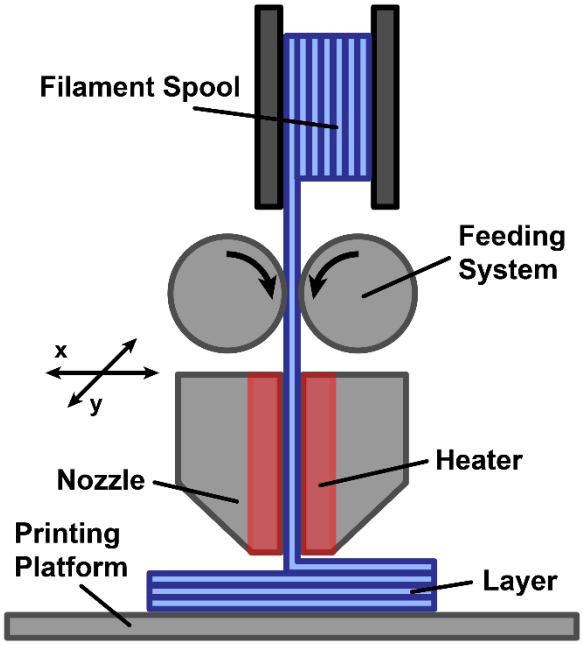

Figure 3. Illustration of fused deposition modeling.

2.1.1.3 Selective Laser Sintering

Another AM technology that must be mentioned here, is selective laser sintering (SLS). SLS was first developed by Dr. Carl R. Deckard and Dr. Joe Beaman at the University of Austin, which resulted in the startup company DTM and a patent in 1989 [22]. It was further improved by the researchers Wilhelm Meiners, Dr. Konrad Wissenbach and Dr. Andres Gasser from Fraunhofer ILT inventing selective laser melting (SLM) patented in 1998 [23]. The main working principle is the same for both techniques as they use a laser that is scanning over a bed of powdered material to generate the desired construct [24, 25]. The main difference between the two lies in the merging of the particles. While SLS only fuses particles with each other, SLM generates enough heat to fully melt the material generating more homogeneous pieces with higher strength, which saves a post-treatment step [26]. Both techniques can process several different materials such as polymers, ceramics, and metals [24, 25, 27, 28]. In **Figure 4** an illustration of selective laser sintering is shown.

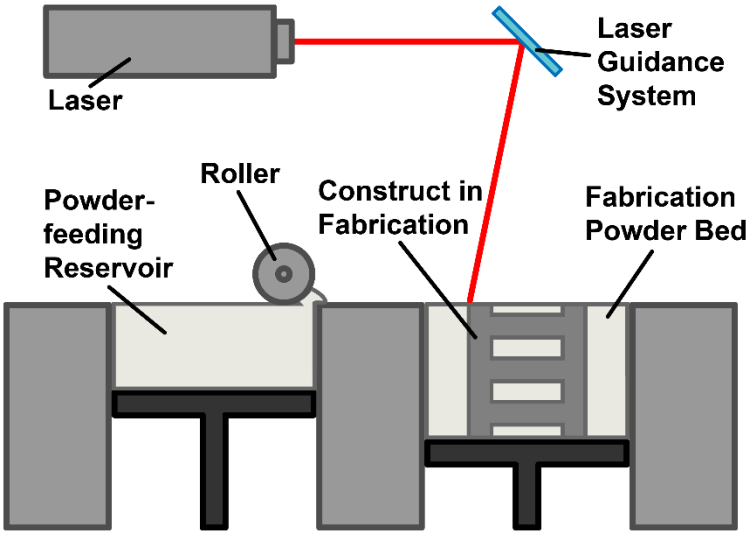

Figure 4. Illustration of selective laser sintering.

The family of AM techniques is substantiative and diverse. There are more AM techniques such as inkjet printing (3DP) or laminated object manufacturing (LOM), which are not further discussed in this work.

2.1.2 Additive manufacturing principle

AM processes follow a specific workflow that is schematically shown in **Figure 5**. This workflow contains five steps (adapted from [29]):

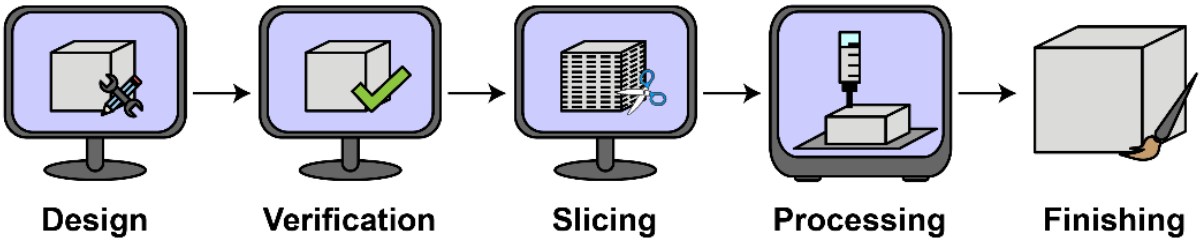

Figure 5. Workflow of AM processes. In the first three steps the desired constructs are digitally created, cleaned up and sliced. After processing in an AM "printer" the construct is finished in a post processing step.

1) The first step includes conception of the desired construct with the help of computer-aided design (CAD) tools. Even though a designer has complete freedom in modelling with CAD tools, depending on the AM technique there are some limitations. An example would be creating void space in techniques that use a liquid

(SLA) or powder (SLM) bath as this would encapsulate the material. Alternatively, a 3D model can also be generated by 3D scanning [30, 31] to utilize the high customizability of these techniques. Alternatively, the model of the construct can be generated using medical imaging.

2) After creation of the 3D model, it needs to be exported as a file that can further be used by the individual AM techniques. A common file format is STL and its acronym can be defined as “standard triangle language”, “stereolithography language” or “stereolithography tessellation language” [32]. The conversion of the CAD files to STL files is necessary for the following slicing process. As STL is an approximation of the original 3D model based on triangles, it needs to be made sure that no unwanted artefacts are generated [33].

3) As already mentioned, the next step is the slicing of the STL files to generate 2D slices of the 3D model together with the machine code needed for the AM machines to create these layers.

4) In this step the actual production takes place, and its details are dependent on the individual technique.

5) The last step consists of post-processing and its extent is also dependent on the used technique. The most common finalization steps are removal of excess material such as supports or edges and a heat or light treatment for improved layer conjunction.

All AM techniques have these five steps in common, however they differ depending on the printing process itself. To classify AM processes different criteria have been used such as the physical state of the process material [5, 34, 35] distinguishing between liquid, solid and powder materials or by the working principle [36] divided into laser-based, nozzle-based and printer-based systems. A more detailed categorization, which also used the working principle, has been introduced by the ASTM “International Technical Committee F42 on additive manufacturing techniques” [37] in 2015 with a total of seven different categories shown in **Figure 6**.

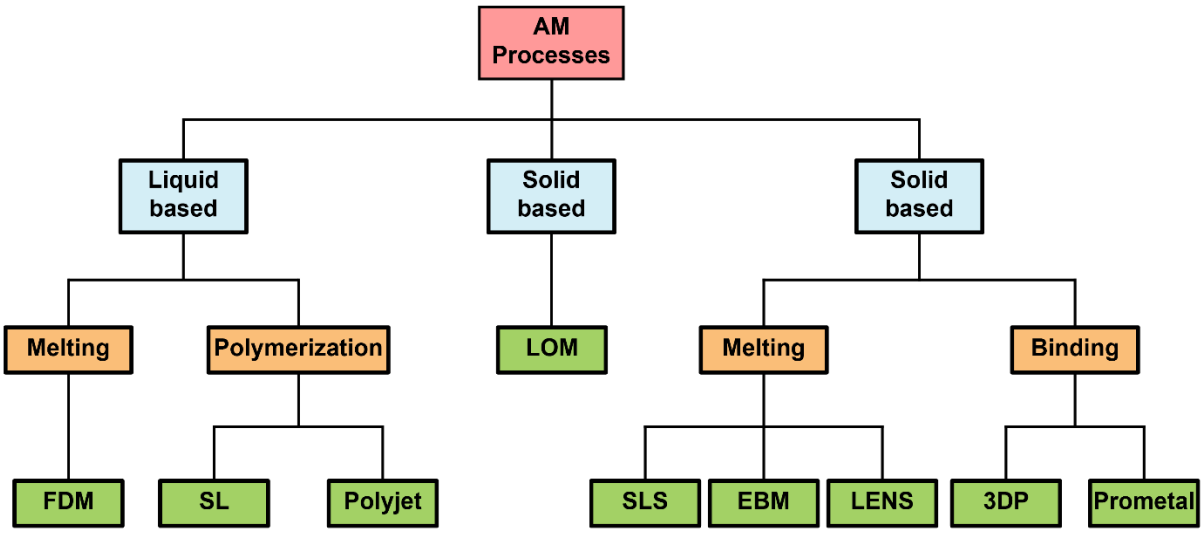

Figure 6. Categories of established AM processes. Adapted from [35].

One of these categories is material extrusion, which will be discussed further as it has the most relevance for MEW. Material extrusion is based on the continuous dispensing on material into the desired construct in a layer-by-layer process. The extrusion itself can be done pneumatic or mechanical. With a pneumatic system the material is extruded by applying an air pressure via a valve. Mechanically driven extrusion can be further divided into screw- and piston-based systems. Piston-based systems can be controlled by the displacement of a plunger, which directly translates into the volume being dispensed. In screw-based systems the volume flow is dependent on the speed of the screw as well as design of the screw [38]. The last one is based on piston-driven system and uses a polymer filament fed into a heater, which is the method used in FDM [39, 40]. These extrusion methods can be used to dispense all sorts of different materials such as polymer solutions, polymer melts, biomaterial inks and bioinks [38].

2.2 Melt electrowriting

2.2.1 Historical outline

The technologies that led to MEW span over four centuries, beginning with the discovery of the transfer of charges to materials to generate forces that deform them. William Gilbert observed in the 17th Century, that amber can attract a liquid, reshaping it from an ordinary droplet into a cone [41]. This was the first report of a phenomenon that would eventually be further developed into becoming of what we know as “Taylor cone”

today. Around the turn of the 20th Century, John Francis Cooley was the first person who filed a patent for what is known today as solution electrospinning (SES) [42]. In this patent he described four different spinning heads, which are all indirectly charged. He proposed the use of a dielectric liquid as medium instead of a gas and used pyroxylin (nitrocellulose) in ether as his preferred material. In 1912 Wiegand and Burton investigated the behavior of charged water streams and the relationship between surface tension and charge. They also offered a mathematical explanation of the behavior of two charged spheres to describe charged water droplets [43].

John Zeleny published a series of papers looking into the influence of an electrical field on a liquid drop emitted from a capillary. The first paper of interest was published in 1914 and mainly focused on the discharge of an electric potential from a liquid drop [44]. He continued by switching liquids, from diluted hydrochloric acid to ethyl alcohol and glycerin, as the first one discharged too early. With ethyl alcohol he was able to describe different phenomena the liquid meniscus undergoes when being electrocuted, such as formation of a Taylor cone and breakup into very small droplets. By switching to glycerin, which has a higher viscosity compared to ethyl alcohol, he could also observed that by applying an electrical field a thin thread is emitted which later dispersed into small droplets [45]. In his last paper, Zeleny investigated the lag between applying voltage and the reaction of the liquid droplet and he also makes a first attempt to mathematically describe the behavior of a liquid drop when electric charge is applied [46]. A big contribution on the development of SES and subsequent technologies was given by Anton Formhals, who published a total of 22 patents between 1931 and 1944. In his first patent he mainly focused on machine design using a fiber emitter that consisted of a rotating saw blade dipping into a bath of spinnable liquid. With a voltage source hooked up to the blade the charge on the edges caused jets accelerating towards roller or rotating disc collectors [47]. He continued his work 1937 by searching the optimal nozzle design suggesting a conical taper that can be disassembled for easier cleaning [48]. In 1939 Formhals published a patent of a device with which he tried to manipulate a fiber in flight by adding more electrodes between the emitter and the collector [49] as well as proposing to fabricate meshes of neutral charge made by stacking fibers of opposite charge [50]. The last patents he published in 1940 [51] and 1943 [52] mainly focused on the collection of fibers using winding devices to produce a usable form of threads. In parallel to Formhals, Charles Ladd

Norton filed a patent in 1936 were he described the world-first melt electrospinning (MES) device which utilized an electrostatic field combined with an air-jet system to produce fibers [53]. This device additionally used auxiliary electrodes to further stabilize the jet in flight and together with the air stream the point of collection could be extended out to 6 m away from the emitter. The next important contribution towards the establishment of electrospinning was the work of Sir Geoffrey Ingram Taylor. In 1964 he introduced a mathematical explanation for the formation of a cone of a fluid droplet under the influence of an electrical field [54], which is nowadays known as *Taylor cone*. Another important contribution of Taylor was done in cooperation with J. R. Melcher in 1969. They developed the leaky dielectric model, which describes the movement of charge within a dielectric material [55]. These early developments in electrospinning are discussed in further detail within a review by *Tucker et al.* [56].

In 1996, Darrel H. Reneker and Iksoo Chun published a seminal paper where they successfully produced nanofibers from many different polymers dissolved in different solvents using the SES technique [57]. After this publication SES experienced a rapidly increasing attention by researchers mainly using it for biomedical applications.

Larrondo and Manley published three papers in 1981 as a series in which they looked at melt electrospinning, however only one paper involved experiments with polymer melts. They constructed a melt electrospinning device based on a melt flow index device and were able to produce randomly deposited fibers of polyethylene and isotactic polypropylene [58]. In the second paper they focused on the influence of an electrical field on the flow field. This investigation was conducted using a viscous silicone oil blended with 10 µm glass beads as tracer particles and two cameras 90° apart to allow for a triangular tracing of the beads [59]. In the third and final paper they looked at the deformation of a pendant drop of molten nylon 12 and polyethylene under the influence of an electrical field. In 2003 Reneker also published an article together with Rangkupan on MES of polypropylene in vacuum [60]. In 2006 Dalton *et al.* looked into the benefits of melt processing by electrospinning PCL directly onto a culture plate with living cells and showed that cells could survive this process [61]. In a first attempt to control the placement of fibers Dalton *et al.* used a metal tweezer to align fibers produced via melt electrospinning [62]. In 2007 and 2008, further observations on the melt electrospun jet let to their focused deposition onto a computer controlled collector [63]. This demonstration of precise control

would then eventually lead to the conceptualization of MEW in 2011 [4]. In the following years MEW would achieve increasing interest and eventually surpassed MES in the annual number of journal articles in 2018 [64].

2.2.2 Working principle of MEW

A setup of a MEW device is presented in **Figure 7**. It contains of a container for the polymer melt reservoir, usually a disposable plastic or glass syringe equipped with a nozzle of a defined diameter.

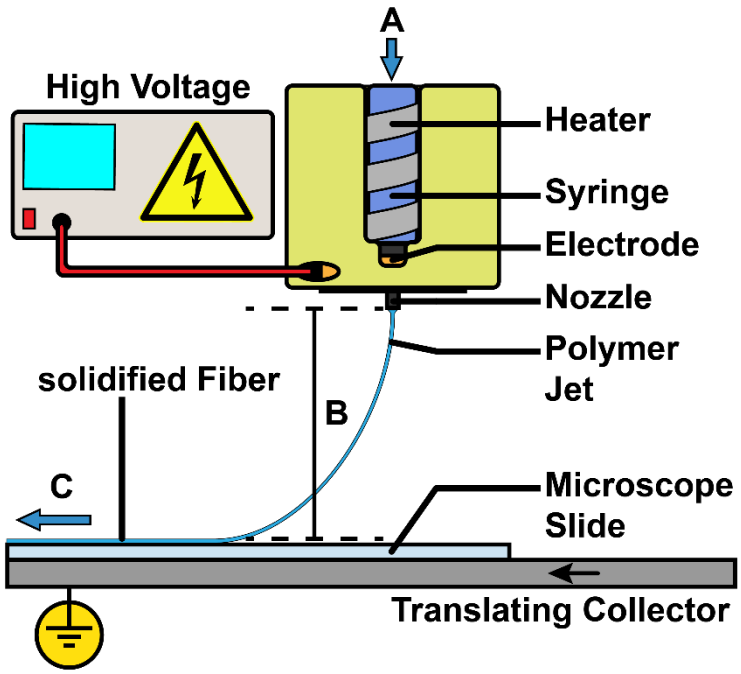

Figure 7. Setup of a MEW device showing three different regimes: A material-feed regime, B free-flight regime and C collection regime. Based on [65].

This syringe is heated to processing temperature and the polymer melt is pushed out of the nozzle, most commonly using air pneumatics. A high voltage source is used to create an electrical field between a ring electrode, which is located around the nozzle, and the grounded or oppositely charged collector. This electrical field is responsible for the generation of a stable jet, that is accelerated towards the collector. The jet can then be precisely collected by moving the collector, usually in an x-y-plane, to produce a construct in a layer-by-layer process. To simplify the process, it can be divided into three stages: a material-feed part (**Figure 7A**), the free-flight regime (**Figure 7B**) and the collection area (**Figure 7C**). In the following chapters a detailed look at the different regimes of the MEW process will be given.

2.2.2.1 Material-feed part

This first section mainly describes how the material flows out of the reservoir through an opening. Important parameters to influence this section are the used material (type of polymer, molecular weight), the temperature, the applied pressure, and the nozzle diameter and length. All these parameters determine the volume flow, an important value in MEW. How the nozzle specifics and applied pressure influence the volume flow can be mathematically described by Hagen-Poiseuille equation for a fluid flowing through a nozzle with a round profile [66]:

$$Q = \frac{dV}{dt} = \frac{\pi \, \Delta p \, r^4}{8 \, \eta \, l} \quad (1)$$

with Q = volumetric flow rate, V = volume, t = time, Δp = pressure gradient, r = pipe inner radius, η = fluid viscosity and l = pipe length.

This equation also accounts for the influence of the viscosity of the flowing liquid, but it is only true for Newtonian fluids. As polymer melt are non-Newtonian liquids and show a shear-thinning behavior, the relationship between Δp and Q is not linear, but

$$\Delta p \propto Q^n \quad (n < 1) \quad (2)$$

This relationship can be reasonably depicted by a decreasing viscosity with an increasing shear rate. A popular model to describe the shear rate dependent viscosity of polymer melts is the power-law, which was first proposed by Ostwald and de Waele [67, 68].

$$\eta = m\dot{\gamma}^{n-1} \quad (3)$$

With m = consistency index, $\dot{\gamma}$ = shear rate and n = degree of non-Newtonian behavior with n = 1 means Newtonian and n < 1 for shear thinning polymers.

This means that the applied pressure and therefore the applied shear rate influence the viscosity of the polymer melt. The influence of the applied temperature is indicated by the consistency index m, which can be described as an Arrhenius-type function

$$m = m_0 \exp\left[\frac{\Delta E}{R}\left(\frac{1}{T} - \frac{1}{T_0}\right)\right] \quad (4)$$

with m_0 = m at T_0, ΔE = flow activation energy, R = universal gas constant, T/T_0 = temperature.

With further simplification a more convenient equation can be depicted as

$$m = m_0 \, e^{-a(T-T_0)} \quad (5)$$

with a = empirical parameter.

This relationship expresses that with increasing temperature the consistency index decreases which also results in a decrease in viscosity. The last contribution to the viscosity and therefore to the volume flow is the polymer itself. The relationship between viscosity and molecular weight of polymers is described in the Mark-Houwink equation

$$[\eta] = KM^a \quad (6)$$

with [η] = intrinsic viscosity, M = (viscosity) average molecular weight and K, a = empirical parameters.

Therefore, viscosity also increases with increasing molecular weight. This can be explained by an increasing interaction between the chains as well as more entanglement between chains being present at higher molecular weights.

As this regime includes the most tunable parameters, there are several publications that are predominantly using this regime to influence the printing outcome. In an important publication Hrynevich *et al.* showed that the fiber diameter could be predominantly changed by changing the applied air pressure [69]. Blum *et al.* varied nozzle diameter as well as pressure amongst other variables to influence different fiber attributes, like diameter, fiber roughness and crystallinity [70].

2.2.2.2 Free-flight regime

The free-flight regime is entered when the material leaves the nozzle. For many extrusion-based techniques such as FDM and 3D plotting the strand undergoes extrudate swelling. This behavior can be explained by looking at a polymer melt on a molecular level. When a polymer melt is entering a nozzle, random polymer coils undergo stretching which leads to an alignment of polymer chains. As soon as the melt leaves the nozzle the chains relax back into random coils causing a observable swelling (**Figure 8A**) [71]. Additionally, a

flowing liquid column usually undergoes Plateau-Rayleigh instabilities which are causing a breakup of the column into droplets (**Figure 8B**) [72, 73].

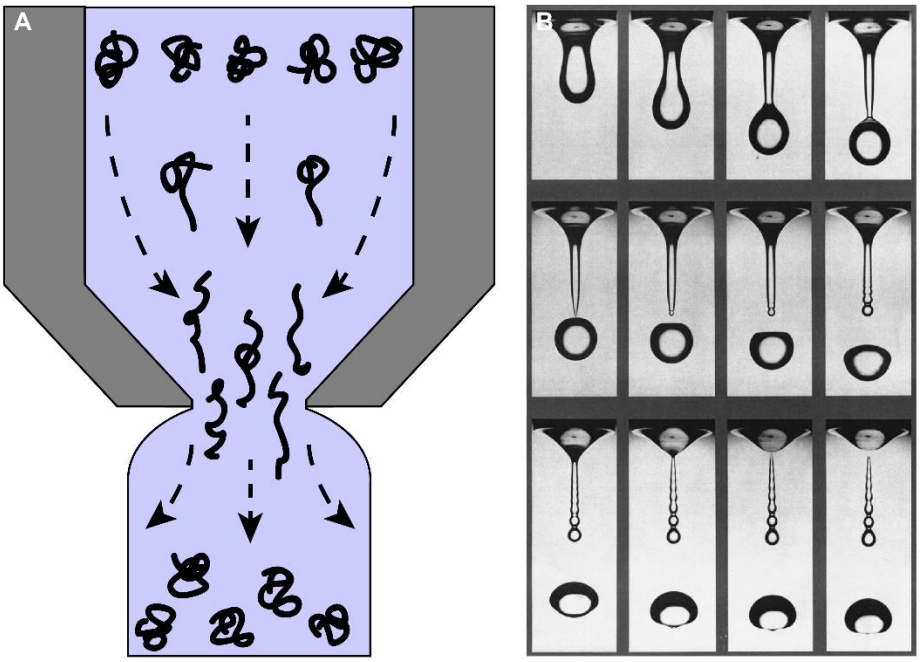

Figure 8. A Scheme of dye swelling of polymer melts or solutions. **B** Progression of the breakup of a flowing liquid column by Plateau-Rayleigh instabilities. Reprinted with permission from American Physical Society.

In MEW this behavior is circumvented by using the effects of an electrohydrodynamic (EHD) effect. When applying a high voltage electrical field between the nozzle and the collection area charge carriers are introduced on the surface of the liquid drop [74]. As polymer melts are usually dielectric, the dielectric leaky model of Melcher and Taylor can be applied [55], which describes that charge carriers can move freely within the fluid and accumulate on its surface. These charges interact with the electrical field applying shear stress by electrostatic force. When this force exceeds the surface tension and viscosity a Taylor cone [45, 54] is formed and a jet is accelerated towards the collector [75, 76]. While the jet generated with SES undergoes whipping instabilities after travelling a certain distance [77], MEW is performed with a polymer melt with a higher viscosity compared to polymer solutions and the collector distance is smaller avoiding instabilities and therefore enable direct-writing. Within this threshold the collector distance can be tuned to influence the jet flight time.

During flight of the jet, it is not only stretching, but also solidifying. As the ambient temperature is low compared to the processing temperature the jet undergoes substantive cooling. When amorphous polymers cool down the chains become more tightly packed leading to a more rubber-like behavior. As soon as the temperature drops below the glass transition temperature (T_g) the polymer vitrifies becoming stiff and brittle [78]. For semi-crystalline polymers the solidification starts out similar by chains becoming more and more immobile while cooling down resulting in an increasing viscosity. As soon as the temperature drops below the melting temperature (T_m) the chains start to arrange into crystalline and amorphous regions. As crystallization generates heat, this heat must be removed by the surrounding media to continue the crystallization process. As the glass transition temperature for semi-crystalline polymers is often below ambient temperature, the resulting solidified material is usually tougher compared to amorphous materials [78]. Here again, the collector distance can be tuned to influence the degree of solidification when the fiber reaches the collector or previously deposited fibers, which can influence e.g., fiber fusion between the different layers.

Controlling this regime is very important as it predominantly defines the stability of the printing process. As the jet is in flight, it is influenced by the electrical field. Hochleitner *et al.* investigated the stability of the MEW jet in relation to the electrical field strength [79]. They found out that depending on the flow rate a certain voltage threshold must be applied to receive a stable jet. If the applied voltage is slightly to low pulsing can be observed and if it is significantly to low long beading occurs. These instabilities can be described an imbalance of the melt flow and the mass that gets pulled by the electrical field, which leads to an inconsistent fiber diameter. Another important contribution to how electrical field manipulation can enhance the outcome is the work of Wunner *et al.* [80] on the creation of large volume scaffolds. They investigated the influence of an increasing layers of fibers on the precision of fiber deposition. Their results show that with increasing layers the precision decreases due to accumulation of excess charge from the produced fibers distorting further fiber deposition. To avoid this precision loss, they changed both the collector distance and the applied voltage with increasing layer number to keep the electrostatic force constant. With these adjustments, Wunner *et al.* could reach higher layer count of around 7 mm compared to keeping these parameters fixed. Finally, this regime is also crucial when scaffolds with small pores need to be fabricated. Pore size is dependent on the fiber

spacing and usually fiber spacing of 100 µm or higher was used for scaffold production with MEW. For this, collector distances of 3 mm or higher are feasible [69, 81, 82]. Tylek *et al.* though went way below that and successfully produced high quality scaffolds with fiber spacing of 40 µm [83]. To avoid fiber bridging [84] a small collector distance of 1.4 mm was employed. As the travel time of the jet is dependent on this distance, a small distance reduces the time window of the jet being able to be influenced by inconsistencies of the electrical field due to already deposited fibers. As small pore scaffold has a higher density of fibers, reducing this window is crucial.

2.2.2.3 Collection area

The last regime is mainly about using a collector to precisely deposit fibers into ordered structures. To successfully utilize the collector, there are two important values that needs to be understood: critical translation speed (CTS) and jet lag.

The CTS is defined to be the lowest collector speed to generate straight fibers. As shown in **Figure 9** fibers undergo different shapes while increasing the collector speed until they are straight.

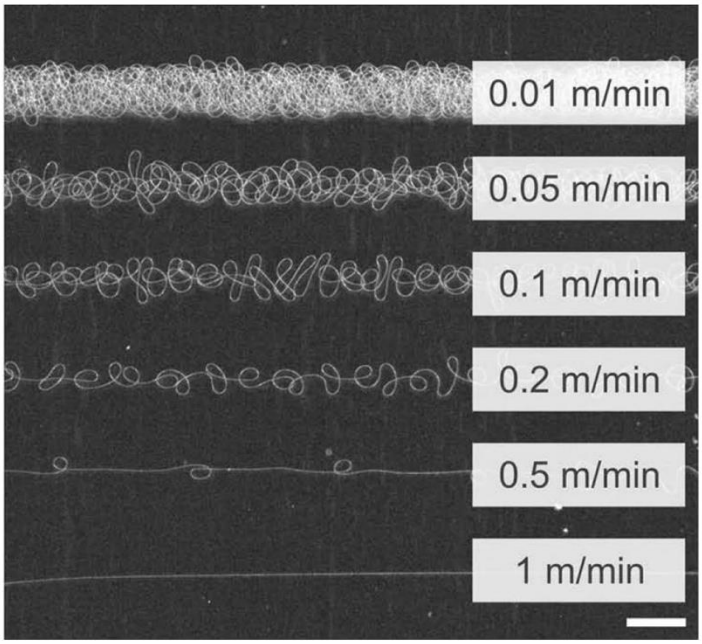

Figure 9. MEW fibers undergoing different geometries. Reprinted with permission from John Wiley and Sons.

Above the CTS, the fiber is stretched, which can be used to adjust the diameter of the fiber besides changing the applied pressure as discussed earlier [69]. Adjusting the fiber diameter can also tailor other properties of the fiber, such as surface roughness, mechanical properties and crystallite size [70]. Additionally, in the work of this thesis the CTS was used to monitor changes of the polymer melt, be it inhomogeneities of the melt or degradation of the used material.

Jet lag is determined by the distance between the position of the nozzle and the actual deposition of the fiber. In comparison with other extrusion-based methods such as FDM the ratio of the collector distance to the fiber diameter is very high for MEW. Therefore, the jet lag of MEW has a much bigger influence on the outcome of a print.

If these requirements are well understood, a high control over fiber placement can be achieved. This was shown by Youssef *et al.* as they were able to generate highly ordered scaffold with different layout patterns to finetune scaffold porosity [85]. To further enhance the fabrication possibilities, Hrynevich *et al.* produced suspended fibers by using a high collector speed in combination with an increased collector distance as well as a low processing temperature [86]. As jet lag becomes more crucial for structure that utilize sinusoidal structures, Hrynevich *et al.* provided a tool for precise prediction of laydown patterns [87]. This knowledge could be utilized by Liashenko *et al.* to produce sinusoidal walls of fibers [88]. To account for layer shifting of the waves due to changing jet lag when building up layer, they introduced a correction factor applied each layer to generate ideal walls of sinusoidal fibers. Additionally, adjusting printing paths layer-by-layer allowed them to also produce nonlinear geometries such as overhangs, wall texturing and branching.

2.2.3 Materials for MEW

A sufficient material database is crucial for any AM process and especially when biomedical requirements need to be met. Being able to not only define the architecture, but also finetune other features such as mechanical properties [89-91] and biodegradability [92, 93] matching the requirements of natural tissue can enhance its application for TERM purposes [94].

Polycaprolactone

MEW is a young AM process, and the library of materials remains small. There are some materials established, but the gold standard that has been investigated intensively is PCL [69, 79, 95]. PCL is a thermoplastic synthetic polyester that is predominantly synthesized by ring-opening polymerization (ROP) of ε-caprolactone (**Figure 10**) catalyzed by tin(II) 2-ethylhexanoate with number average molecular weights (M_n) between 530 and 630 000 g mol^{-1} [96]. It is a semi-crystalline polymer that can reach up to 69% crystallinity [97] with a T_g between -65 and -60 °C and a T_m between 56 and 65 °C [98-100]. The low melting temperature together with a rapid solidification [101] make it an excellent candidate for melt processing. PCL also has properties that are sought after in TERM as it is biocompatible and bioresorbable with a total *in vivo* degradation time of 2-4 years depending on molecular weight [102, 103]. The degradation itself is achieved in a 2-step process: In the first step, the material is degraded by non-enzymatic hydrolysis of the ester bonds until the molecular weight gets low enough (under 3000 g mol^{-1}). The resulting fragments are then taken up by phagosomes of macrophages and giant cells to further break them down until they are resorbed by intracellular degradation [104]. These properties make it a stand-out material for TERM approaches [101, 105, 106].

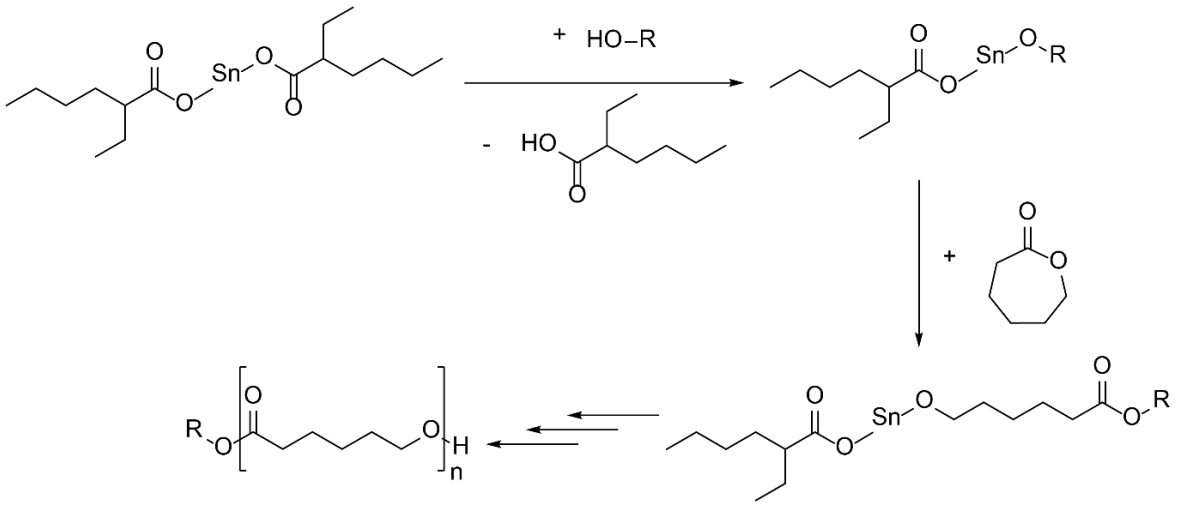

Figure 10. Ring-opening polymerization of PCL catalyzed by tin(II) 2-ethylhexanoate.

2.2.3.1 Other materials

Beyond PCL there are other materials that have been used for MEW. A possible deviation from the gold standard are blends of different polymers or additives with PCL.

Castilho *et al.* blended PCL with poly(hydroxymethyl glycolide-*co*-ε-caprolactone) to produce a material that can be processed via MEW and tested in cardiac tissue engineering. This blend was beneficial for cardiac cells as it showed higher biocompatibility and with a suitable scaffold architecture guidance of cardiac cell growth was possible [81]. In another approach to change the properties of PCL Abdal-hay and colleagues mixed it with hydroxy apatite nanoparticles and processed it via MEW to promote osteoblast cell seeding, infiltration and growth [107].

Besides blends, new polymers have also been established to expand the MEW library with materials having different properties. An example would be the thermoplastic elastomer based on a urea-siloxane copolymer used by Hochleitner and colleagues [108] that combines the properties of a thermoplastic with an elastic polymer. It is also possible to generate hydrogel scaffolds with MEW as shown by Nahm *et al.* [109]. They used poly(2-ethyl-2-oxazine) functionalized with furan and maleimide and processed a mixture via MEW. The functionalization caused a reversible crosslinking while the fibers cooled down due to Diels-Alder click chemistry, which allows swelling of the fibers when being exposed to water. It has also been shown that it is possible to process electroactive polymers. Florczak *et al.* processed polyvinylidene fluoride and showed that MEW processing favors the generation of β-phase and therefore enhances the piezoresponse of the material [110]. An overview of all materials processed so far with MEW is shown in a review of Kade *et al.* [111].

2.2.3.2 Poly(lactic-co-glycolic acid)

To enlarge the library of polymers, Chapter 5 focuses on the establishment of PLGA. PLGA is copolymer consisting of the monomer units of polyglycolic acid (PGA) and polylactic acid (PLA) and can be polymerized by enzymatic ROP [112], ROP [113] or polycondensation [114-116] reactions (**Figure 11**). Controlling the synthesis is very important as molecular weight, polydispersity, ratio of the monomers and the PLGA sequence have an influence on the physico-chemical properties of the material [117, 118]. Due to its hydrolytic degradation behavior, PLGA is a well-used polymer in TERM [119, 120], especially for drug delivery applications [121, 122]. PLGA undergoes biodegradation in a hydrolytic mechanism generating glycolic and lactic acid [117]; these acids then get resorbed by the organism and further metabolized in the Krebs cycle [123]. Additionally, PLGA has a history of use in

clinical biomaterials [124]. To process PLGA into usable devices many different techniques have already been used such as solvent casting/salt leaching [125], microsphere fabrication [126] and electrospinning [127, 128]. As most of these techniques are solvent-based, the received scaffolds can be harmful for the patient, if residual solvent cannot be fully removed. MEW processing of PLGA would bypass this issue as scaffolds are prepared directly from melt.

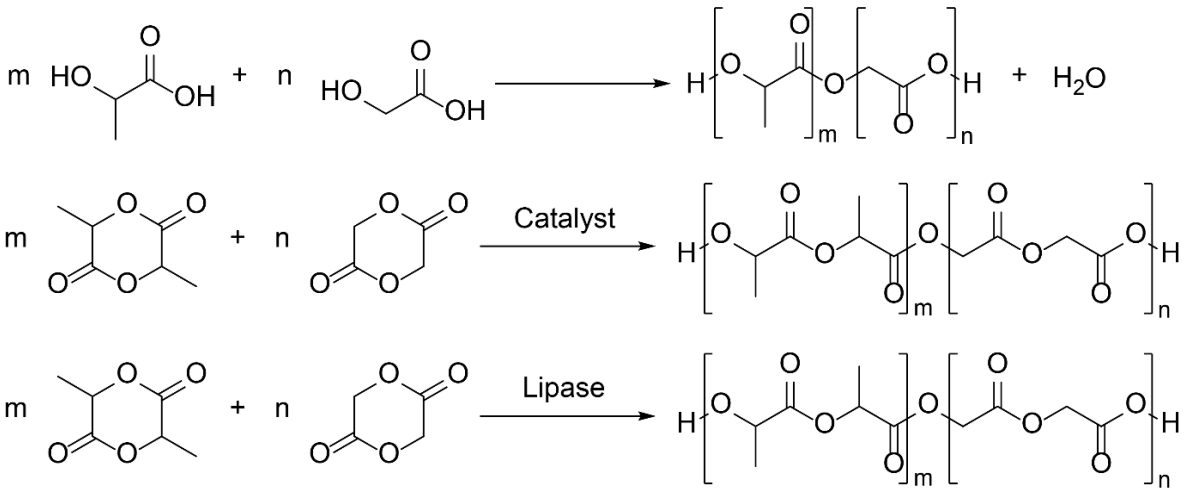

Figure 11. Polymerization of PLGA by polycondensation, ring-opening polymerization with the help of a catalyst and enzymatic ring-opening polymerization.

2.3 Thermal degradation

MEW is a melt-based process and therefore requires elevated temperatures to keep the process materials in a molten state. Since biodegradable materials are desired in TERM, polyesters are a very popular class of polymers that are experiencing wide application. Due to their biodegradable nature, these polymers are often also susceptible to thermal degradation. To know the degradation rate and the generated degradation products is very important as the processing stability in a prolonged print can be affected by degradation and the product may be harmful for patients. Therefore, an overview of the literature of the thermal degradation of PCL and PLGA will be given here.

2.3.1 Polycaprolactone

As PCL was rising in popularity as a biodegradable polymer Ouhadi *et al.* were particularly interested in the mechanism of the degradation of PCL under thermal conditions [129]. They would artificially age PCL synthesized by metallo-organic catalysts with and without acetylated hydroxy groups at 120 °C under oxygen and inert atmosphere. For characterization they would use dilution viscometry, gel permeation chromatography (GPC) and membrane osmometry. What they found is that PCL degrades with a radical initiated thermo-oxidative mechanism. They also mentioned a second mechanism in statistical ester interchange reactions. Another contribution was done by Persenaire *et al.* that utilized non-isothermal thermogravimetric analysis (TGA) coupled with mass spectrometry (MS) and Fourier transform infrared spectrometry (FTIR). They proposed a two-step degradation with a statistical rupture via ester pyrolysis reaction as first step forming gases of H_2O, CO_2 and 5-hexenoic acid. The second step consist of an unzipping mechanism generating ε-caprolactone in the process. Although TGA is normally used in a non-isothermal mode, Aoyagi and colleagues additionally looked at degradation of PCL under isothermal conditions at 170, 250 and 290 °C [130]. From their data they deduced that the thermal degradation of PCL happens predominantly by unzipping. Lastly, Sivalingam *et al.* performed non-isothermal as well as isothermal (300, 320, 340 and 350 °C) TGA experiments in combination with GPC to investigate the thermal degradation of PCL [131]. The activation energy calculated by the Friedman and Chang method for analysis of the non-isothermal measurements showed a 3-fold change suggesting that the contribution of the two parallel mechanisms of random scission and unzipping is changing with increasing temperature. Under isothermal conditions only unzipping could be observed.

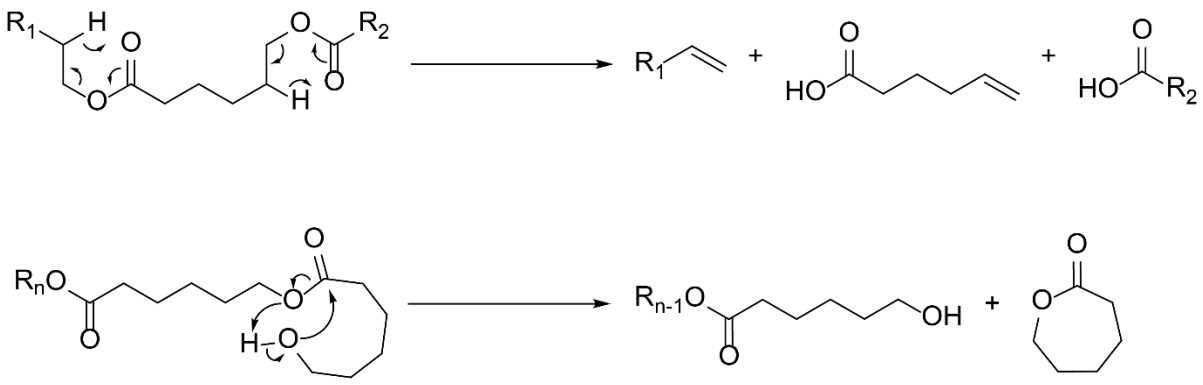

Figure 12. Thermal degradation mechanisms of PCL including random scission and unzipping.

To better illustrate the two mechanisms of random scission and unzipping, respective reaction schemes are shown in **Figure 12** adapted from the work of Persenaire [132] and Sivalingam [131]. As conventional thermal degradation studies are either done under non-isothermal condition or at isothermal conditions beyond 100 °C and in an accelerated setup, this work aims at looking at the changes PCL undergoes under MEW conditions in terms of printability but also chemical changes.

2.3.2 Poly(lactic-*co*-glycolic acid)

There are numerous studies on the *in vitro* and *in vivo* degradation of PLGA of different compositions, but studies on the thermal stability are rare. To give an overview over the thermal degradation of PLGA also some information on PLA and PGA will be provided.

McNeill and Leiper looked at the thermal decomposition of PGA with TGA and thermal volatilization analysis (TVA) coupled with a mass spectrometer under non-isothermal and isothermal conditions [133]. Their findings suggest that PGA degrades in ester interchange reactions when temperatures are below 270 °C forming glycolide and higher oligomers in the process as well as CO_2 being formed by decarboxylation at the carboxyl chain end. Above 270 °C PGA undergoes ester interchange reactions as well as random chain scission. Sivalingam and Madras also contributed to the mechanism of the thermal degradation of PGA with the help of non-isothermal and iso-thermal TGA experiments in inert atmosphere [134]. They found that PGA would degrade predominantly by ester interchange reactions at lower temperatures leading to the formation of olefinic chains with small amounts of glycolide and methyl glycolate by decarboxylation of chain

ends. This agrees with the study of McNeill and Leiper but was more detailed due to the usage of the Friedman plot observing a switch in the activation energy of the degradation.

Like PGA there is a plethora of publications about the thermal degradation of PLA. McNeill and Leiper also investigated the thermal degradation of PLA under non-isothermal and isothermal conditions. For their non-isothermal approach, they used TGA, differential scanning calorimetry (DSC) and TVA with a heating rate of 10 K min^{-1} [135]. They could show that 50 % of the degradation product they found were oligomers and other volatiles mainly consisted of CO_2 and acetaldehyde. In their isothermal approach they looked at the degradation of PLA at temperatures between 230 and 440 °C with the help of TVA, MS and IR spectroscopy [136]. Additionally, they added 1,4-diaminoanthraquinone as a radical inhibitor to investigate the radical nature of the degradation. They concluded that the main degradation mechanism is a non-radical, backbiting ester interchange reaction producing degradation products such as lactide, oligomers of different sizes depending on the location of the interchange reaction and acetaldehyde (**Figure 13**). Going beyond 270 °C other mechanisms rise in significance that generate radicals such as alkyl-oxygen homolysis and acyl-oxygen homolysis (**Figure 14**). Kopinke *et al.* also looked at the degradation of PLA using TGA, DSC, time resolved pyrolysis-MS and pyrolysis gas chromatography coupled with mass spectrometry (GC-MS) [137].

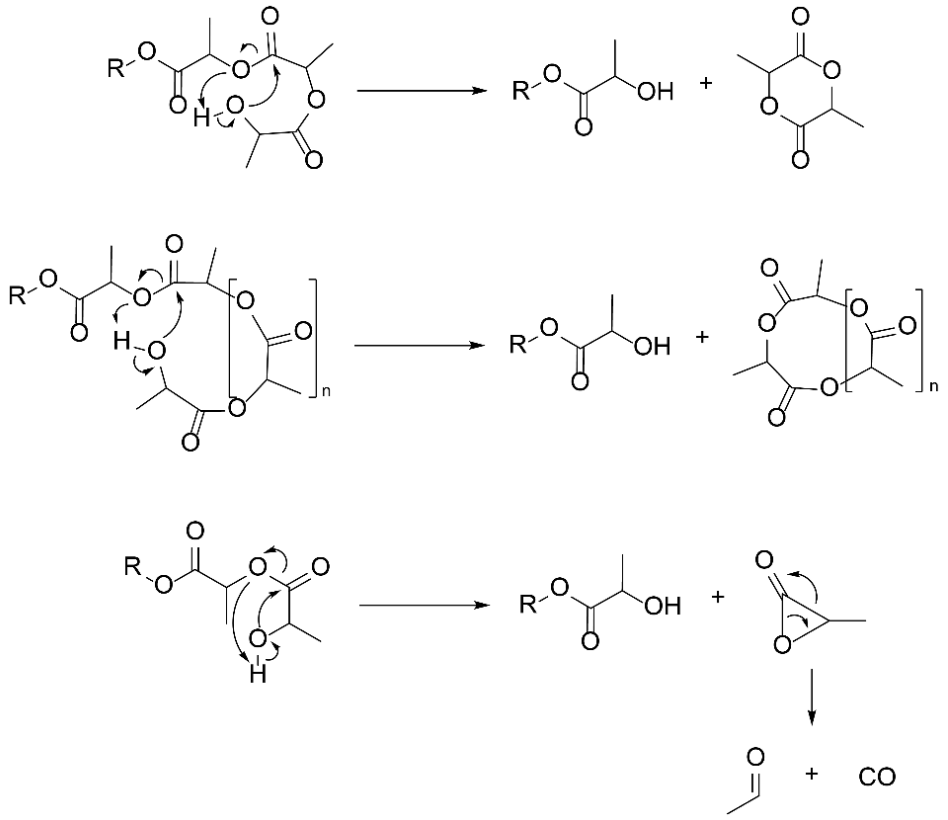

Figure 13. Predominant thermal degradation mechanisms of PLA at temperatures between 230 °C and 440 °C.

Their results confirmed the findings of McNeill as they could identify the intramolecular ester exchange reaction forming lactide and oligomers to be the main degradation route. The radical reactions could also be identified, again consistent with the work of McNeill [135, 136]. A new reaction mechanism was introduced in form of the *cis*-elimination which requires a C-H bond in β-position of the ester oxygen. Sivalingam and Madras also investigated the thermal degradation of PLA with the help of non-isothermal and isothermal TGA measurements under N_2 atmosphere [134]. They could again confirm the findings of McNeill *et al*. but shed more light on the change from random chain scission to specific chain end scission with the help of the Friedman plot showing a switch in activation energy of the degradation.

To conclude their study on PGA and PLA, Sivalingam and Madras also looked at the influence of PLA on the degradation of PGA in their copolymer PLGA (85 % lactic acid : 15 % glycolic acid) [134]. What they found is that the addition of PLA increases the degradation rate of PGA compared to pure PGA probably because of the released acid of PLA degradation autocatalyzing the degradation process.

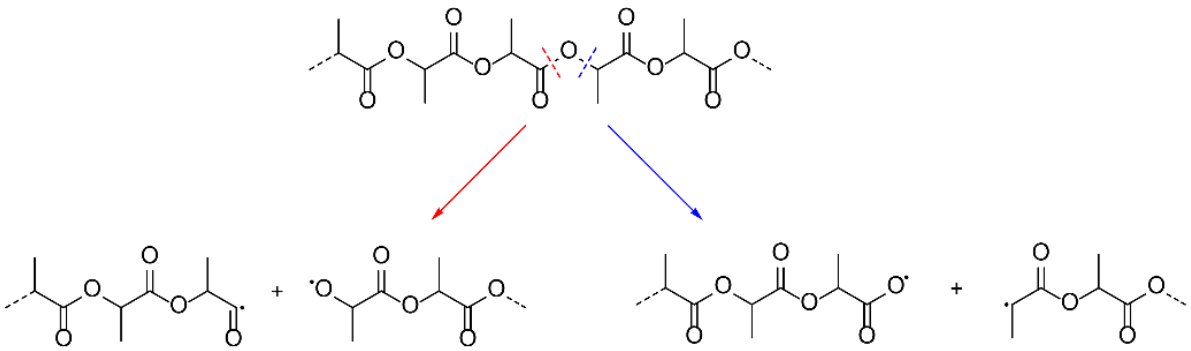

Figure 14. Radical degradation mechanisms of PLA at temperatures beyond 440 °C.

As already stated in the PCL section the investigation of thermal degradation of these polymers is predominantly done by an accelerated process with the help of TGA measurements. As these measurements rely on the generation of volatiles, degradation steps that might affect MEW processing by changes in e.g., the viscosity of the melt are not depicted in these studies. Therefore, this work aims to give insight into changes in the printing behavior of PLGA (50:50 lactide:glycolide) during processing at the lowest suitable processing temperature.

2.4 Plasticizer

Since PLGA is a rapidly degrading polymer, measures need to be taken to enlarge its processing window in MEW. This can be done by reducing the processing temperature to also reduce the degradation rate. To achieve this reduction, the application of plasticizer is a well-known approach. In general plasticizers are nonvolatile, high boiling and low molecular weight substances that can be added to polymers to change their thermal and mechanical properties [138]. Some of these changes can improve the processability of the material such as reduction of T_g or changing the rheological properties of the melt, but also tailor the mechanical properties of the final product such as flexibility or ductility [138-140]. A plasticizing effect can be accomplished internally or externally. For the internal approach the plasticizer is chemically bound to the polymer [141, 142], while in the external approach the plasticizer is blended within the polymer [143-145]. There are different classes of chemicals that are commonly used as plasticizers. The most used class is phthalates, but terephthalates, trimellitates and citrates are also often used. There are several theories that describe the mechanism of plasticizer action. The most popular ones

are the lubricity theory, the gel theory, and the free-volume theory. The lubricity theory is the oldest one and is attributed to Kirkpatrick [146], Clark [147] and Houwink [148]. It assumes that intermolecular friction between polymer chains cause the rigidity of the material. If small molecules are added they act as a lubricant letting the chains slide against each other more easily [149]. The gel theory expands on the lubricity theory by accounting for the secondary interactions such as Van-der-Waals forces and hydrogen bonds between chains. Plasticizer break these interactions and prevent reformation, which would again facilitate sliding of chains against each other [149]. As these theories were not sufficient to describe the plasticizer effect, the free-volume theory was developed as it also allows for the explanation of the success and failure of plasticizers [150]. Free volume describes the internal space available for chain movement, which increases sharply at T_g. Plasticizer can now occupy and increase this space and maintain it when the material is cooled down preventing the reformation of a rigid structure [149]. As already stated, adding plasticizer reduces the T_g of a polymer. This can result in a reduction of the processing temperature that might enlarge the processing window of the material.

Chapter 3

THE MULTI-WEEK THERMAL STABILITY OF MEDICAL GRADE POLY(ε-CAPROLACTONE) DURING MELT ELECTROWRITING

Chapter 3 has already been published as original research article (Böhm, C., Stahlhut, P., Weichhold, J., Hrynevich, A., Teßmar, J., Dalton, P. D., The Multiweek Thermal Stability of Medical-Grade Poly(ε-caprolactone) During Melt Electrowriting. *Small* 2021, 2104193.)

The chapter is based on the work of the author of this thesis Christoph Böhm, who mainly worked on the conceptualization, experiments, data evaluation, and composition of the manuscript.

The author contributions of the related research article are as follows:

Contributor	**Contribution**
Christoph Böhm	Designed and performed experiments; mainly analyzed data; wrote the manuscript
Philipp Stahlhut	Operating of the SEM for the visual analysis of fibers
Jan Weichhold	Data analysis of XRD data
Andrei Hrynevich	Provided G-Code for the experiment; revised and provided feedback on the manuscript
Jörg Teßmar	Provided support on experiment planning and evaluation; revised and provided feedback on the manuscript
Paul D. Dalton	Provided support on experiment planning and evaluation; revised and provided feedback on the manuscript

3.1 Abstract

MEW is a high-resolution AM technology that places unique constraints on the processing of thermally degradable polymers. With a single nozzle, MEW operates at low throughput and in this study, medical-grade PCL is heated for 25 d at three different temperatures (75, 85 and 95 °C), collecting daily samples. There is an initial increase in the fiber diameter and decrease in the jet speed over the first 5 d, then the MEW process remains stable for the 75°C and 85°C groups. When the collector speed was fixed to a value at least 10% above the jet speed, the diameter remained constant for 25 d at 75°C and only increased with time for 85°C and 95°C. Fiber fusion at increased layer height was observed for 85°C and 95°C, while the surface morphology of single fibers remained similar for all temperatures. The properties of the printed material were assessed with no observable changes in the degree of crystallinity or the Young's modulus, while the yield strength decreased in later phases only for the 95°C group. After the initial 5-day period, the MEW processing of PCL at 75°C is extraordinarily stable with overall fiber diameters averaging 13.5±1.0 µm over the entire 25-day period. The stable, multi-week processing capability of this thermally degradable polymer provides an insight into its adoption as the gold standard for MEW.

3.2 Introduction

AM technologies are an essential part of biomaterials processing [151], tissue engineering and regenerative medicine (TERM) applications [152] and, more recently, biofabrication [153]. PCL is appealing as a scaffold material in this context, as it is hydrolytically stable for sufficient periods in cell culture as well as having long-term degradation *in vivo*. PCL also has excellent processing characteristics in general; multiple manufacturing technologies use this polymer extensively [154], including SES, templating, and emulsion formation. Increasing the resolution of controlled manufacturing also allows the possibility to produce hierarchical structures necessary for more complex tissue replacements [155] as well as personalized implants [156].

There are several AM technologies already used to process biomaterials and the ones that have successfully translated to the clinic to date have all been based on solvent-free techniques [157]. These include electron beam melting, extrusion-based direct writing [152, 158] and SLM. Another solvent-free AM process that is being developed within

academia with the intent for clinical translation is MEW, follows the principles of melt extrusion but produces higher resolved structures than the afore-mentioned AM technologies. MEW fills the dimension gap between SES and extrusion-based direct writing by achieving fiber diameters typically ranging between 2 µm and 100 µm [159].

MEW has already been applied to a large variety of biomedical applications including cartilage TERM [160], cancer research [161] and heart valve replacement [162]. Additionally, MEW has been combined with other biofabrication technologies to create hybrid systems with superior properties compared to constructs created by one method alone [155]. Examples include fiber reinforced hydrogel constructs to better mimic soft tissue mechanical properties [163] or scaffolds utilizing both SES and MEW to control spreading behavior of cells [164].

MEW, however, places certain requirements on materials that push the boundaries of what is previously investigated. The closest related well-established AM technique using polymer melts is extrusion-based direct writing, which includes using a feedstock filament drawn into a heated nozzle [11]. Due to the relatively high flow rate of extrusion-based direct writing [39], the polymer is exposed to the high temperature required for melting only for a short time. This short heating period is also applicable for SLM, where polymeric particulates are thermally fused together using a laser source [28].

MEW on the other hand requires very low throughput; typically in the order of 2 to 50 µL h^{-1} (**Figure 15A**) [165, 166] and therefore, the molten polymer is typically heated for prolonged periods of time, in the order of hours and days [167]. From a design and regulatory perspective for implantable biomaterials, the thermal degradation and impact on the printed material is essential to ascertain. For this reason, we performed a comprehensive study on the stability of PCL during MEW over a multi-week time frame, to 1) identify the stable operating regime for the process and 2) identify time periods that would indicate thermal degradation. The PCL used in this study was synthesized and purified under Good Manufacturing Practice (GMP) conditions and is the current gold standard polymer for MEW [168]. The investigated extended heating of PCL at moderate temperatures is herein notably different to previous thermal degradation studies, which focus on higher temperature stresses for shorter periods of time [130-132, 169].

3.3 Results and Discussion

Biomaterials are one primary application for MEW and translation from university-led research to implantable devices is governed by the regulatory agencies that prioritize safety and reliability [157, 170]. There is a relatively fast-track regulatory pathway for biomaterials in the US, termed the 510(k) route that allows new implants based on similarities to previous devices. In this context, GMP-manufactured polymers with a history of use in the clinic are essential for conforming to this process. The PCL used here is made under such conditions and is the basis for several medical devices, including those that are made by melt-extrusion based AM [158]. The low flow rates associated with MEW, however, result in the PCL being exposed to heat for longer periods than melt extrusion and knowledge of the effects of these elevated heating conditions on manufacturing is important for clinical translation as a biomaterial.

3.3.1 Melt electrowriting

We established MEW over a 25-day period, using a daily print collection strategy that allowed multiple analysis including also X-ray diffraction (XRD) and mechanical testing. Using two microscope slides per day, the programmed printing paths are shown in **Figure 15B** and contain several regions including 1) a 25-layer scaffold to stabilize the jet and for XRD measurement, 2) three iterations of printing to determine the jet speed, fiber diameter/morphology and 3) four fiber walls consisting of 25 stacked fibers for morphological analysis and mechanical testing.

3.3.2 Critical translation speed

Knowing the CTS is important throughout a print since this value can influence the fiber diameter and fiber placement when changing printing direction [6, 25]. Corresponding to the jet speed, the CTS provides a value above which the jet will stretch and therefore reduce in final diameter [159]. The CTS was investigated as a part of this study as a measure of process stability and **Figure 15E** shows the typical progression of the experiment for 85 °C. This shows sets of four fibers direct-written with increasing collector speeds and the CTS was determined when they are linear. Changes in parameters can affect the CTS; for example, a higher processing temperature will reduce the viscosity and results in a higher

flow rate to the nozzle. Lower viscosity, in turn, produces a higher CTS since the collector speed must be increased to prevent the jet from buckling (**Figure 15C**).

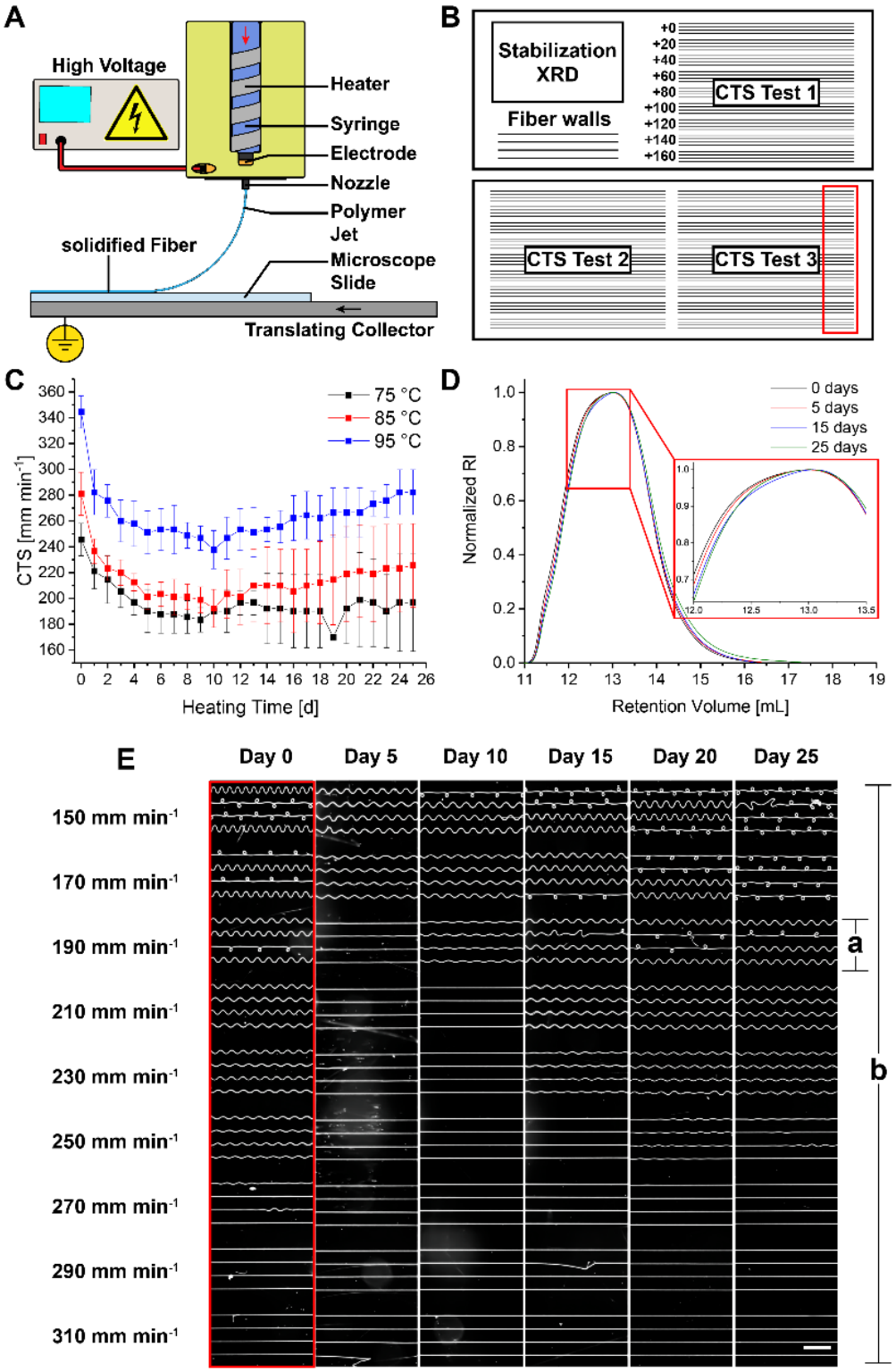

Figure 15. Overview for multi-week stability MEW experiments. **A** Schematic of the MEW process and **B** the printing design on the glass microscope slides, developed to minimize the collection area and to perform multiple analysis with daily prints. It consists of a

stabilization area that was used for XRD measurement, three CTS tests were straight lines of fibers were produced at increasing collector speeds and four walls of 25 fibers were printed to investigate fiber stacking and mechanical properties. **C** development of the CTS at 75 °C (black), 85 °C (red) and 95 °C (blue); **D** development of GPC curves measured of PCL samples artificially aged at 95 °C for 0 (black), 5 (red), 15 (blue) and 25 (green) d. **E** Stereomicroscope images of the CTS measurement for one printing iteration at 85 °C over 25 d; each four fibers (a) were defined as a "block" and all printed fibers (b) as an "array".

The change in CTS trends similarly for all three temperatures and commences with a decrease during the first 5 d (**Figure 15C**). The decrease in the CTS during the first 5 d was 23% for 75 °C, 28% for 85 °C and 23 % for 95 °C, respectively. The CTS continued to change after day 9 for 85 °C and 95 °C, while for it remains stable for 75 °C with only small variations. On day 19 microscopy slides of one printing iteration were destroyed before analysis, which explains the observable outlier. From day 13 on an upward trend for 85 °C and 95 °C can be observed, which is explainable by ongoing degradation of the material. To confirm the degradation GPC measurements with samples artificially aged at 95 °C have been performed and their results can be found in **Figure 15D**. The measured GPC curves shift towards higher retention volume values with increasing heating time, which translates into polymer chain lengths decreasing with time. The changes are very subtle indicating a very slow degradation of PCL. This is also confirmed by measurements of the viscosity over 24 h that show a very slow decrease (**Figure 16A**).

3.3.3 Fiber diameter

Since the collector speed stretches the jet above the CTS [159] into a catenary shape and affects the fiber diameter, a distinction was made between the diameter of fibers produced at the CTS (**Figure 17B**) and at a fixed collector speed above the CTS (v_{fix}, **Figure 17C**). The collector speeds of v_{fix} were 270 mm min^{-1} (75 °C), 310 mm min^{-1} (85 °C) and 360 mm min^{-1} (95 °C) and were selected to ensure that all research was performed above the CTS for the entirety of experiments (**Figure 17C**), as the vast majority of MEW research is performed at a fixed collector speed above CTS; here it is 10 to 76 % above the CTS.

The fiber diameter at CTS shows an initial increase as the CTS decreases during the first 5 d, when the development of **Figure 17B** and **Figure 15C** is compared. In the following

days, the diameter of the samples produced at 95 °C increases, while the diameters of the other two temperatures remained stable. The fiber diameter at v_{fix} for both 85 °C and 95 °C show a steady increase over 25 d. In contrast, the diameter at v_{fix} when processing at 75 °C remains almost constant over all 25 d of printing.

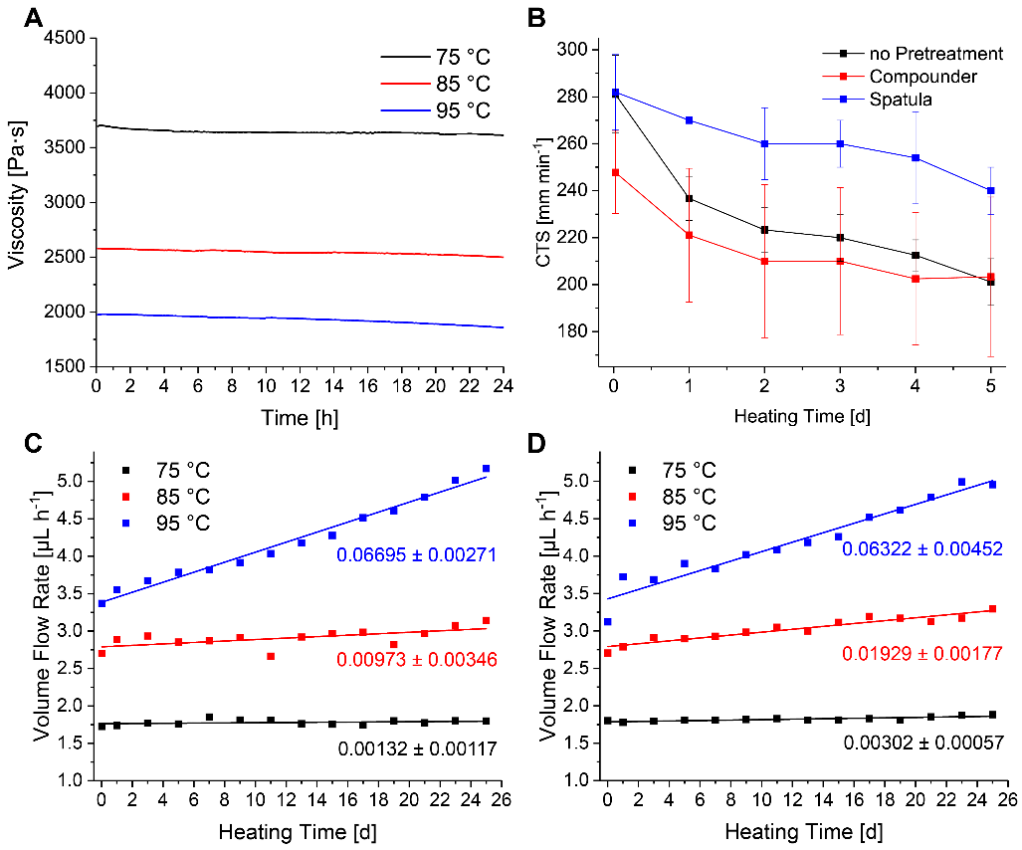

Figure 16. A Development of the viscosity over 24 h measured at 75 °C (black), 85 °C (red) and 95 °C (blue). **B** Development of the CTS during the first 5 d of heating after no pretreatment (black), pretreatment in a micro-compounder (red) and mixing of PCL melt insight the syringe with a spatula (blue). Development of the calculated volume flow rate over 25 d of heating at 75 °C (black), 85 °C (red) and 95 °C (blue) at **C** CTS and **D** v_{fix}.

This small fiber diameter variation with a fixed collector speed well above the CTS reflects the situation in numerous studies, aiming at the production of straight fibers [79, 95, 159]. With information on the diameter at CTS and the CTS we could evaluate the respective melt flow rate for all three temperatures. Shown in **Figure 16C** and **D**, the volume flow rate at 75 °C does not significantly change throughout the 25 d of printing. For 85 °C and 95 °C the melt flow rate increases steadily over 25 d with 95 °C increasing at a higher rate. This, as well as the GPC data, suggests a steady degradation of PCL throughout the 25 d of heating.

3.3.4 Changes in printing properties

The most likely cause of a decrease in CTS during the first 5 d would be an increase in viscosity of printing, which has several explanations. The first one involves increasing the average molecular weight by transesterification reactions/post-polymerization [129]. Transesterification might cause a change in viscosity if the initial chain length distribution is shifted towards the low molecular proportion which leads statistically to longer chains as it reaches a thermodynamic equilibrium. Secondly, the behavior could be explained by physical changes of entanglement in the melt. We wanted to test if an inhomogeneity of the melt caused this reduction in CTS during the first 5 d, by using two different thermal pretreatment methods. Firstly, we compounded the pellets and immediately transferred a hot filled syringe into the heater. This did not have the desired mixing effect, perhaps due to an unavoidable transient cooling when placing the syringe into the MEW printer. In the second approach, we mixed the melt with a spatula directly inside the print head, which indeed resulted in a more stable CTS during the first 5 d. The results of these experiments can be found in **Figure 16B**, which show that the initial drop in CTS was most effectively reduced by mixing the melt with a spatula.

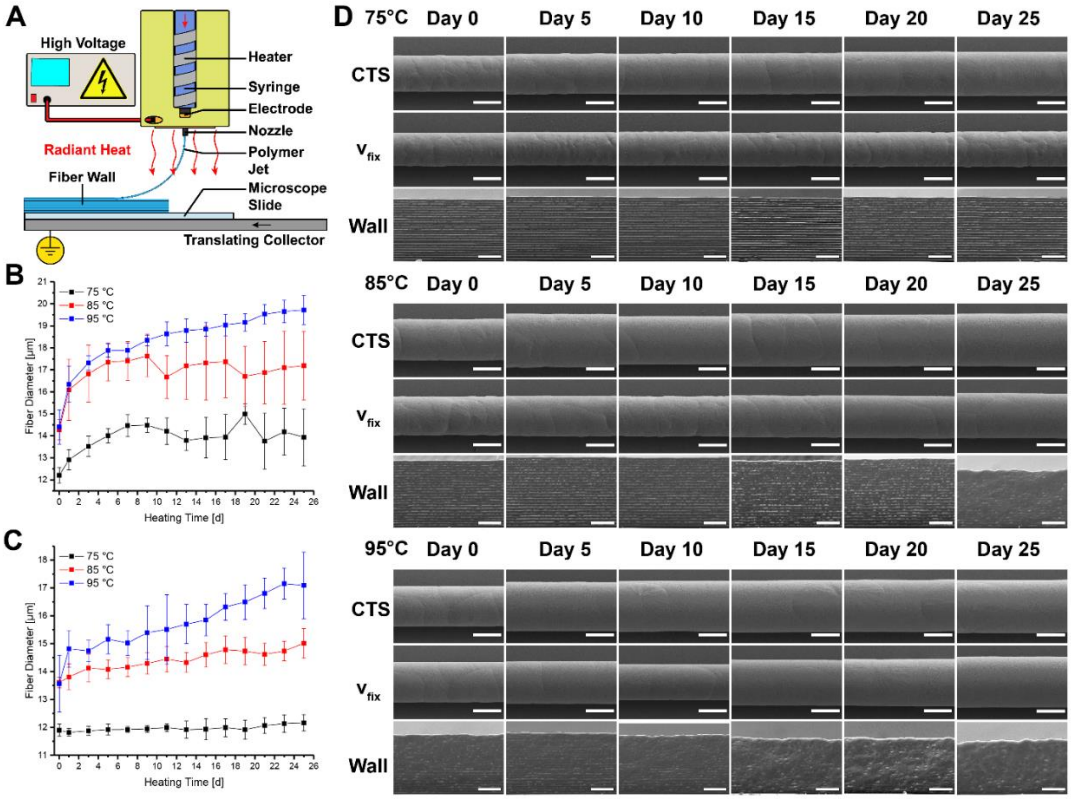

Figure 17. A Production of the fiber walls. **B** Development of the diameter of fibers produced at CTS with heating time. **C** Development of the diameter of fibers produced at

v_{fix} with heating time. **D** SEM images of showing the fiber surface after printing at CTS and v_{fix} and the fiber walls produced with 75 °C, 85 °C and 95 °C. Scalebars: 10 µm (CTS and v_{fix}) and 100 µm (fiber walls).

Later in the multi-week period, thermal degradation for 85 and 95 °C becomes observable, with a rising CTS, fiber diameter and therefore overall flow rate. For 75 °C the print is again exceptionally stable with no major changes visible for CTS and the fiber diameter at v_{fix}. This shows that with optimal processing conditions MEW can be exceptionally stable but is susceptible to small alterations in the printing properties of the material probably due to changes of the molecular weight if less optimal parameters are chosen.

3.3.5 Fiber morphology

PCL crystallizes in spherulites which should add to the rough appearance of its fibers [171]. **Figure 17D** provides an overview of the fiber solidification and surface morphology with time. The fibers are generally consistent over the 25 d of printing for the 75 °C group, while fibers produced at 85 °C and 95 °C with v_{fix} become slightly smoother with time, with fewer spherulites visible. Printing at both v_{fix} and CTS shows a slight decrease in visual roughness of fibers when increasing the temperature from 75 °C to 95 °C. These differences are very small and probably not significant, but it is possible to change the surface morphology by changing printing parameters as has been shown before [70].

3.3.6 Fiber Stacking

The fiber stacking behavior affects the 3D structure and inter-fiber mechanics. All fiber walls were produced at v_{fix}, as setting a single collector speed is standard practice for scaffold production [81, 83, 85]. At higher layer number the fibers are closer to the printhead where the ambient temperature is higher, which resulted in a more molten appearance in the upper layers with fibers merging (**Figure 17D**). At 85 °C the changes during the first 10 d are minor but with increasing time the fiber merging of the upper layers becomes substantial. The fibers at 95 °C behave similarly but this shrinkage already occurs at day 10. Conversely, there were no visible changes in the wall morphology of fibers throughout 25 d for prints performed at 75 °C.

3.3.7 X-ray Diffraction

A change in the number and size of crystallites may provide an insight in an overall material change however the crystallinity remains at a value of 52.5±3.4 % across all temperatures (**Figure 18A**). For all samples, crystallites are 25.6±2.3 nm with no major changes observed for all temperatures (**Figure 18B**). As the crystallinity of PCL is dependent on the molecular weight [172], changes due to thermal treatment must be too small to have an observable effect with this technique. Some preparation issues account for small difference seen in the first 5 d for experiments performed at 85 °C and are outlined further in the Chapter 3.5.10.

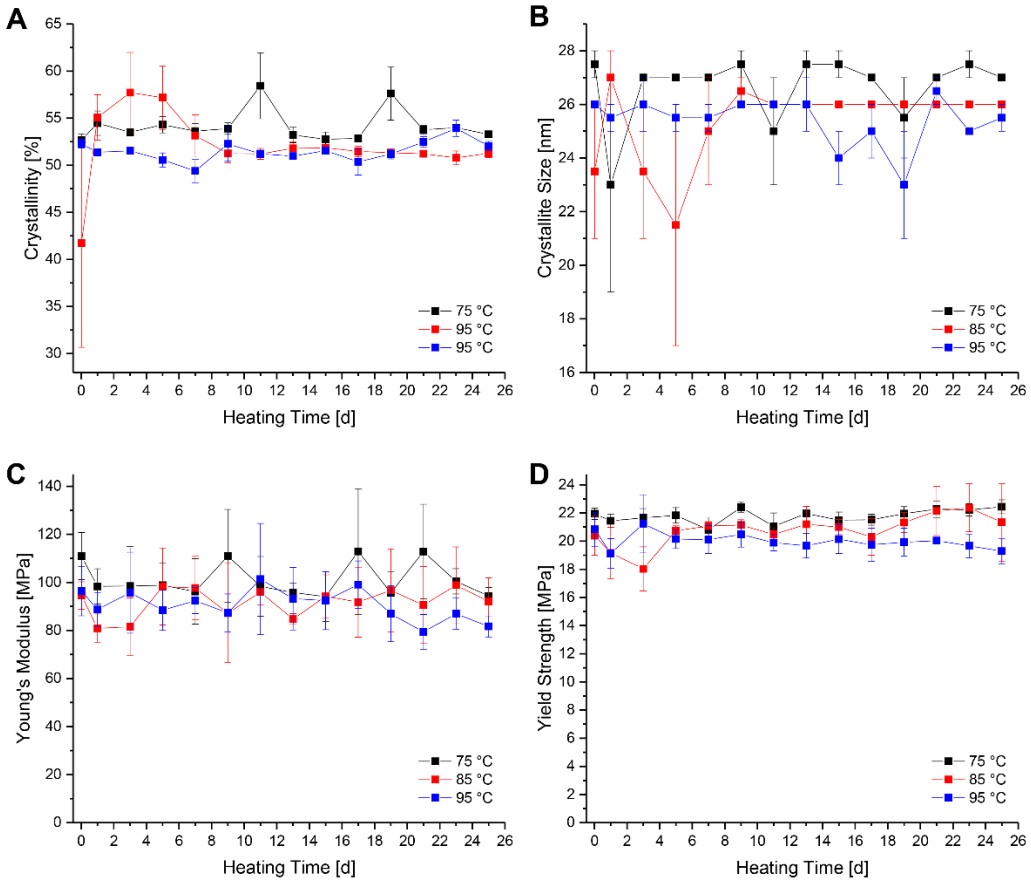

Figure 18. Crystallinity (A) and crystallite size (B) of PCL scaffolds with 25+25 layers. Young's modulus (C) and yield strength (D) of PCL fiber walls with a stack height of 25 layers.

3.3.8 Mechanical Testing

Tensile testing was performed using walls of 25 fibers printed at v_{fix}. Similar to XRD results, the Young's modulus showed no changes throughout the experiment duration for any of the three temperatures (**Figure 18C**). This is in alignment with Grosvenor *et al.* [173]

who showed that small changes in the molecular weight don't affect the Young's modulus. The yield strength (**Figure 18D**) is also mostly unaffected at 75 °C and 85 °C during printing with calculated values ranging from 19-22 MPa. The yield strength is reported to be influenced by the molecular weight [173], meaning changes due to thermal degradation at 75 °C and 85 °C were too small to affect the yield strength. There is a reduction in the yield strength at the later periods for 95 °C, perhaps reflecting the thermal degradation changes seen using CTS measurements (**Figure 15C**). Overall, PCL is very durable over 25 d of constant heating for 75 °C and 85 °C and shows only small changes in the yield strength for 95 °C.

3.4 Conclusion

MEW is a high-resolution AM technology that is sensitive to small changes in the physical properties of the melt. When processed at temperatures just above its melting point for 25 d and with a mass flow rate of 1 to 5 µL h^{-1}, PCL is a remarkably stable polymer to process. In the study, small changes in the CTS occurred in the first 5 d at 75 °C, followed by a stable period out to 25 d. There were several changes to the prints while processing at 85 °C and 95 °C – notably with the CTS and fiber diameter. The Young's modulus, yield strength or crystallinity, however, did not change with time for any of the temperatures used, indicating that the CTS is an especially sensitive measure of processing changes. Overall, our study found that PCL is an extremely durable polymer to process via MEW, and a major reason that this polymer is the gold standard for this AM technology.

3.5 Materials and Methods

3.5.1 Materials

Medical-grade PCL (Corbion Inc., Netherlands, PURASORB PC 12, Lot# 1712002224, 05/2018) was used for all the experiments. To avoid changes of the material due to storage, the material was aliquoted into 50 mL Falcon tubes and sealed after argon purging. The aliquots were stored at -80 °C and fully warmed to room temperature prior to opening the Falcon tube, to prevent condensation of water vapor on the PCL pellets.

3.5.2 MEW Printer

For the printing experiments, a custom-built MEW printer was used as described previously [174] and is shown in **Figure 19**. Briefly, a HV source (LNC 10000-05 pos, Heinzinger Electronic GmbH, Rosenheim, Germany) was connected to the nozzle through a brass piece that was also heated with a SiN ceramic heater (Bach RC, Germany). The polymer was extruded using compressed air controlled by a pressure valve (SMC, Germany) to a nozzle, positioned above a grounded stainless-steel collector mounted on x-y linear axis (Aerotech Inc., Pittsburgh, USA), controlled via G-code run by A3200 Motion Composer (A3200, version 4.09.000.0126, Aerotech Inc., Pittsburgh, Pennsylvania, USA).

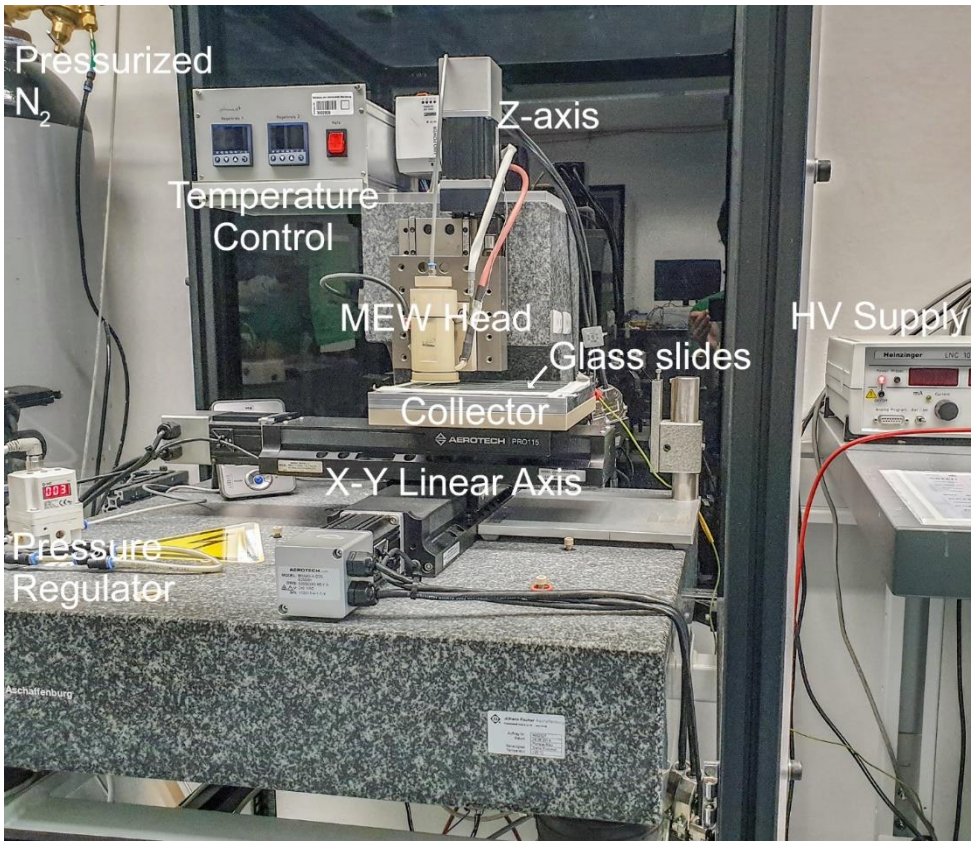

Figure 19. Photograph of MEW printer.

3.5.3 Printing Parameters

MEW processing was performed using a 3 mL syringe (3 mL FORTUNA OPTIMA Luer Lock Tip, Poulten & Graf GmbH, Wertheim, Germany) equipped with a 25 G nozzle (length 7 mm; Unimed S.A., Lausanne, Switzerland) protruding 0.5 mm beyond the HV brass

electrode. The syringe was filled with 2 mL of PCL pellets before heating to 75 °C, 85 °C and 95 °C without any pre-treatment. A constant collector distance of 3.5 mm, voltage of 4.5 kV and an air pressure of 2.0 bar were used for all experiments. A weather station (TFA Dostmann GmbH& Co. KG, Reicholzheim, Germany) recorded the ambient air temperature and relative humidity (21.8±0.3 °C and 40.6±3.9 %). Each experiment was set to a single temperature and was performed in triplicate (i.e., a total of 9 x 25-day prints) and the MEW printer was not used for any other activities during each 25-day printing experiment. As the material was kept at the respective temperature for 24 hours per day, a total heating time of 600 h was achieved per iteration.

3.5.4 Collector Configuration

Glass microscope slides (76 x 26 x 1 mm, VWR, Radnor, Pennsylvania, USA) were placed upon a stainless-steel collector and printing was performed once per day for a total of 25 d at the respective temperature (75, 85 or 95 °C). A schematic of the printing setup can be observed in **Figure 15B**. A box-shaped structure (25 + 25 fiber layers) with an overall dimension of 25 x 18 mm, a fiber spacing of 500 µm and a stacking height of 25 layers was initially printed for XRD measurements. The XRD sample was printed at a collector speed of 500 mm min^{-1} with a total printing time of 112 min. Immediately following this sample, three arrays containing blocks (**Figure 15C** a) of four lines were printed with 9x4 fibers in total per array (**Figure 15C** b). Every fourth fiber the collector speed was increased by 20 mm min^{-1} to determine the CTS and the fiber diameter. The G-code described above is provided as Supporting Information.

Commencing with a collector speed of 110 mm min^{-1} (75 °C), 150 mm min^{-1} (85 °C) and 260 mm min^{-1} (95 °C), each block the collector speed was increased by 20 mm min^{-1}, which was repeated three times. After that, four walls of straight fibers for following mechanical testing were produced by moving back and forth on the x-axis 25 times at the highest employed speed for each temperature defined as v_{fix}, which would be 270 mm min^{-1} (75 °C), 310 mm min^{-1} (85 °C) and 360 mm min^{-1} (95 °C), respectively. The G-code described above is provided in Chapter 8.1. To further compare the printing behavior of PCL at the different temperatures, the volume flow rate Q has been calculated with the following formula:

$$Q = \pi \left(\frac{d}{2}\right)^2 v \quad (7)$$

with d is the average diameter of fibers produced at CTS/v_{fix} and v is the average collector speed at CTS/v_{fix}. For this calculation a cylindrical fiber shape was assumed.

3.5.5 Thermal pre-treatment of PCL

To investigate, if thermal pre-treatment makes a difference for processing PCL via MEW, a set of experiments with two different configurations was performed. Firstly, the print head was preheated to 85 °C together with an empty syringe, while PCL was added to a micro compounder (Micro Compounder MC 5, Xplore Instruments BV, Sittard, The Netherlands) and heated to 85 °C with a screw speed of 100 rpm. The melt was then mixed for 30 min at 50 rpm before releasing it into the pre-heated syringe. After placing the syringe back into the heater, a waiting period of 30 min was applied before commencing printing, to ensure thermal equilibrium (n=3). For the second approach the PCL filled syringe was placed inside the preheated print head and molten for 30 min. Then the melt was mixed inside the syringe with the help of a spatula, before letting the material sit for another 25 min (n=2). The MEW processing is identical in both cases and to what was described above, however daily samples were only collected for a period of 5 d.

3.5.6 Determination of fiber diameter

The fiber diameter was determined using scanning electron microscopy (SEM) (Crossbeam 340 SEM, Carl Zeiss Microscopy GmbH). After sputter coating a 3 nm layer of platinum (Leica EM ACE600, Wetzlar, Germany), images at day 0, day 1 and then every 2nd day including day 25 were taken. The images were then processed via a custom-made ImageJ macro. This macro consisted of a segmentation step adapted from the ImageJ plugin “DiameterJ”[175] using the “traditional” algorithm, and the “local thickness” plugin. This method analyzes the entire image and results are the mean of the diameter over the entire image. These mean values were then determined for all images (1008 images per temperature) to generate the mean value and the standard deviation of the fiber diameter for each second day for each temperature. Using the information about fiber diameter and CTS, the volume flow rate was calculated as described in Chapter 3.5.4.

3.5.7 Gel permeation chromatography

PCL samples (n=1) were artificially aged using an oven (Memmert GmbH & Co. KG, Schwabach, Germany) at 95 °C for a total of 25 d. Samples were drawn after 2 h (0 d), 5 d, 15 d and 25 d. The samples were then dissolved in chloroform (Carl Roth, Karlsruhe, Germany) with a concentration of 5 mg ml^{-1} and mixed for 2 h. The samples were then filtered through a 0.45 µm polytetrafluoroethylene (PTFE) filter, before measuring them using a GPC device from Malvern (Herrenberg, Germany) with a Viscotek GPCmax (in-line degasser, 2-piston-pump and autosampler) equipped with a column oven (35 °C), refractive index (RI) detector (Viscotek VE3580), a pre-column (Viscotek CGuard) and two columns (2x Viscotek LC4000L, length = 300 mm, width = 8 mm, porous styrene divinylbenzene copolymer, particle size 7 µm). The flow rate was kept at 1.0 mL min^{-1}.

3.5.8 Rheology

The viscosity development of PCL over 24 h at 75 °C, 85 °C and 95 °C has been determined with a Physica MCR 301 rheometer (Anton Paar, Graz, Austria). The test was performed with a 25 mm parallel plate configuration with a gap of 0.5 mm. After heating up the lower plate to the respective temperature the material was applied, trimmed, and measured in a rotational setup with a shear rate of 0.1 s^{-1}. The setup was encapsulated in a cover to ensure temperature isolation.

3.5.9 Mechanical testing

Mechanical testing was carried out using the fiber wall (Collector Configuration) fixed via double-sided tape to a frame, cut out of cardboard with a laser cutter (Rayjet 50 C30, Trotec Laser GmbH, Ismaning, Germany). The prepared frames (**Figure 20**) were then used to test mechanical strength of PCL fibers using a dynamic mechanical analysis device (BOSE ElectroForce 5500, TA Instruments, New Castle, USA) in static testing mode (triplicate for N=2 different prints at each temperature). The maximum strain was 150% and the rate 0.05 mm/s. To determine the Young's modulus (σ) and the yield strength the cross section (A) of the fiber wall has been modelled as a perfect 25-stack of fibers using the measured fiber diameter (d) and using Equation 9.

$$A = 25 \cdot \left(\frac{d}{2}\right)^2 \cdot \pi \qquad (8)$$

After the calculation of the tensile stress the Young's modulus was determined by the slope of the elastic region of the stress-strain curve. To specify the yield tensile strength, the highest value at the transition from elastic to plastic region has been determined.

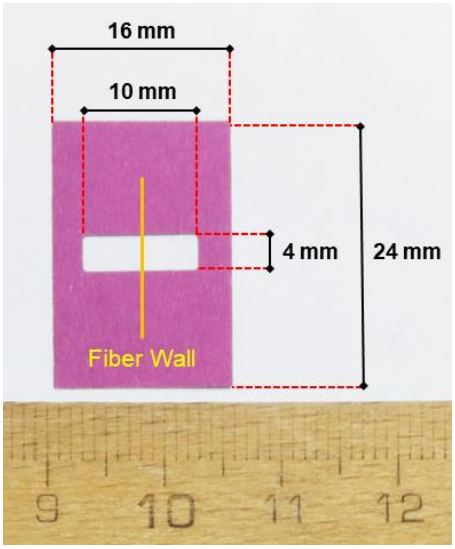

Figure 20. Specifications of the used frames used for mechanical testing of the fibers.

3.5.10 X-Ray diffraction

The scaffold described in the printing section was used for XRD measurements. Therefore, the scaffold has been brought onto the sample holder consisting of a silicon single crystal wafer designed to minimize background signals fixed via static electricity. The sample holder was fixed in the XRD (D8 DaVinci Design, Bruker, Karlsruhe Germany) and examined with CuKα radiation (λ = 1.54060 Å) in a range from 10-50° 2θ, in 0.01° steps, a dwell time per step of 0.85 s while the sample was rotating at 15 rpm (n = 2). To ensure a minimal background a voltage and current for the X-Ray tube of 30 kV and 53 mA were chosen respectively and a beam knife was fixed in the beam path to cut off non diffracted X-Rays at low angles. After the measurement, the obtained intensities per angle were analyzed qualitatively with the program Diffrac.EVA (Bruker, Karlsruhe Germany) and quantitatively with Diffrac.TOPAS (Bruker, Karlsruhe Germany). To calculate the theoretical peak positions and peak shapes of PCL and compare it to the obtained diffractogram, the crystal structure presented by Bittiger H. *et al* [176] was used and refined to values for the

lattice parameters of a = 7.485 Å, b = 4.974 Å and c = 17.935 Å. The crystallite size was determined on the basis of the Scherrer equation [177, 178]:

$$\mathrm{B}(2\theta) = \frac{K\lambda}{L\cos\theta} \qquad (9)$$

Where B(2θ) is the integral breadth, which is calculated as the total area under the peak at the position 2θ divided by its maximum height. K the Scherrer constant = 1 and L the volume average of the crystal thickness or crystallite size in the following parts.

To distinguish the crystalline signals from the amorphous contributions to the diffractogram the sample holder was also measured empty, and the signal was then calculated in as the remaining background in further calculations. Furthermore, in the calculation the difference between the obtained diffractogram and the calculated PCL curve plus the background signal was seen as the contribution of the amorphous phase content. A quotient of the areas under the respective curves for PCL or the amorphous content with their sum gave the value for the crystallinity.

Chapter 4

INVESTIGATION OF MULTI-WEEK THERMAL STABILITY OF MEDICAL GRADE POLY(ε-CAPROLACTONE) USING PHYSICAL AND CHEMICAL ANALYSIS

Manuscript is in final preparation step. The chapter is based on the work of the author of this thesis Christoph Böhm, who mainly worked on the conceptualization, experiments, data evaluation, and composition of the manuscript.

4.1 Abstract

PCL is an often-used material for biomedical applications as it is biodegradable and, due to its melting temperature of around 60 °C, it can be processed at relatively low temperatures (70-100 °C). Even at these relatively mild temperatures, thermal degradation can alter the chemistry of the material and therefore change its physical as well as its biochemical properties. In this study, PCL was kept at 75 °C, 85 °C and 95 °C for a total of 25 d, before various analytical techniques including GPC, GC-MS, DSC and rheology were used to investigate chemical and physical changes. Using GPC and rheology we were able to observe that PCL degraded slowly during the 25 d heating period with rheology particularly indicating a higher degradation rate with increasing temperature. In terms of the physical changes, we looked at the onset melting temperatures which did not change significantly over 25 d as the changes in the molecular weight were too small to affect it. As PCL degrades in a random scission as well as an unzipping mechanism, GC-MS was used to determine the development of the caprolactone content. At 95 °C the expected development of an increasing monomer content could be observed, while for 75 °C the caprolactone content decreased. This behavior could be explained by ester interchange reactions that can reintroduce released monomer back into the polymer backbone. The combination of these properties explains why PCL is an excellent material for melt processing as it thermally degrades very slowly.

4.2 Introduction

AM techniques are being increasingly used for the last three decades. Especially in the field of TERM, 3D printing approaches are very popular due to their ability to design both new and patient specific scaffolds. At the same time, the possibility to produce hierarchical structures is given, which is necessary for complex tissue replacements [179, 180]. Scaffolds for TERM are usually produced by using biocompatible polymers processed via different techniques. These techniques can have two different approaches as they need to use either polymer solutions or polymer melts to generate the desired product. A popular example for solvent-based process is SES, which produces fibers in a sub-micron range to mimic the extra cellular matrix [181]. Its melt-based counterpart is MES. SES is the more popular choice due to the simple setup, but MES has some advantages, especially when biocompatibility is of importance. Firstly, no potentially toxic solvents are necessary, which obviates a post-process step to remove them. Secondly, the viscosity of polymer melts is higher, therefore whipping instabilities do not appear as early as in SES. While SES is predominantly used to create nonwoven meshes, MES allows better control over fiber deposition for more complex shapes. This principle was further optimized by the development of MEW, which reduced the distance between the print head and the collector to achieve high precision [4]. With these advantages several disadvantages also appear. The thermal properties of the used polymer are very important, besides being biocompatible and biodegradable. Many naturally derived polymers with relevance in TERM such as collagen or fibronectin cannot be readily processed, as they undergo decomposition at elevated temperatures and often are not really meltable. Additionally, all polymers need to be kept molten in a reservoir for prolonged durations for MEW. This often leads to massive degradation, which can alter the printing properties and become potentially harmful to cells, if toxic byproducts are generated.

As already stated, materials that can be degraded and absorbed by the body are preferred, which put polyesters at the forefront due to their degradability by hydrolysis. Popular polyesters, that are used in TERM are poly-L-lactic acid, PLGA and PCL. Looking at the thermal properties of these materials, both PLLA with a melting temperature of around 170 °C [182] and PLGA with a processing temperature of around 240 °C [183] are prone to higher thermal stress when compared to PCL. PCL is a semi-crystalline thermoplastic polymer with a melting temperature of around 60 °C [96], which makes it the ideal

candidate for prolonged melt processing. That is the reason why PCL is the gold-standard material for MEW, which requires a melt reservoir because the required flow rates are so low. It has become apparent that PCL is very durable during prolonged heat exposure, however for medical application it must be guaranteed, that the degradation does not lower the quality of product neither by changes in the processability nor by generation of toxic byproducts. Therefore, it is important to investigate and comprehend the thermal degradation route of PCL.

Thermal degradation of PCL has already been investigated intensively. Persenaire *et al.* showed 2001 primarily with TGA that PCL degrades in a two-step process. The first step was identified as random scission leading to the formation of water (H_2O), carbon dioxide (CO_2) and hex-6-enoic acid [132]. The second step only took part at temperatures beyond 430 °C and followed a depolymerization or unzipping mechanism where ε-caprolactone was generated. Sivalingam *et al.* investigated the thermal degradation of PCL under isothermal and non-isothermal conditions. They found that PCL degrades with both random chain scission as well as unzipping under non-isothermal conditions, while showing pure unzipping at isothermal heating. These isothermal experiments have been carried out at 300 °C, 320 °C, 340 °C and 360 °C [131]. So far, all data concerning the thermal degradation of PCL have been collected in accelerated studies, predominantly looking at TGA data and using temperatures beyond what is usually used to process this material. As this is a follow-up of our publication about the printing stability of PCL under MEW conditions, we decided to also look at the chemical and physical changes over a 25-day time span applying standard processing temperatures of 75 °C, 85 °C and 95 °C. As syringes filled with PCL for MEW are usually used for days or even weeks, this work investigates the thermal stability of PCL over a three-week period.

4.3 Results

4.3.1 Gel permeation chromatography

To investigate the changes of molecular weight PCL undergoes during 25 d of constant heating, GPC of samples drawn on day 0, day 1 and then every second day have been measured. Since the system runs on chloroform and molecular weight is determined by conventional calibration via polystyrene (PS) standards, the measured values have been

normalized to day 0 to achieve a good comparability between all three temperatures. As can be seen in the collected data (**Figure 21A**) PCL degrades linearly over 25 d for all three temperatures. In terms of kinetics, GPC shows no major differences between the three temperatures. Even though degradation continues throughout the heating time, after three weeks (21 d) of constant heating the molecular weight drops to 92 % (75 °C), 91 % (85 °C) and 92 % (95 °C) of the respective initial value. A comparison of the development of the polymers' dispersity (**Figure 21B**) shows that the samples produced at 85 °C and 95 °C show a slight upward trend with ongoing heating time, while at 75 °C dispersity shows an overall downward trend.

4.3.2 Transesterification experiments

One possible explanation for why PCL is very stable under processing conditions could be transesterification reaction (**Figure 21C**), which would slow down the effect of degradation and therefore its effect on physical properties like viscosity. To investigate these reactions a fluorescence labelled, low molecular weight PCL (Pyr-PCL) was synthesized. **Table 1** shows the calculated molecular weight, as well as the number-average molecular weight determined by GPC, which were in good agreement with each other. To further analyze, if the transesterification mechanism proclaimed is accurate, we also synthesized an end capped version of Pyr-PCL, which should show a slower reaction when mixed with an end capped PCL compared to the unmodified setup, if free alcohol groups are main contributors. As Pyr-PCL was synthesized with tin(II) 2-ethylhexanoate as catalyst, we had to remove it to reduce its effect on these reactions. Therefore, the material was dissolved in chloroform and washed with 1M hydrochloric acid (HCl). Residual tin content was determined by inductively coupled plasma mass spectrometry (ICP-MS) measurements, which confirm successful removal of tin (**Table 2**). The washed Pyr-PCL (Pyr-PCL_W) has then been used for the end-capping reaction to introduce the above-mentioned protective group generating Pyr-PCL_{Ac}.

Table 1. Calculated and measured molecular weight of Pyr-PCL.

Method	Molecular weight [g mol^{-1}]
Calculated	3013.72
GPC (M_n)	2965

After mixing Pyr-PCL_W with PCL and Pyr-PCL_{Ac} with PCL_{Ac} in a micro compounder, the received blends were aged with an oven over 25 d. The samples were then measured using a GPC system with a refractive index and fluorescence detector. The results can be seen in **Figure 21C**. The blend of Pyr-PCL_W and PCL as well as Pyr-PCL_{Ac} and PCL_{Ac} show a linear increase of the fluorescence signal with ongoing heating time, while the later one is increasing by approximately half the rate. The late outliers of the non-protected experiment could be explained by overlap of the measured curve with a big fluorescence peak of Pyr-PCL that has not yet reacted with higher molecular weight chains.

Table 2. Tin content of Pyr-PCL (before HCl wash), Pyr-PCL_W and Pyr-PCL_{Ac} determined by ICP-MS measurements.

Material	Tin content [ppm]
Pyr-PCL (before HCl wash)	9558.40 ± 1788.39
Pyr-PCL_W	2.21 ± 0.62
Pyr-PCL_{Ac}	0.67 ± 0.07

4.3.3 Gas chromatography

Another explanation for the durability of PCL could be its thermal degradation mechanism. As Sivalingam *et al.* showed PCL degrades with an unzipping mechanism when kept at isothermal conditions [131], which would lead to the formation of ε-caprolactone. To investigate, if the ε-caprolactone content is changing during the thermal degradation of PCL, the monomer content of the samples was measured via gas chromatography. The results are shown in **Figure 21D**. As can be seen all three temperatures behave somewhat differently. To start off at 75 °C a downward trend with heating time can be observed,

while samples at 95 °C show a slight upward trend. 85 °C is somewhat in the middle showing a stable regime until day 19 and then quickly increasing.

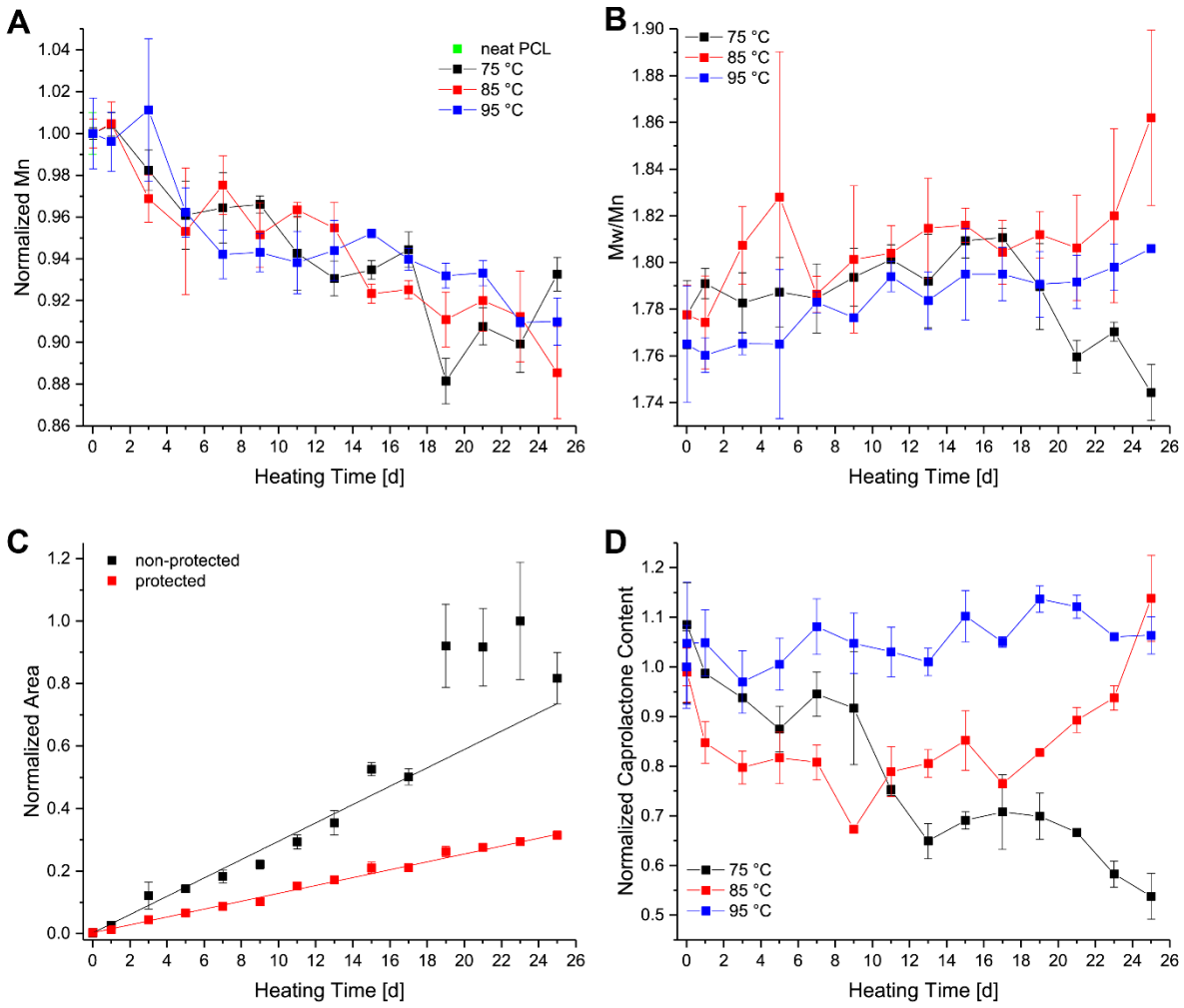

Figure 21. Development of **A** the number-average molecular weight at 75 °C (black), 85 °C (red) and 95 °C (blue), **B** the polydispersity at 75 °C (black), 85 °C (red) and 95 °C (blue), **C** the curve area of the fluorescent signal of uncapped (black) and capped (red) PCL, and **D** the caprolactone content at 75 °C (black), 85 °C (red) and 95 °C (blue) with ongoing heating time.

4.3.4 Differential scanning calorimetry

To see the influence of the chemical changes on the physical properties of PCL, we used DSC to look at the development of the melting onset as well as the melting enthalpy. Firstly, looking at the melting onset (**Figure 22A**) there is a minor upwards trend for all temperatures, but these changes are very small. Secondly, the development of the melting

enthalpy (**Figure 22B**) is also very stable with the 75 °C and the 85 °C samples showing melting enthalpies around 58 J g^{-1} and the 95 °C samples varying around 55 J g^{-1}.

4.3.5 Rheology

To investigate the viscoelastic properties of PCL with ongoing heating time, frequency sweep measurements with PCL artificially aged at 75 °C, 85 °C and 95 °C were conducted and the development of the cross over point of the storage (G') and loss modulus (G'') was determined. The development of this cross over with heating time can be seen in **Figure 22C**. It can be observed that the frequency increases with heating time but at different rates with samples produced at 75 °C showing the slowest change, then 85 °C and 95 °C experiencing the fastest change. Due to the physical limits of the rheometer, frequency sweeps for 95 °C samples could only be measured until day 9 as after that the crossover frequency exceeded 100 Hz.

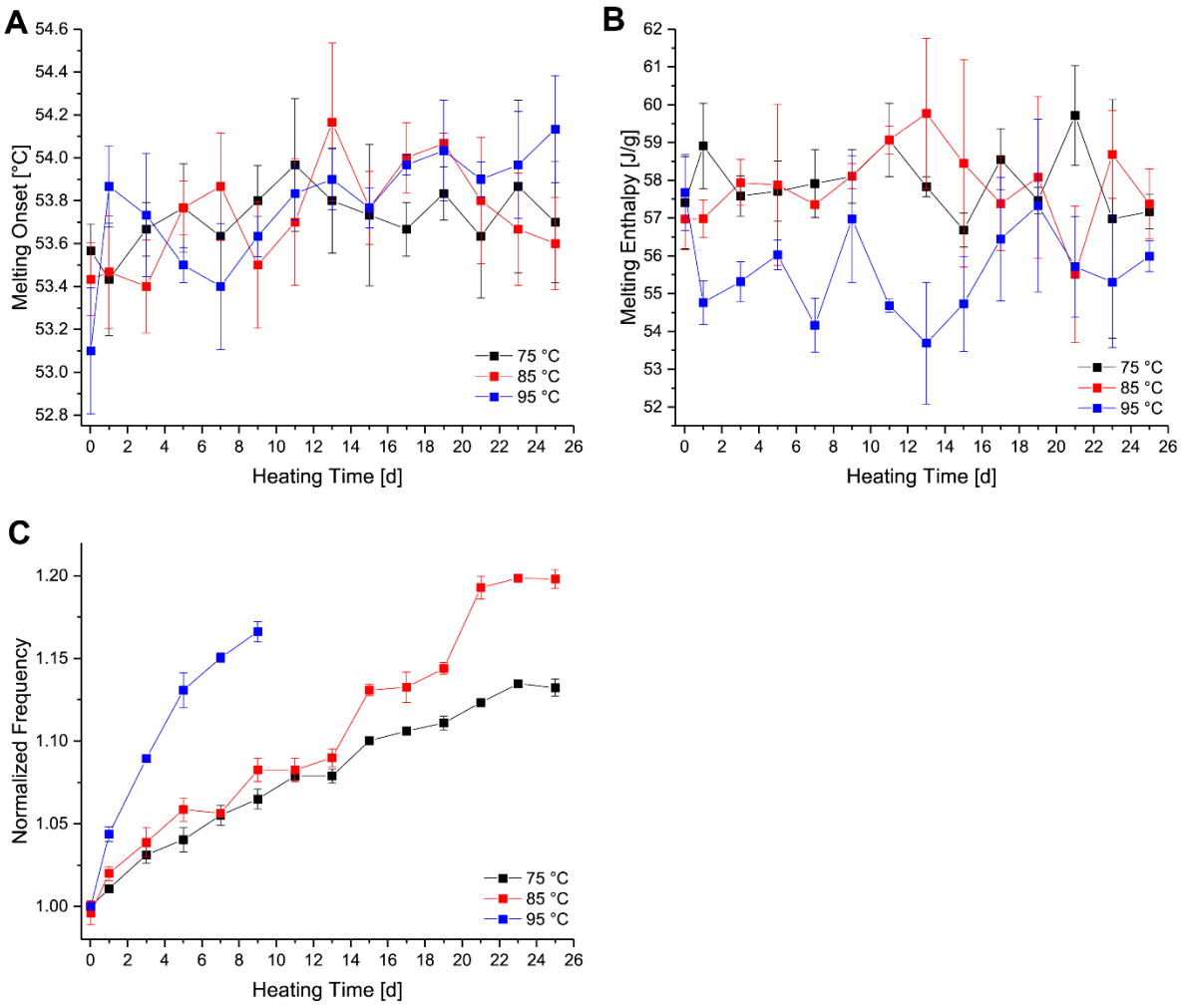

Figure 22. Development of the melting onset (**A**), melting enthalpy (**B**) and the normalized frequency of the crossover point of G' and G'' with heating time at 75 °C (black), 85 °C (red) and 95 °C (blue).

4.4 Discussion

For MEW it is important to understand how chemical changes of the material are influencing the physical properties such as the melting temperature as well as the rheological behavior. To investigate these changes, firstly the chemistry of the thermal degradation of PCL was examined with GPC and GC-MS before translating the findings to its physical and rheological behavior with the help of DSC and rheology measurements.

4.4.1 Determination of chemical changes

For over 25 d of heating, the changes to the M_n weight according to GPC are very small. Additionally, M_n decreases gradually with heating time for all three temperatures. Looking at the polydispersity, information on whether predominantly larger or smaller chains degrade can be gathered. For the samples generated at 85 °C and 95 °C an upward trend with heating time can be observed leading to the conclusion that M_n decreases faster than the weight average molecular weight (M_w). In contrast at 75 °C the development of the polydispersity shows a downward trend with M_w decreasing faster than M_n. The development of the polydispersity also gives insight into the degradation mechanism. According to Yoon *et al.* polydispersity should converge toward 2 if degradation follows a random scission mechanism [184]. Since at 85 °C and 95 °C polydispersity is increasing and approaching the value of 2, at 75 °C polydispersity drops which means that there must be another mechanism contributing. Literature about the thermal degradation shows that PCL can additionally degrade in an unzipping mechanism generating ε-caprolactone in the process. As literature predominantly focuses on the degradation of PCL under pyrolysis conditions, results might be different when investigated under processing conditions as temperatures are lower. Persenaire *et al.* investigated the pyrolysis with the help of TGA coupled MS using a non-isothermal program and found H_2O, CO_2 and hex-6-enoic acid as well as ε-caprolactone [132]. This leads to their conclusion that the reaction is two-fold with a random scission and an unzipping mechanism (**Figure 23**). In contrast Sivalingam *et al.* conducted isothermal degradation experiments at temperatures between 280 °C and 330 °C and could only observe unzipping from the hydroxyl end for PCL bulk [169].

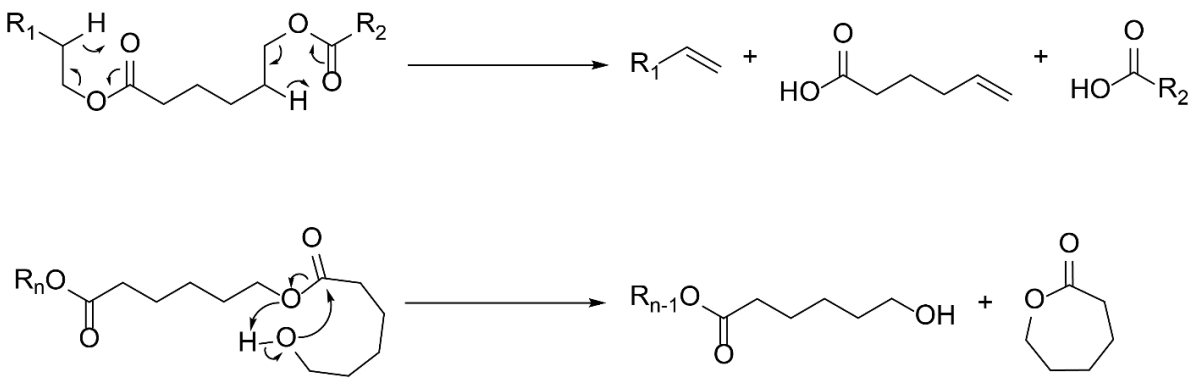

Figure 23. Thermal degradation mechanisms suggested by Sivalingam *et al*. with random scission (upper) and unzipping (lower) mechanism.

Since we used much lower temperatures and since the polydispersity development of the 75 °C samples showed a different behavior compared to the other two temperatures, we decided to investigate the change of the ε-caprolactone content via GC-MS. At 85 °C and 95 °C we could observe an overall increase in monomer content. However, while samples produced at 95 °C experienced a steady growth in caprolactone content, a drop could be seen during the first 3 d for the 85 °C samples followed by a stable regime until day 19 before the content is increasing until day 25. In contrast, 75 °C again shows a different behavior as monomer content decreases steadily with ongoing heating time. These results lead to three conclusions: The first one is the presence of a monomer generating degradation mechanism, which is most likely unzipping, as monomer generation can be observed for the 85 °C and 95 °C samples. Secondly, as the samples produced at 75 °C seem to reincorporate monomer, but the overall molecular weight still decreases according to GPC, there must be a second mechanism with a big effect on molecular weight. This would be most likely a random scission mechanism, even though we could not observe any hex-6-enoic acid generation with the help of GC-MS. But as we were not operating at pyrolysis conditions, it was not likely to degrade the material that severely to observe low molecular degradation products besides ε-caprolactone. The third conclusion which can also be drawn by looking at the data of the 75 °C samples is a reaction that is capable to reincorporate monomer. This probably hints towards some sort of post-polymerization or interchange reaction, which would not only include monomer-polymer- but also polymer-polymer-interaction.

These reactions have already been investigated, especially with polymer blends. In a review of Kotliar in 1981 [185] three different possible mechanisms for polyesters were discussed (**Figure 24**): intermolecular alcoholysis [186], intermolecular acidolysis [187] and transesterification [188]. To test this conclusion, we set up an experiment, where we mixed a low molecular weight PCL carrying a fluorescently active pyrene group with the commercial PCL that we use for our printing experiments. The idea behind it was that if transesterification reactions are happening the low molecular PCL should be fusing with the high molecular PCL. Mixing these two, thermally aging them and then monitoring the samples with a GPC device equipped with a fluorescence detector should show a growing fluorescent signal at retention times where the high molecular weight PCL can be found. This is indeed what we observed in our collected data (**Figure 21C**).

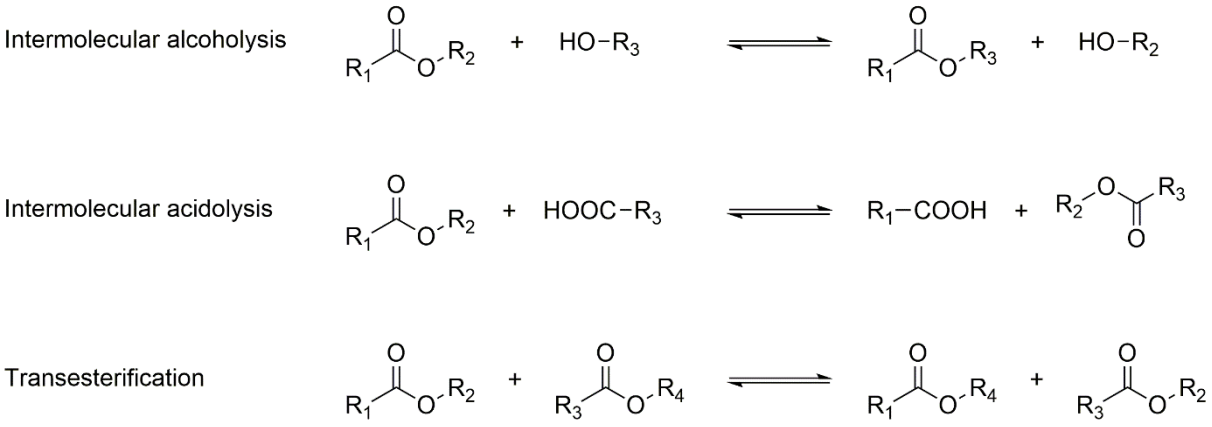

Figure 24. Possible pathways for ester interchange reaction.

We also compared these findings with the mixture of hydroxyl-protected Pyr-PCL (Pyr-PCL_{Ac}) and PCL (PCL_{Ac}). Blocking the alcohol resulted in a reduced growth of pyrene-carrying high molecular PCL. These results suggest that intermolecular alcoholysis is the dominant mechanism for interchange reactions in melt PCL. We neglected intermolecular acidolysis, for once because Flory *et al.* suggested, that these reactions are slow [189], and also because all polymers that we used in this study carried a capped acid group according to the supplier. What we cannot answer unequivocally is the influence of transesterification reactions, since we could not ensure that all alcohol groups were capped. This leaves room for speculation, if a small amount of uncapped alcohol could lead to the rate of increasing fluorescent signal that we saw for the capped reaction partners. We would therefore

suggest that transesterification reactions are happening, but we cannot give any answer on what the ratio between intermolecular alcoholysis and transesterification is.

Overall, it can be said, that PCL is a very durable polymer at processing temperatures due to ester interchange reaction. These reactions have an equilibrizing effect on the average chain length correcting the generation of short chains that might occur due to degradation via a random scission mechanism. Additionally, these reactions make sure that monomer units that have been generated by an unzipping mechanism are reincorporated into the polymer. This slows down the overall degradation via this mechanism or even reverse it partially as can be seen for the samples collected at 75 °C.

4.4.2 Determination of physical changes

To observe the physical changes PCL undergoes under processing conditions, we looked at the melting onset determined by DSC measurements. As shown in **Figure 22A** and **B**, the changes are very small, and no clear trend is visible. According to literature a reduction of the number average molecular weight of PCL to about 87.5 % only leads to a reduction of the melting temperature of 10.7 % [190]. This means, that PCL did not degrade that strongly over the period of 25 d regardless of the chosen temperature to detect any significant changes in its melting behavior, which is in good agreement with its chemical stability discussed above.

Rheology proved to be more sensitive for small changes on a molecular level. The development of the crossover points of G’ and G’’ with heating time allows for an observation of thermal degradation. Since the crossover point represents the frequency at which the melt does no longer follow the oscillating movement of the measuring system by flow but by elastic movement, it can give insights on the average chain length of the tested polymer. If the average polymer chain length decreases, the smaller chains can follow an increasing frequency longer, since the overall viscosity is lower. This means that with ongoing degradation and the average polymer chain length becoming smaller, the frequency of the crossover point increases. This is the behavior that can be seen in **Figure 22C**. It also shows the expected trend for an Arrhenius-type degradation, since the degradation rate increases with increasing temperature. In terms of PCL the viscosity of the melt is not only dependent on the molecular weight of the material but also on plasticizing

effects of the monomer. As could be observed in the GC-MS experiments the monomer content does change with time showing a downward trend for samples produced at 75 °C and an upward trend for 95 °C samples and 85 °C being in between. The release of monomer in the 95 °C samples could increase the rate at which the frequency of the crossover point increases.

4.5 Conclusion

In this work we heated PCL for 25 d at MEW processing temperatures of 75 °C, 85 °C and 95 °C and showed that it is degrading slowly throughout the heating time. The results from GPC, GC-MS and rheology suggest that the mechanism of degradation is two-fold: random chain scission and unzipping from the alcohol end. Even though, PCL is degrading steadily the rate is rather slow, which can be explained by ester interchange reactions, which are able to reintroduce short chains or monomer generated by unzipping. As these mechanisms slow down the degradation process this translates into a very slow change of the thermal properties like the melting onset temperature and the melting enthalpy. Overall, we could show that PCL is material of outstanding thermal stability, if processed at moderate temperatures.

4.6 Materials and Methods

4.6.1 Material

Medical-grade PCL (Corbion Inc., Netherlands, PURASORB PC 12, Lot# 1712002224, 05/2018) was used for all the experiments. According to the supplier, the carboxylic end of the polymer chain is protected via an ester with an aliphatic alcohol. To avoid changes of the material due to degradation, the material was aliquoted into 50 mL Falcon tubes and purged with argon. The aliquots were stored at -80 °C.

4.6.2 Synthesis of Pyr-PCL

The synthesis was performed under argon atmosphere. Tin(II) 2-ethylhexanoate (269 mg, 0.66 mmol, Sigma Aldrich, St. Louis, USA) was added to dry toluene (20 ml, Fisher Scientific, Schwerte, Germany), which was then reduced to 15 mL to azeotropically remove residual water at 130 °C. After addition of 1-Pyrenebutanol (182 mg, 0.66 mmol, Sigma

Aldrich, St. Louis, USA) and ε-caprolactone (1.83 g, 15.9 mmol, Sigma Aldrich, St. Louis, USA), the mixture was stirred for 24 h at 80 °C. The mixture was then dissolved in 5 mL dichloromethane (DCM, Fisher Scientific, Schwerte, Germany), before solvent was removed under vacuum. The residue was dissolved in DCM (3 ml) and precipitated in 150 mL cold methanol (MeOH, Fisher Scientific, Schwerte, Germany). The suspension was centrifuged and after decantation of the supernatant the residue was washed three times with cold MeOH (40 ml), and any residual solvent was removed by applying vacuum. A pale-yellow solid was obtained (1.84 g, 92.2 %), which will be called Pyr-PCL in the following chapters. As it is known that the tin catalyst remains in the product, 1.5 g was dissolved in 30 mL DCM before washing it with 100 mL 1 M HCl. The organic phase was then washed once with 100 mL 0.5 M sodium hydroxide (NaOH) solution and three times with 100 mL of deionized water until the water phase was no longer acidic. The volume of the organic phase was then reduced to 10 mL under vacuum before precipitation in 450 mL cold MeOH. The suspension was transferred into 50 mL falcon tubes and centrifuged for 5 min at 2500 rpm. Then the supernatant was removed, and the residual solid was washed three times with 40 mL cold MeOH, before it was dried under vacuum. A pale-yellow solid was obtained (1.38 g, 92.6 %), which will be called Pyr-PCL_W in the following chapters. For characterization Pyr-PCL_W nuclear magnetic resonance (NMR) spectra were measured using a 300 MHz NMR (Bruker NMR 300 Fourier). The NMR spectrum of Pyr-PCL is shown in **Figure 25**. ^{1}H NMR (300MHz, $CDCl_3$): δ [ppm] = 8.28-7.85 (m, 9H, aromatic protons from pyrene), 4.17-4.13 (t, ^{3}J = 6.51 Hz, 2H, e), 4.08-4.04 (t, ^{3}J = 6.62 Hz, 35H, j), 3.66-3.62 (t, ^{3}J = 6.45 Hz, 2H, o), 3.41-3.36 (t, ^{3}J = 7.46 Hz, 2H, b), 2.33-2.28 (t, ^{3}J = 7.47 Hz, 37H, f/k), 1.99-1.76 (m, 4H, c/d), 1.70-1.54 (m, 80H, g/i/l/n), 1.43-1.33 (m, 39H, h/m).

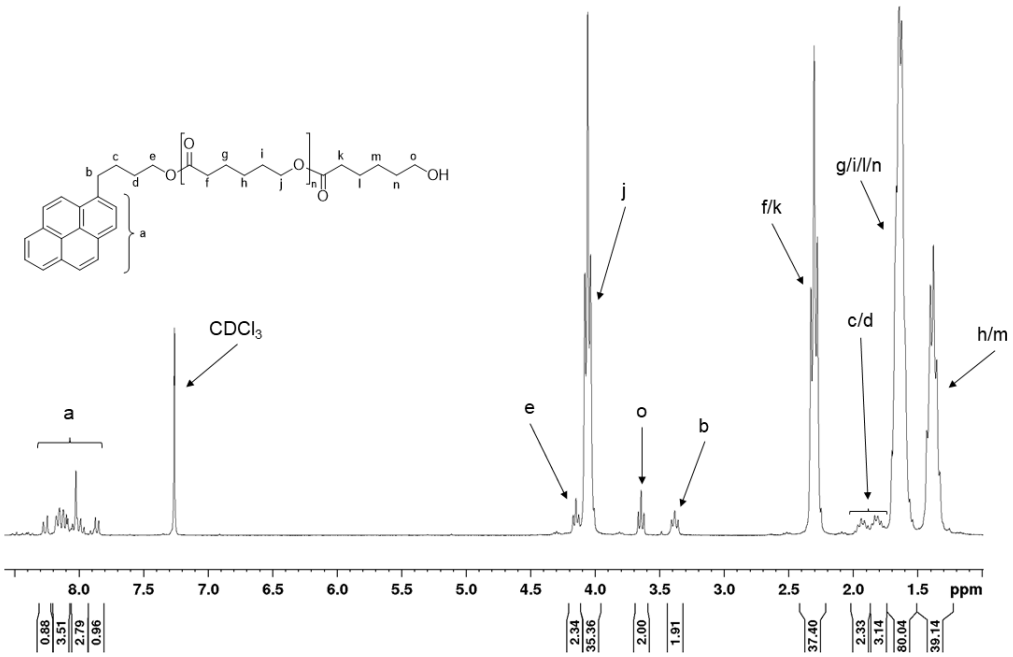

Figure 25. NMR spectrum of Pyr-PCL.

4.6.3 End capping of Pyr-PCL and PCL

Pyr-PCL_W (300.5 mg) was dissolved in 100 mL chloroform and heated to 60 °C. Acetic anhydride (18.9 mL, 200.3 mmol) was added and stirred at 60 °C for 3.5 h. Acetylation of PCL was done similarly to Pyr-PCL: PCL (10 g, PURASORB PC 12, Lot# 1712002224, 05/2018, Corbion Inc., Netherlands) was dissolved in 300 mL chloroform and heated to 60 °C. Acetic anhydride (25.2 mL, 267.1 mmol) was added and stirred at 60 °C for 3.5 h. In the following chapters these will be referred to as Pyr-PCL_{Ac} and PCL_{Ac}.

4.6.4 Inductively coupled plasma mass spectrometry

The Tin content of Pyr-PCL, Pyr-PCL_W and Pyr-PCL_{Ac} was determined by ICP-MS (ThermoFisher Scientific, Waltham, USA). Therefore, samples of this polymers were dissolved in 69 % nitric acid (Carl Roth, Karlsruhe, Germany) overnight. The resulting solutions were then diluted stepwise to 1:10 and 1:100 solutions with MilliQ water and to 1:1000 solutions with 0.69 % nitric acid and measured against standard solutions of different dilutions (10, 1, 0.1, 0.01, and 0.001 mg L^{-1}).

4.6.5 Compounding

For the mixing of a blend of 0.1 wt-% Pyr-PCL_w in PCL as well as 0.1 wt-% Pyr-PCL_{Ac} in PCL_{Ac} a micro compounder (MC5, Xplore Instruments BV, Netherlands) was used. A temperature of 85 °C has been used for blending at 50 rpm for 20 min.

4.6.6 Oven degradation

To artificially age PCL, samples (n=3) were kept at 75, 85 and 95 °C in an oven (Memmert GmbH & Co. KG, Schwabach, Germany) for up to 25 d with samples drawn after 2 h, 1 d and then every second day. These samples were then used to investigate thermal degradation of PCL via GPC, DSC, Rheology and GC-MS. For the investigation of transesterification reaction three samples of Pyr-PCL_w/PCL and Pyr-PCL_{Ac}/PCL_{Ac} were heated at 85 °C using the same time schedule as mentioned above. Until measurements were done all samples were kept under argon atmosphere at -80 °C to avoid any alteration.

4.6.7 Gel permeation chromatography

Samples were dissolved in chloroform (Carl Roth, Karlsruhe, Germany) with a concentration of 5 mg ml^{-1} and mixed for 2 h. The prepared sample were then filtered using a 0.45 µm PTFE filter. For the measurement, a GPC device from Malvern (Herrenberg, Germany) was used with a Viscotek GPCmax (in-line degasser, 2-piston-pump and autosampler) equipped with a column oven (35 °C), RI detector (Viscotek VE3580), a pre-column (Viscotek CGuard) and two columns (2x Viscotek LC4000L, length = 300 mm, width = 8 mm, porous styrene divinylbenzene copolymer, particle size 7 µm). The flow rate was kept at 1.0 mL min^{-1}. PS standards were used for a relative calibration to determine molecular weight values.

4.6.8 Transesterification study using HPLC

Samples were dissolved in chloroform (Carl Roth, Karlsruhe, Germany) with a concentration of 5 mg ml^{-1} and dissolved for 2 h. The prepared samples were then filtered using a 0.45 µm PTFE filter. For the quantification of high molecular weight fluorescence, a GPC System from Shimadzu (Duisburg, Germany) was used with a HPLC Pump (LC-20AT),

autosampler (SIL-20AC), column oven (CTO-20AV, 35°C) and fluorescence detector (RF-20A) together with a pre-column (Viscotek CGuard) and two columns (2x Viscotek LC4000L, length = 300 mm, width = 8 mm, porous styrene divinylbenzene copolymer, particle size 7 µm). The fluorescence detector was operated at an excitation wavelength of λ_{ex} = 325nm and an emission wavelength of λ_{em} = 380nm. Samples of 100 µl volume were injected at a flow rate of 1.0 mL min^{-1}. Extent of transesterification was quantified using the integral of the high molecular peak in front of the signal of the low molecular weight Pyr-PCL with or without the end capping.

4.6.9 Gas chromatography

To measure the residual monomer content of PCL samples aged at 75 °C, 85 °C and 95 °C, GC-MS experiment have been conducted using a GC-MS device from Agilent Technologies (Santa Clara, USA) with a 7820 A GC system equipped with a MS detector (5977B MSD), an autosampler (PAL RSI, CTC Analytics AG, Zwingen, Switzerland), a (5%-phenyl)-methylpolysiloxane column (HP-5ms Ultra inert) and He as carrier gas. Measurements were run in splitless mode at an inlet temperature of 180 °C, a temperature ramp from 40 °C, held for 2 min, to 150 °C with 10 K min^{-1} and a flow rate of 1 mL min^{-1}. For sample preparation 20 mg of the neat polymer as well as the samples described above were dissolved in 2 mL of chloroform for 2 h before being pushed through a 0.45 µm PTFE filter. To calibrate the measurement, six different standards (n=3) in chloroform, which are shown in **Table 3**.

Table 3. Calibration standards for GC-MS measurement.

Standard	Concentration [mg mL^{-1}]
1	0.1
2	0.08
3	0.06
4	0.04
5	0.02
6	0.001

Standards and samples were measured using a temperature ramp from 40 °C to 150 °C with a rate of 10 °C min^{-1} and a helium flow rate of 1.0 mL min^{-1}. The peaks were then integrated using Enhanced ChemStation software (version F.01.03.2357) and the caprolactone content was then calculated with the help of the calibration curve.

4.6.10 Differential scanning calorimetry

Samples of around 15 mg were encapsulated in pierced lid aluminum crucibles (Netzsch, Selb, Germany) and measured using a DSC 204 F1 Phoenix® (Netzsch, Selb, Germany). After heating up to 120 °C at 10 K min^{-1}, a temperature ramp from -50 to 120 °C with a heating rate of 10 K min^{-1} under nitrogen atmosphere has been used. This ramp was repeated two times in total. For evaluation, the onset melting temperature and the melting enthalpy have been determined via Proteus Thermal Analysis (Netzsch, Selb, Germany, version 5.2.1) software.

4.6.11 Rheology

Rheology measurements have been conducted with a MCR702 rheometer (Anton Paar, Graz, Austria). The samples that were generated by oven degradation were loaded at 120 °C using a 25 mm plate-plate-setup with a gap of 0.3 mm. After loading a shear rate of 15 s^{-1} is applied for 1 min to remove any thermal history of the sample. Following that, the temperature is removed without rotation over 6 min to reach the respective temperature of either 75 °C, 85 °C or 95 °C depending on the temperature at which the samples was aged at. This temperature is kept for 3 min before a frequency sweep is conducted within a range of 100 Hz to 0.1 Hz and an amplitude of 1 %.

Chapter 5

PROCESSING OF POLY(LACTIC-*CO*-GLYCOLIC ACID) MICROFIBERS VIA MELT ELECTROWRITING

Chapter 3 has already been published as original research article (Böhm, C., Tandon, B., Hrynevich, A., Teßmar, J. and Dalton, P.D. (2022), Processing of Poly(lactic-co-glycolic acid) Microfibers via Melt Electrowriting*. Macromol. Chem. Phys.*, 223: 2100417.)

It is based on the work of the author of this thesis Christoph Böhm and Dr. Biranche Tandon, who mainly worked on the conceptualization, experiments, data evaluation, and composition of the manuscript.

The author contributions of the related research article are as follows:

Contributor	**Contribution**
Christoph Böhm	Designed and performed experiments; analyzed data; wrote the manuscript
Biranche Tandon	Designed and performed experiments, analyzed data, wrote the manuscript
Andrei Hrynevich	Provided support in establishing the printing process; revised and provided feedback on the manuscript
Jörg Teßmar	Provided support on experiment planning and evaluation; revised and provided feedback on the manuscript
Paul D. Dalton	Provided support on experiment planning and evaluation; revised and provided feedback on the manuscript

5.1 Abstract

Polymers sensitive to thermal degradation include PLGA, which has not yet been processed via MEW. After an initial period of instability where mean fiber diameters increase from 20.56 µm to 27.37 µm in 3.5 h, processing stabilizes through to 24 h. The jet speed, determined using CTS measurements, also reduces slightly in this 3.5 h period from 500 mm min^{-1} to 433 mm min^{-1} but generally remains constant. Acetyl triethyl citrate (ATEC) as an additive decreases the glass transition temperature of PLGA from 49 °C to 4 °C, and the printed ATEC/PLGA fibers exhibits elastomeric behavior upon handling. Fiber bundles tested in cyclic mechanical testing display increased elasticity with increasing ATEC concentration. The processing temperature of PLGA also reduces from 165°C to 143°C with increase in ATEC concentration. This initial window of unstable direct writing seen with neat PLGA could also be impacted through the addition of 10 wt-% ATEC, producing fiber diameters of 14.13±1.69 µm for the first 3.5 h of heating. Our investigation shows that the initial changes to the PLGA printing outcomes seen in the first 3.5 h are temporary and that longer printing times result in a more stable MEW process.

5.2 Introduction

MEW is a technique that allows for deposition of fibers in the lower micrometer range in a very precise manner [191, 192], and PCL is the current gold standard material [168]. With its low melting point and slow degradation, PCL can remain being heated for long periods without measurable degradation [193]. This is essential for a system such as MEW that relies on applying heat to an entire volume of the melt, since an air pressure-type delivery of the molten polymer to the nozzle is important to achieve small diameter fibers [194]. MEW processing requires a low, stable flow rate to the nozzle while filament-type and screw-driven systems, generally deliver higher flow rates that result in large diameter fibers [159]. For example, a screw-driven melt electrospinning system reported 360 µL hr^{-1} as the lowest extrusion flow rate for linear PCL [195], corresponding to 100 µm fiber diameter. This contrasts to a calculated extrusion rate of 1.5-5 µL $hr^{-1}$for 12-25 µm diameter PCL fibers using air pressure [193]. The smallest diameter MEW fibers produced to date are 0.8 µm and are also made from PCL [196].

While polymers have been processed or developed for MEW, thermal degradation or crosslinking limits the library of processable materials [168]. The viscosity of the melt affects the flow rate to the nozzle and the processing of materials can be challenging as MEW currently requires keeping a material in a sustained molten state, which can change the printing behavior in prolonged processing time frames.

There are several materials that have already been successfully processed with MEW [168], many of which are polyesters. These include poly(L-lactide-co-ε-caprolactone) [197] or a 60:40 mixture of PCL and (poly(hydroxymethyl glycolide-co-ε-caprolactone) to promote changes in surface wetting or mechanical properties [81]. Furthermore, 45S5 bioactive glass could be added to a blend of PLA and poly(lactide-block-ethylene glycol-block-lactide) (PLA-PEG-PLA) and successfully processed via MEW [198]. Conversely, crosslinking can occur during heating that affects the process stability. Recently, a system of furan and maleimide functionalized poly(2-ethyl-2-oxazine) that crosslink with the help of Diels-Alder reactions was MEW processed which was later peptide-functionalized to enhance the attachment of cells [109]. There is, however, a limited period of processing due to the two components start to crosslink in the heated reservoir increasing the viscosity until material flow stops.

A potential new polyester to include within the MEW-processable library is PLGA. PLGA is a versatile polymer that has a long clinical history and is mostly used as a drug delivery system [123] or as a scaffold in tissue engineering [199, 200]. The degradation of PLGA is favorable as it undergoes hydrolysis of the ester group in the presence of water to release lactic and glycolic acid over month-long periods. These acids are byproducts of metabolic pathways and can further be metabolized by the Krebs cycle [201], which causes minimal toxicity at sufficiently high scaffold porosities [200, 202]. Additionally, it is possible to tune the degradation time frame by changing the initial molecular weight, the ratio of glycolic and lactic acid and the dimensions of the implantable device [201].

As beneficial as a controlled degradation rate is for drug release and TERM applications, the processability of PLGA with a melt processing technique such as MEW can be challenging. In a comparative study of thermal degradation of PCL, PGA and PLA, Sivalingam *et al.* showed that PLA and PGA decompose at lower temperatures than PCL [134]. At a processing temperature of 165 °C for neat PLGA compared to around 85 °C for PCL, PLGA should degrade faster, which will have an influence on the viscosity of the MEW jet material. This study additionally investigates the inclusion of ATEC (**Figure 26**) as a plasticizer for lowering the T_g and printing temperature of PLGA. The increase in flexibility of PLGA fibers due to addition of ATEC is a direct effect often observed in polymers for various plasticizers [138, 203]. Such plasticizers can reduce the tensile strength and Young's modulus of polymers, as well as increase the elastic recovery [204]. To compare these blends and determine their printing stability, the jet speed was determined, as measured by the CTS.

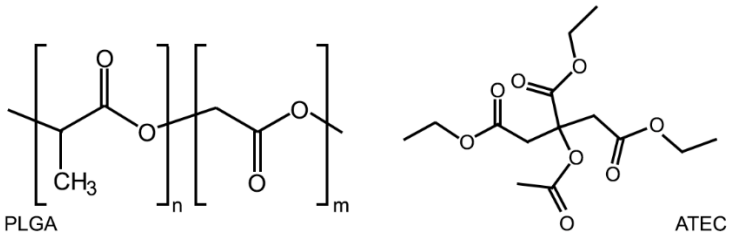

Figure 26. Chemical structure of PLGA and ATEC used in this study.

5.3 Materials and Methods

5.3.1 Material

PLGA with a 1:1 lactic to glycolic acid ratio (Evonik Operations GmbH, Darmstadt, Germany, RESOMER RG 505, Lot# D161000569) and an inherent viscosity of 0.73 dl g^{-1} (25 °C, 0.1 %, $CHCl_3$) was used for all experiments. The material was aliquoted into 50 mL Falcon tubes, purged with argon and stored at -80 °C. The tubes were fully warmed to room temperature prior to opening to prevent condensation of water vapor on the PLGA. ATEC (Sigma-Aldrich, St. Louis, USA) was used as plasticizer as received.

5.3.2 Preparation of the PLGA/ATEC blends

Different ratios of the PLGA/ATEC blends were prepared according to Table 1 by using a 25 wt-% solution of PLGA in dichloromethane (Thermo Fisher Scientific, Waltham, USA) and adding the respective amount of ATEC. The resulting mixture was vigorously stirred for 3 h before drawing films (COATMASTER 510, ERICHSEN GmbH & Co. KG, Hemer, Germany). The films were air dried overnight, cut into pieces, and further dried under vacuum for 3 h. The blends were stored at -80 °C under argon to prevent degradation.

Table 4. Nomenclature used and ratio between PLGA and ATEC for different blends, and the $T_{Syringe}$ and T_{Nozzle} for each formulation.

Blend	PLGA [wt-%]	ATEC [wt-%]	$T_{Syringe}$ [°C]	T_{Nozzle} [°C]
PLGA	100	0	165	144
PLGA10	90	10	157	136
PLGA20	80	20	155	128
PLGA30	70	30	143	118

5.3.3 MEW Printer

A custom-built MEW printer with SiN ceramic heater (Bach RC, Germany) and a brass electrode connected to a HV source (HCP 14-20000, FuG Elektronik GmbH, Schechen, Germany) set to positive polarity was used. Compressed nitrogen was utilized to pressurize the syringe (pressure valve - Aventics, Laatzen, Germany). The nozzle is positioned above an aluminum collector connected to a second HV source with a negative polarity. The x-y linear axis (Bosch Rexroth AG, Schweinfurt, Germany) of the collector was controlled via G-code run by IndraMotion MTX (Bosch Rexroth AG, Schweinfurt, Germany). To control the ambient conditions of temperature and humidity, the MEW device was enclosed into an airtight casing connected to a climate chamber (DM340 C AC, ATT Umweltsimulation GmbH, Ofterdingen, Germany).

5.3.4 Preparation and pre-treatment

The 0 h timepoint was neat, untreated PLGA. MEW was performed using a 3 mL syringe (FORTUNA OPTIMA Luer Lock, Poulten & Graf GmbH, Wertheim, Germany) with a nozzle (25-G, length 7 mm; Carl Roth GmbH & Co. KG, Germany). The syringe was loaded with different quantities of the material depending on the experiment and purged with nitrogen for 15 min using a pressure of 0.3 bar before placing it inside the head preheated at the respective temperature. The first print was performed after 1 h of heating.

5.3.5 Collector configuration

All printing experiments were performed with a G-code designed to automatically print fiber arrays at all the heating times. The fibers were direct-written onto microscope slides (76x26x1 mm, VWR, Radnor, Pennsylvania, USA) and each slide has three areas. The first is the stabilization region, where the jet was stabilized by printing straight fibers for 8 mins. Following this, the second area has a total of 26x4-line fiber arrays with increasing collector speeds of 100 mm min^{-1} for each array from the initial 100 mm min^{-1} value. Finally, there is a second stabilization region, where adjustments such as processing temperature and applied pressure are made for the next slide. A schematic of the slide layout is shown in **Figure 27**.

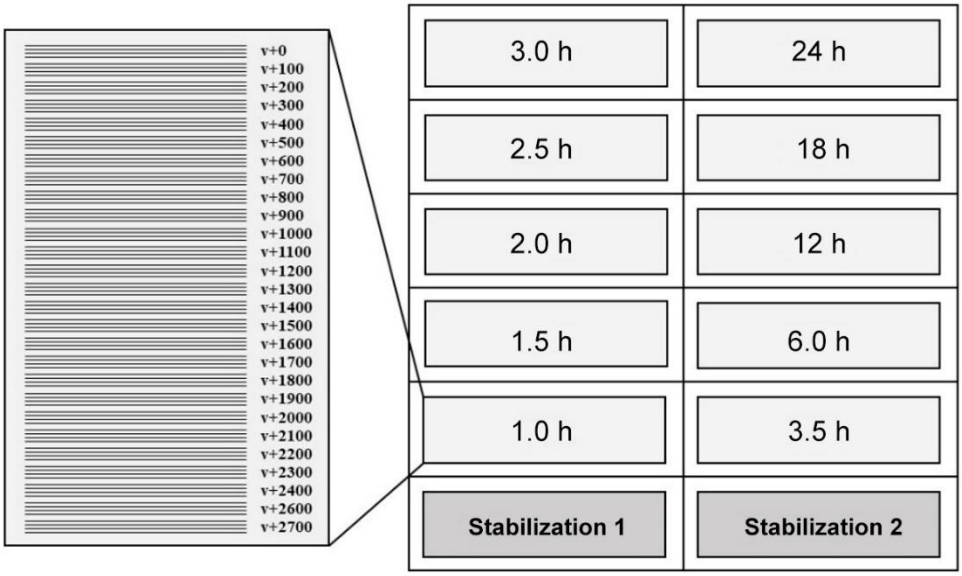

Figure 27. Calculating the CTS. The tool path used to determine the CTS and fiber diameter with heating time of PLGA, PLGA10, PLGA20 and PLGA30 shown. The left-hand slide shows how the sets of four lines of fibers are printed. At low speeds, the fibers will be coiled towards sinusoidal before becoming straight with increasing collector speed. When the MEW fibers are all straight, this determines the CTS at that heating timepoint.

5.3.6 Identifying the minimal printing temperature

The minimal printing temperature for the syringe ($T_{Syringe}$) and the nozzle (T_{Nozzle}) of different blends were determined. Two separate temperature sweeps were used for $T_{Syringe}$ and T_{Nozzle} using the G-code shown in Appendix where a heating rate of 5 K per slide was followed by 2 K per slide to narrow on these values. The fiber diameter consistency was determined by stereomicroscopy (Discovery V.20, Carl Zeiss AG, Oberkochen, Germany) and repeated until the printing speed was reliable after 1 h heating. The resulting $T_{Syringe}$ and T_{Nozzle} for each blend are shown in **Table 4**.

5.3.7 Critical translation speed and fiber diameter

For jet speed determination using CTS, the same collector setup as described above was used and temperatures set according to **Table 4**. A collector distance of 3.5 mm, nozzle protrusion of 0.5 mm, a voltage of 5.0 kV (head) and -0.5 kV (collector) were used. The climate chamber for the MEW printer was set to maintain a constant ambient temperature

of 20 °C and relative humidity of 40 %. Samples were produced after 1, 1.5, 2, 2.5, 3, 3.5, 6, 12, 18 and 24 h of heating to investigate the influence of prolonged high temperature exposure. Diameter determination was done using SEM (Crossbeam 340 SEM, Carl Zeiss Microscopy GmbH) after sputtering the samples with a 3 nm layer of platinum using a sputter coater (Leica EM ACE600, Wetzlar, Germany). The fiber diameters were determined for arrays printed at CTS and for a collector speed that was above CTS for the first 6 h of heating (v_{fix}). The second speed was chosen to simulate the usual approach to scaffold printing with a constant collector speed above CTS. A total of eight images per speed were used and this procedure was repeated three times.

5.3.8 Mechanical properties of fibers

Bundles of 30 fibers were printed for each material, detached from the glass slide collector, and affixed to a cardboard frame with a gap of 4 mm (effective length) using a double-sided tape. Cyclic and tensile testing was performed using Bose ElectroForce 5500 (TA Instruments, New Castle, USA). The sample was attached to the tensile grips of the mechanical testing equipment and the edges of the cardboard frame were cut before initiating the tests. A strain rate of 0.05 mm min^{-1} was used for tensile tests. For cyclic testing, the samples were pre-loaded to 50 % strain at 0.05 mm min^{-1} followed by a half sine wave with a 1 mm amplitude (total 75% strain) and 1 Hz frequency. The sample was held at this position (50 % strain) for 30 seconds to allow elastic recovery of fibers and the cycle was repeated 10 times (**Figure 28**). A total of nine samples (three samples for three different batches each) were tested for each blend. PLGA30 could not be used to provide data as sample handling was difficult, and it was not possible to lift fibers from the collector without damaging them. Young's modulus was calculated as the ratio of stress to strain% in the initial onset regions of the data obtained.

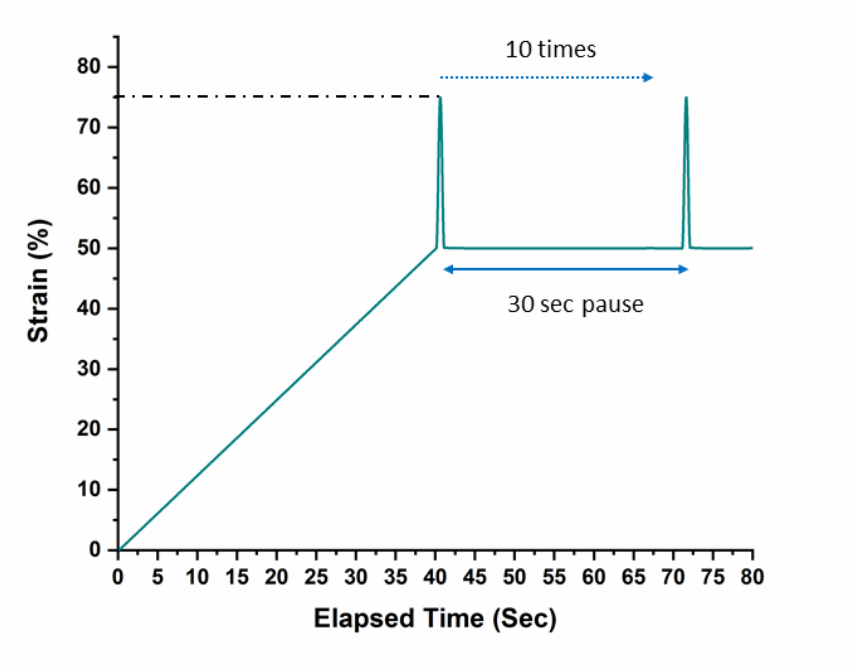

Figure 28. Depiction of the cyclic mechanical testing sequence. Initially, the samples were loaded to 50 % strain at the rate of 0.05 mm min^{-1}. Following this, a half sine wave with 1 mm amplitude was applied (strain 75 %). A 30 s pause was included after the cycle to observe fiber recovery. This whole regime was repeated 10 times.

5.3.9 Videography

All videos were recorded using a Nikon Z6 digital camera with Nikon ED 200 mm lens while editing and compilation was performed in the software Blackmagic Resolve 16 (Blackmagic Design, USA).

5.3.10 Sample preparation for gel permeation chromatography and differential scanning calorimetry

A setup similar to the aforementioned collector configuration was used. Instead of glass slides, glass vials were used to collect samples and the heating times before sample collection were kept the same. To keep the collection time at a minimum, a 21 G nozzle (length 7 mm; Carl Roth GmbH & Co. KG, Germany) was utilized and the syringe was filled with material to the 0.6 mL mark. To extrude the material, a pressure of 3.0 bar was applied. As the height of the glass containers was 45 cm, the head-to-collector distance was set to 60 mm and a total voltage of 6.0 kV (3.0 kV for head and -3.0 kV for collector) was applied

to accelerate the collection of the viscous melt. Three samples were drawn for each material at every heating time point and the resulting samples were stored under argon at -80 °C before further analysis.

5.3.11 Gel permeation chromatography

All samples (n=3) were dissolved in chloroform (Carl Roth, Karlsruhe, Germany) at a concentration of 5 mg ml^{-1} and mixed for 2 h. The resulting solutions were then filtered through a 0.45 µm PTFE filter. The measurement was carried out using a GPC device from Malvern (Herrenberg, Germany) with a Viscotek GPCmax (in-line degasser, 2-piston-pump and autosampler) equipped with a column oven (35 °C), RI detector (Viscotek VE3580), a pre-column (Viscotek CGuard) and two columns (2x Viscotek LC4000L, length = 300 mm, width = 8 mm, porous styrene divinylbenzene copolymer, particle size 7 µm). A flow rate of 1.0 mL min^{-1} was kept throughout the measurement. To determine the M_n of the samples, PS standards were used.

5.3.12 Differential scanning calorimetry

To determine the T_g of the blends, around 10 mg per sample were encapsulated inside a pierced lid aluminum crucible (Netzsch, Selb, Germany) and measured with a DSC 204 F1 Phoenix® (Netzsch, Selb, Germany). The sample was heated to 120 °C and cooled to -50 °C with 10 K min^{-1} to eliminate any thermal history. After that, another heating cycle from -50 °C to 120 °C and cooling from 120 °C to -50 °C with 10 K min^{-1} was measured. Samples of the neat material and all the blends were collected after 1 h, 2 h, 3 h, 6 h, 12 h and 24 h and measured (n=3). To determine T_g, the data was evaluated using Proteus Thermal Analysis (Netzsch, Selb, Germany, version 5.2.1) software.

5.4 Results & Discussion

5.4.1 General Jet behavior

The addition of plasticizer significantly lowered the glass transition temperature of PLGA which could impact the jet behavior. For PLGA and PLGA10, the jet solidifies before landing, fails to attach to the collector surface and gets attracted towards the MEW head.

However, this effect is reduced in PLGA20 and not observed for PLGA30 (**Supporting Video 1** in Appendix).

MEW of neat PLGA

MEW processing of PLGA results in fibers with visually smooth surfaces and a diameter that ranges between 20.56 to 27.37 µm. A minimum temperature of 144 °C (T_{Nozzle}) and 165 °C ($T_{Syringe}$) was required to process the neat polymer. In what may initially appear as an unstable process, the fiber diameter of PLGA at the CTS becomes consistent after 3.5 h of heating. This unstable processing period sees an increase in diameter of 33 % while the CTS did not change substantially. This initial effect on the fiber diameter was also recently observed for PCL, albeit over a longer period of 5 d before stabilization for the following 25 d of heating [193].

The most common approach to MEW, however, is to use collector speeds that are substantially higher than the CTS – typically 1.10 to 1.5xCTS – so that straight lines are direct-written. **Figure 29A** shows smooth, well-formed fibers of neat PLGA printed above the CTS which generally have a smaller diameter. This has previously been shown for PCL, and it is important to note for researchers who aim to direct-write non-linear fibers, i.e., sinusoidal morphologies for auxetic properties. The CTS data of PLGA is shown in **Figure 29B** with a zoomed-in graph shown in **C**. To present results that reflect the unstable and the stable printing period, the heating time was divided into two sections: up to and including the initial 3.5 h of heating and everything thereafter. Notably, the CTS for PLGA is relatively stable during this period. The cause of this CTS stability but increase in fiber diameter is not fully elucidated. A similar behavior was observed for PCL in a different study [193]. Since the MEW process operates in a balance of many instrument parameters, changes in the properties of the processed polymer are likely to have a visible effect on the outcome.

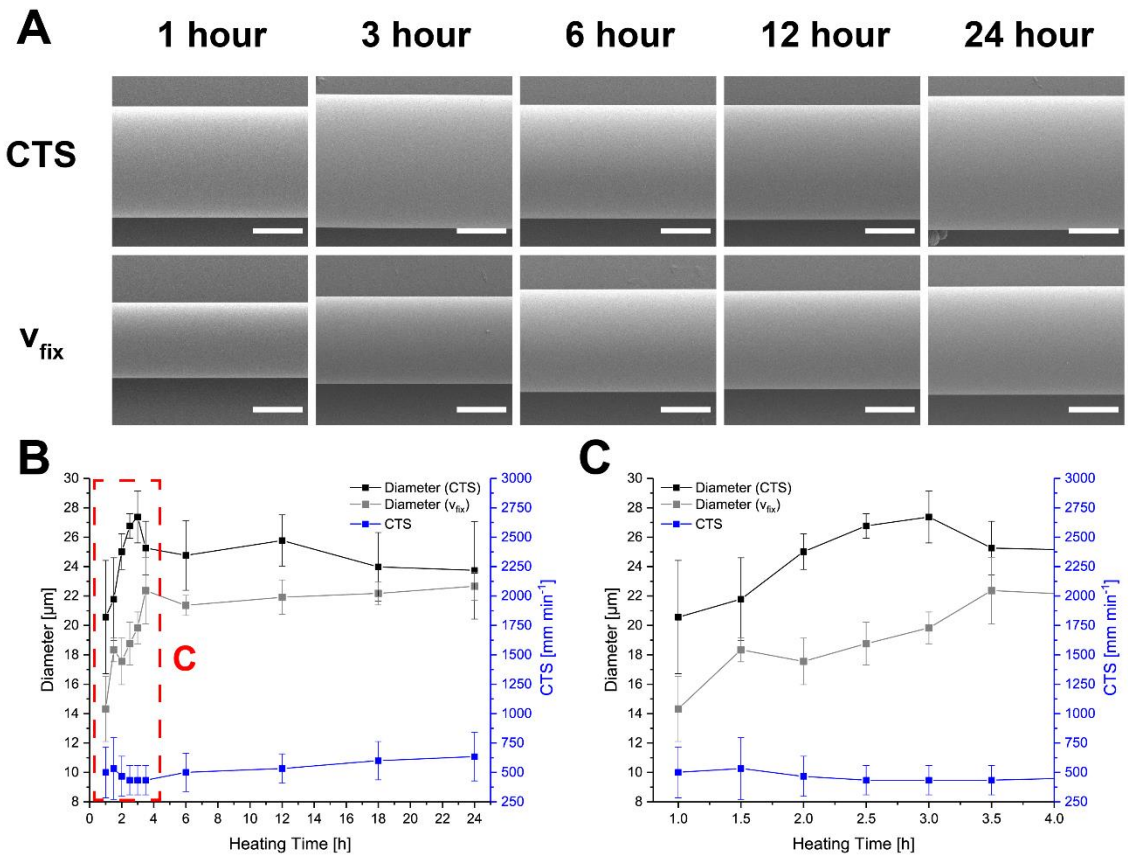

Figure 29. MEW of neat PLGA. SEM images of fibers printed at different time-points at CTS and v_{fix} (**A**), diameter and CTS development over time (**B**) and zoomed in version of the graph for first 3.5 h (**C**). It was observed that after 3.5 h of printing, PLGA stabilizes as a process.

5.4.2 Fiber morphology

A smooth fiber morphology was observed for all polymer blends and was unaltered with heating time. Due to a 2600 mm min^{-1} collector speed limit for the testing routine, only the first 3 h for CTS and V_{fix} of PLGA30 are shown. The fibers degraded in quality with time (**Figure 30A** and **B)** and CTS exceeded the speed limit of the test after 6 h (**Figure 31A** and **B**). The PLGA30 fibers are no longer round, but merged with the glass slide, likely caused by the reduced T_g of 4 °C affecting the speed at which a solid fiber is formed. Fibers produced at v_{fix} from PLGA20 (**Figure 30C**) and PLGA10 (**Figure 30D**) also have smooth surfaces and did not appear to flatten.

5.4.3 CTS and fiber diameter

The CTS data and fiber diameters of PLGA and its blends are shown in **Figure 31**. During the first 3.5 h, the CTS of PLGA10 is very stable. To better visualize the stability, the change in CTS with time is calculated by applying a linear fit to the graph (**Figure 31A**) determining its slope. The results of this operation are shown in **Figure 30E**. PLGA shows a ΔCTS of -31.6±10.8 mm min^{-1} h^{-1} and PLGA10 of -8.3±14.6 mm min^{-1} h^{-1}. In comparison, the CTS of PLGA20 and PLGA30 printing increases with a rate of 90.4±16.9 mm min^{-1} h^{-1} and 241.1±44.3 mm min^{-1} h^{-1}. Beyond 3.5 h, the CTS increases for all blends with PLGA10 being the slowest. In contrast, the change in CTS rate for PLGA remained similar throughout the print with only a gradual increase despite an increase in fiber diameter.

Two different speeds, CTS and v_{fix} were used for diameter determination. In the first 3.5 h of heating, all blends show an increase in the fiber diameter (**Figure 31C**-**F**). For times of 6 h and longer, the diameter was almost stable for PLGA, PLGA10 and PLGA20 showing a small decreasing trend. For PLGA30, no data could be collected beyond 6 h as the CTS was already too high to collect straight fibers. An overview of the mean fiber diameters at CTS and v_{fix} are shown in **Table 5**. Similar to the slope of the CTS progression a slope for the diameter progression was calculated for CTS and v_{fix}. The results are shown in **Figure 30F**. While the rate at which the diameter of fibers produced at CTS was stable for PLGA and all blends, the rate at which the diameter of fibers produced at v_{fix} is different for PLGA and its blends and can be arranged in the following order: PLGA10 (0.98±0.26 µm h^{-1}) < PLGA (1.66±0.62 µm h^{-1}) < PLGA20 (2.85±0.51 µm h^{-1}) < PLGA30 (3.53±0.28 µm h^{-1})).

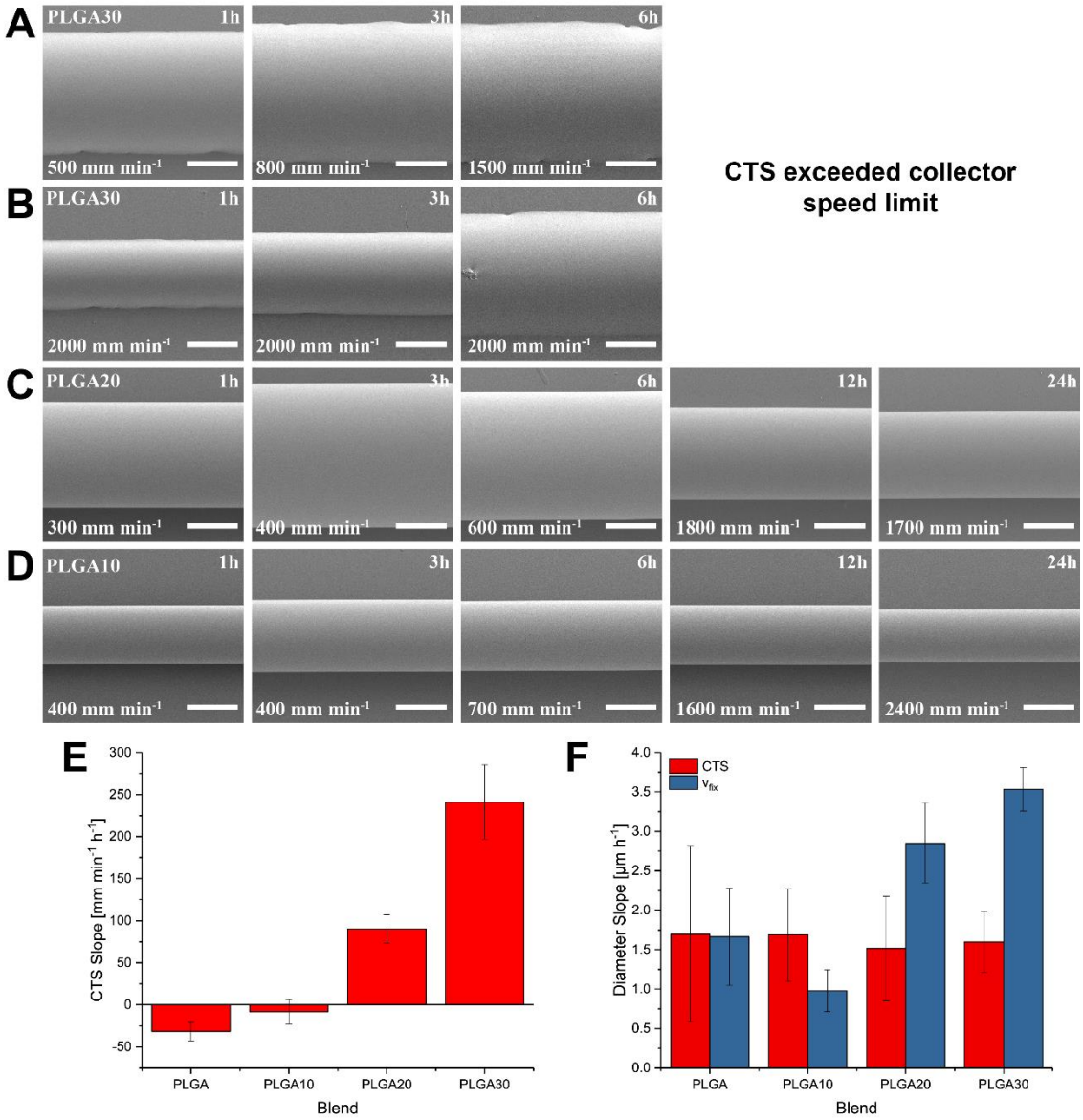

Figure 30. SEM images of fibers showing changes in diameter for PLGA30 at CTS (**A**) and v_{fix} (**B**) as well as for PLGA20 and PLGA10 at CTS (**C** and **D**). Δ CTS 0 to 3.5 h (**E**) and Δ diameter at CTS and v_{fix} (**F**) during the first 3.5 h of heating.

Table 5. Mean fiber diameter values obtained for PLGA/ATEC blends at different collector speeds. Values for the initial 3.5 h of printing are compared with the rest of the printing time.

	initial 3.5 h		from 6 h to 24 h	
Material	**Fiber diameter (CTS) [µm]**	**Fiber diameter (v_{fix}) [µm]**	**Fiber diameter (CTS) [µm]**	**Fiber diameter (v_{fix}) [µm]**
PLGA	24.28±3.35	18.63±3.09	24.45±2.67	22.03±1.03
PLGA10	16.15±2.96	14.13±1.69	13.60±1.68	14.94±0.62
PLGA20	20.99±6.92	15.85±4.44	18.79±5.55	26.92±2.97
PLGA30	25.81±2.37	18.13±4.12	25.79±3.11	25.63±0.58

The addition of plasticizer reduced the minimum processing temperature of the material from 165 °C (PLGA) to 157 °C (PLGA10), 155 °C (PLGA20) and 143 °C (PLGA30) (**Table 4**). In terms of printing performance both PLGA and PLGA10 showed a negative trend in CTS progression during the first 3.5 h of printing, while CTS of PLGA20 and PLGA30 was increasing. Especially PLGA30 showed a higher rate of change in CTS, which could be explained by the GPC as PLGA30 indeed degraded at a higher rate compared to the other blends. This leads to the conclusion that the plasticizer lowers the processing temperature preventing the initial fast degradation, but also seems to accelerate the degradation rate over the prolonged time period. This could be attributed to water being introduced by the plasticizer which is then causing ester hydrolysis. This makes PLGA30 to be the worst polymer candidate of the group for use in MEW fabrication as these changes in CTS are not manageable.

Even though PLGA and PLGA10 showed relatively low, and PLGA20 a manageable rate of increasing CTS, another important parameter is the fiber diameter at v_{fix}. Measuring the fiber diameter at a constant collector speed is a good indication of changes within the material. As can be seen in **Figure 30F**, the change in diameter with heating time is lowest for PLGA10 followed by PLGA. PLGA20 and PLGA30 both show quite high rates, which is not desired for regular scaffolds to be generated via MEW.

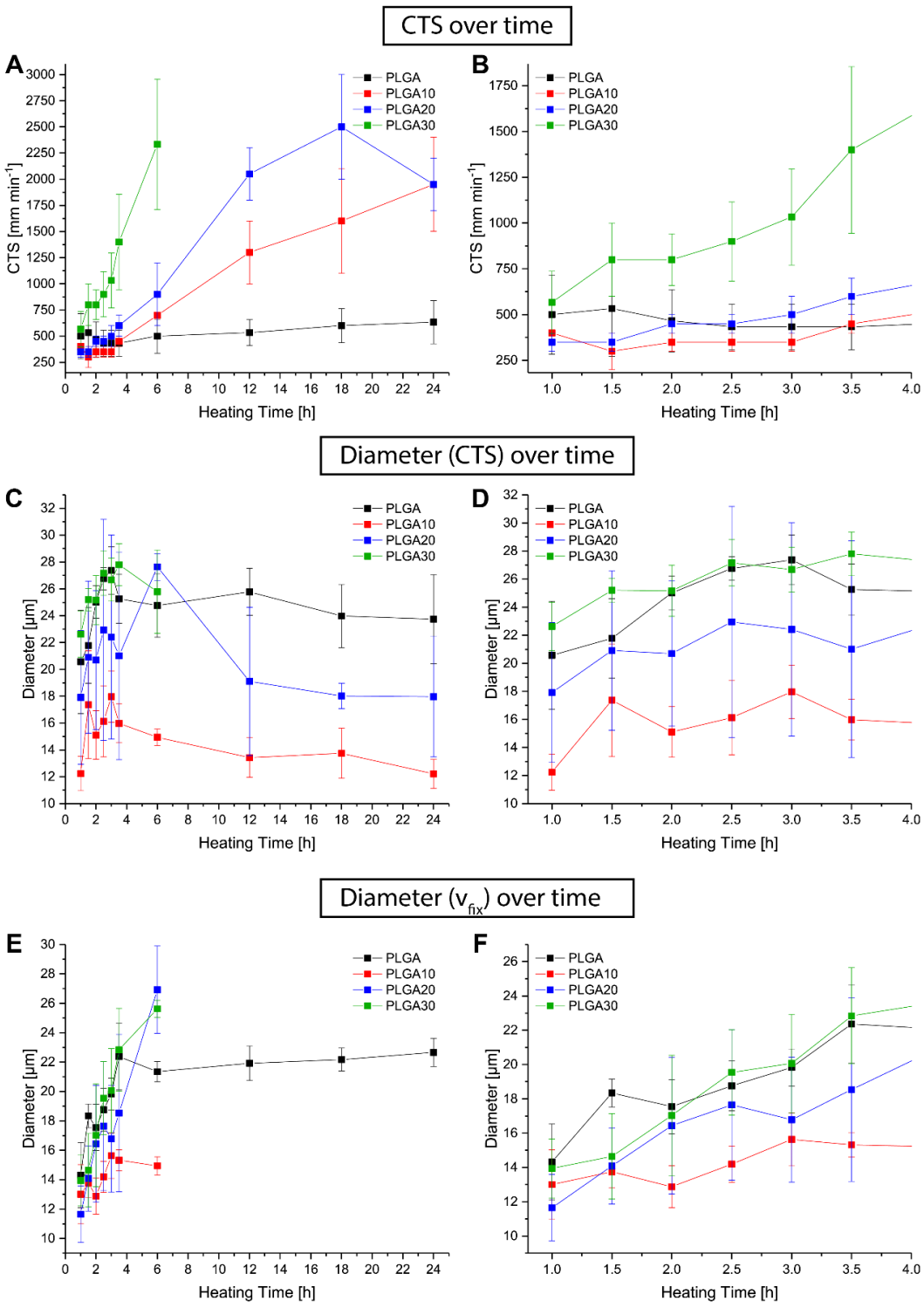

Figure 31. Development of the CTS of PLGA, PLGA10, PLGA20 and PLGA30 (**A**) and a zoomed-in view on the first 3.5 h (**B**); development of the diameter at CTS (**C**) and a zoomed-in view on the first 4 h (**D**) and at v_{fix} (**E**) and a zoomed-in view on the first 3.5 h (**F**).

5.4.4 Mechanical properties

Mechanical properties of the melt electrowritten fibers were assessed to study the influence of ATEC addition to PLGA. The plasticizer softened the polymeric fibers as evidenced by the Young's Modulus. PLGA fibers had the largest value of 9.13±1.49 MPa with PLGA10 and PLGA20 showing values of 7.01±2.35 MPa and 0.72±0.49 MPa (**Figure 32A**), respectively. The samples did not fail/break for strain up to 275 %. The strain recovery of samples was recorded (**Supporting Video 2** in Appendix). It was observed that PLGA underwent a plastic deformation, while PLGA10 showed some signs of partial recovery and PLGA20 showed complete recovery in ~12 s (**Figure 32B** and **C**).

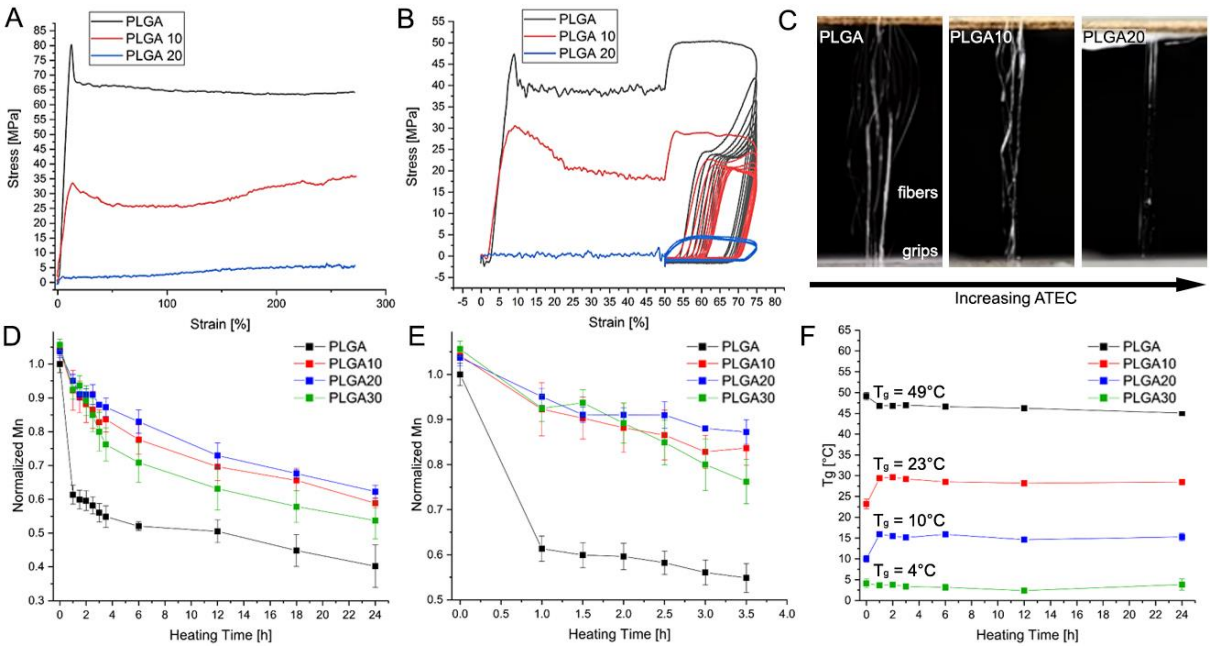

Figure 32. Stress-strain graphs for tensile tests (A) and cyclic tests (B) of fiber bundles (C). Development of the M_n over 24 h (D) and a zoomed-in view on the first 3.5 h (E); development of T_g (F).

5.4.5 Gel Permeation Chromatography

GPC measurements determined the M_n changes of the different PLGA blends with heating time. The normalized data allowed better comparability between the different PLGA blends (**Figure 32D)**. To provide further details, **Figure 32E** shows a zoomed in graph for first 3.5 h. The most outstanding information is the development of the M_n of PLGA as it reduces within the first hour of heating to around 61 % of the initial M_n. This initial reduction was not observed with the PLGA/ATEC blends.

5.4.6 Differential Scanning Calorimetry

The addition of ATEC influences the T_g of PLGA therefore DSC measurements were performed to determine the magnitude and whether this changed with time (**Figure 32F**). With increasing ATEC content, the T_g reduced from 49 °C (PLGA) to 4 °C (PLGA30) and then did not substantially change for the 24 h period. The T_g was found to change after the first hour of heating for PLGA, PLGA10 and PLGA20, reflecting the changes observed for M_n. Thermal hysteresis, also called thermal memory, could be excluded, since the data was collected from the second cycle of the DSC measurement.

5.4.7 Printing Interpretation

PLGA could be successfully processed into fibers using MEW, and the stability of the diameter changed primarily in the first 3.5 h of printing. The CTS for PLGA is remarkably stable from beyond 3.5 h of printing (**Figure 31A**). A possible explanation to this initial period could be given by the GPC data which showed a rapid loss in M_n in the first hour, before it reached a stable regime out to 24 h. To minimize this initial degradation, the processing temperature was lowered by preparing PLGA/ATEC blends [205, 206]. In terms of fiber morphology, there were minor differences between PLGA and its blends, except for PLGA30 where the fibers flattened with increasing processing time (**Figure 30A** and **B**). This could be explained by the low T_g of PLGA30 together with the heat that radiates from the printhead.

5.5 Conclusion

This study reports the first printing study for the MEW of PLGA, and we observed thermal degradation within the initial processing window. After this period, the process was stable out to 24 h. A reduction of the processing temperature was achieved by the addition of the plasticizer, ATEC, and PLGA10 could be reliably printed in this initial 3.5 h period. Printing above the v_{fix} reduced fiber diameter variability, while the addition of ATEC resulted in an elastomeric behavior of the fibers, investigated further with cyclic mechanical testing. ATEC did not substantially reduce the processing temperature, however, without significant addition of the plasticizer. It is especially recommended that future

MEW studies investigate thermal degradation behavior out to much longer times than several hours, as the initial variations in printing stability may be short-lived.

5.6 Supporting Information

Supporting Information is available in the appendix of this thesis.

Chapter 6

CONCLUDING DISCUSSION AND OUTLOOK

This doctoral thesis addressed the thermal stability of PCL and PLGA during MEW processing. This knowledge is important since thermal degradation will change the molecular structure of these polymers, which will have an influence on printing stability and final product properties.

PCL shows a remarkable level of stability over multiple weeks of printing, despite it being a thermally degradable polymer. Especially at the lowest processing temperature used (75 °C) no major changes could be observed in CTS and fiber diameter during this period. Such stability could be linked to the slow thermal degradation of PCL investigated via GPC, rheology, and GC-MS. This investigation showed that PCL is degrading with a random scission mechanism as well as an unzipping mechanism under printing conditions. The rate of the degradation was rather slow as could be shown by GPC. A possible explanation could be transesterification reactions, which were observed throughout the heating duration. This reaction not only introduces an equilibrium of the average chain length, but also reintroduces monomer generated by unzipping degradation. These mechanisms are responsible for the extended integrity of PCL while under thermal stress. Besides the long-term stability a drop in CTS could be observed during the first 5 d of heating for all three temperatures. As this behavior could not be observed in any chemical analysis, the assumption was made that this phenomenon was caused by an inhomogeneous melt. During the first 5 d of heating the polymer pellets provided in a syringe need to be heated up and molten. While melting of the material seems to be complete after 30 min for an observer judged by eye, the melt is not yet in a homogeneous and thoroughly mixed state. A possible explanation could be that polymer entanglement is not homogeneous throughout the melt as the individual pellets first need to mix with each other. As the PCL melt is rather viscous at the processing temperatures this process could be very slow. As a homogeneous entanglement of the polymer chains would slowly form, the viscosity would change during this process, which would ultimately change jet speed and fiber diameter. Even though the viscosity can be tracked with the help of a rheometer, such behavior could not be observed. This can be explained by the procedure that is applied when measuring polymer melts, as the first step is always to erase the thermal memory of a material and achieve thermal equilibrium before starting the measurement. According to the findings of this thesis it took 5 d of heating to fully achieve a thermal equilibrium of the PCL melt without external manipulation.

The second polymer that was investigated for this thesis was PLGA. As it has not been processed via MEW before, many of the fundamentals needed establishing. It is substantially more degradable than PCL and since degradation needs to be minimized during processing the first step was to find the minimal temperature for the stable printing of PLGA. Since thermal degradation is a continuous process that also progresses during the heating time before printing, the minimum temperature was chosen so that a stable jet would be formed after 1 h of heating.

After scanning through different temperatures with the definition mentioned above, a temperature of 165 °C was sufficient to repeatedly fulfil this criterion. Even though the process looked quite stable according to development of the CTS and fiber diameter, GPC revealed that during the first hour of heating the polymer chains almost degraded to half of their initial length before degradation slowed down significantly. To counteract against this premature degradation the attempt was made to reduce the processing temperature of PLGA by addition of up to 30 wt-% of the plasticizer ATEC. This could indeed reduce the processing temperature by up to 13 % for the 30 wt-% blend. But even though the reduction was successful, and the degradation was slower, confirmed by GPC, it could now be observed that CTS and fiber diameter would constantly change during the 24-hour test duration. These changes limit the printing window of the material as a changing CTS eventually will result in sinusoidal structures.

Even though a greater effect was expected in lowering the processing temperature, the addition of plasticizer resulted in interesting properties of the material. With increasing ATEC content the mechanical behavior of PLGA changed towards more elastic behavior and it showed self-healing properties as ripped material could be fused back together applying body temperature. The elastic behavior could be explained by ester interchange reactions between PLGA and the multi-functional ATEC to yield a polymer with loosely crosslinked chains. These properties make it an interesting material for TERM purposes as it is biocompatible and bioresorbable. To further solve the issue of a fast-degrading polymer the most promising approach would be to design a print head that allows to process filaments like a FDM machine. This would drastically decrease the time the polymer is kept in a heated state and therefore decreases the overall degradation.

In comparison PCL and PLGA show big differences in their printing performance. While PCL can be printed at processing temperatures (75 °C, 85 °C and 95 °C) for weeks with only minor changes, PLGA already shows major alterations of CTS and fiber diameter after 24 h. This can especially be observed when looking at the blends with ATEC and their development of the diameter of fibers produced at v_{fix}. This demonstrates why PCL is still the gold standard of MEW: It can be easily processed due to its semicrystalline nature with very small changes to its printing properties due to thermal treatment. PLGA on the other hand is degrading quickly making it difficult to process. Despite this, a processing window of 6 h could be established which makes it usable for small batch scaffold production.

There are several topics for future studies to move MEW forward. For once, investigation of the fundamental working principles of MEW are necessary to gain full control over the process. Therefore, more insights into the physics of electrostatically driven polymer melt jets need to be achieved. A good starting point would be an investigation on how much surface charge is introduced on a polymer jet depending on the voltage and the used material as this is most likely influenced by the chemistry of the material. Another important topic is the improvement of the MEW device itself. As most of the materials that are relevant for TERM applications are degradable, a heating system more similar FDM devices would be beneficially. This would greatly lower the time at which the material needs to be heated, which would be a great improvement over the current reservoir system.

Additionally, a MEW device could be developed placed inside a cooled chamber that is capable of applying temperatures below the freezing temperature of water. This would enable processing viscous protein solutions by electrostatically generating a water/protein jet that solidifies and keeps its fiber shape due to freezing. The produced constructs could then be freeze-dried and eventually crosslinked to obtain scaffolds based on pure proteins.

In conclusion, MEW is still a relatively new fiber-based AM technique that allows to fabricate scaffolds that can be used in TERM applications. Since the scale of its fibers is in the lower micrometer range, MEW fills a gap between SES, which produces fibers in the nanometer range and FDM with fibers with diameters around 0.2 mm. Even though, MEW shares similarities with SES and FDM, its setup is much more complicated as it is required to heat the material with an electrical heater and at the same time apply a high voltage.

Additionally, due to the plethora of variables of this system, such as temperature, voltage, head-to-collector distance, and the material itself to name a few, a lot of know-how is necessary to properly set up a MEW machine.

Chapter 7

SUMMARY / ZUSAMMENFASSUNG

7.1 Summary

The **focus of this thesis** was to investigate how different materials react to the heat exposure that comes with the MEW process over a defined timespan. For this the gold standard PCL, a slow-degrading, and PLGA, a fast-degrading polymer, has been used.

An assessment of the thermal stability of PCL during the MEW process over a timeframe of 25 d has been shown in **Chapter 3**. To guarantee reproducibility, an automated collection of fibers has been used to determine the CTS on each day of heating for three different temperatures: 75 °C, 85 °C and 95 °C. As the CTS is dependent on the physical properties of the material at the respective temperature, it provides information on chemical changes and their effect on the physical properties. The experiment showed that PCL is exceptionally stable over 25 d of heating when processed at 75 °C. For 85 °C and 95 °C a slight upward trend during the last 10 d could be observed, which is an indication for thermal degradation. The same trend could be observed when looking at the fiber diameter of fibers produced at v_{fix}. All three temperatures had in common that during the first 5 d the CTS decreased, which could be explained by inhomogeneities of the melt due to the lack of mixing. Even though changes in CTS during the last 10 d could be observed for 85 °C and 95 °C, physical analysis of the printed fibers by XRD and mechanical testing did not show significant changes in crystallinity, crystallite size, Young's modulus and yield strength. These results indicate that the degradation process is too slow to show significant changes in the physical properties of the fibers. Overall, this work could show that PCL is very durable under thermal condition and can be processed for at least 15 consecutively days without it having a major impact on the printing properties. This timeframe can be expanded to 25 d and probably even beyond that, when the temperature is kept at 75 °C.

To investigate the chemical details on the thermal durability of PCL, a more in-depth analysis had been performed, shown in **Chapter 4**. Therefore, PCL was artificially aged in an oven over 25 d at 75 °C, 85 °C and 95 °C. Then the samples were analyzed with GPC and GC-MS to comprehend the chemical changes and DSC and rheology to investigate the influence on the physical changes. Data from GPC analysis and rheology revealed that PCL is degrading steadily at all three temperatures, but the degradation was too slow to significantly change melting onset temperature or melting enthalpy over the 25-days timespan according to DSC data. In terms of the chemical details of the degradation, two different mechanisms are known in literature: random chain scission and unzipping. As

unzipping produces free monomer, GC-MS measurements were run to look at the development of ε-caprolactone content with heating time. It could be observed that for samples aged at 95 °C indeed an upward trend in monomer content could be observed, which lead to the conclusion that unzipping is taking place. In contrast, a downward trend could be observed for the 75 °C samples. Together with the GPC data, it could be ruled out that unzipping is the only degradation mechanism, but rather a twofold degradation together with random chain scission. Lastly, a second GPC experiment was conducted using a 25-days aged PCL sample that has been mixed with a fluorescence labelled 3 kDa PCL. This data revealed that PCL and labelled PCL were undergoing ester interchange reactions. These reactions could on the one hand clarify how monomer could be reincorporated and on the other hand explain why PCL is so durable under thermal conditions. As chain length decreases with ongoing degradation these short chains could undergo ester interchange reactions to become longer again, slowing down the effects of thermal degradation. Overall, this study could confirm the findings of Chapter 3 by explaining why PCL is chemically stable over long periods of processing via MEW.

Finally, in **Chapter 5** PLGA was established as a processable material for MEW. As PLGA is quickly degrading at high temperature, the first step was to find the minimum temperature at which the material could be reliably printed. Even though, CTS and fiber diameter were surprisingly stable over 24 h of printing, GPC results revealed that the material already degraded heavily in the one-hour preheating period. To tackle this issue, ATEC had been blended with PLGA in 10 wt-%, 20 wt-% and 30 wt-% mixtures to reduce the processing temperature as well as the degradation rate. According to GPC data, the degradation could indeed be slowed down for the blends. The downside was that this slower degradation introduced a steadily changing CTS. Therefore, the blends cannot be reliably processed for 24 h but a processing window of approximately 6 h could be established. Since adding plasticizer could also change the mechanical properties of a material, mechanical testing with fibers produced with PLGA and all three blends was performed. While PLGA was very brittle as expected, the blends, especially the 20 wt-% and 30 wt-% mixtures, showed an elastic behavior. This could probably be explained by ester interchange reactions that might have caused the formation of a loosely crosslinked network with ATEC. Overall, PLGA could be successfully established as a material for MEW, which is a very popular material in TERM approaches. Additionally, it could be shown, that

the addition of ATEC could reduce the processing temperature as well as introducing elastic properties to the fibers.

7.2 Zusammenfassung

Der **Fokus dieser Doktorarbeit** lag auf der Untersuchung, wie sich verschiedene Materialien bei Erhitzung auf die jeweiligen Prozesstemperaturen über einen definierten Zeitrahmen verhalten. Dafür wurde zum einen der Goldstandard PCL, ein langsam degradierendes Polymer, sowie PLGA, ein schnell degradierendes Polymer, verwendet.

In **Kapitel 3** wurde die Druckstabilität von PCL über einen Zeitraum von 25 d bei seiner Verarbeitung mittels MEW untersucht. Um die Wiederholbarkeit über 25 d hinweg zu garantieren, wurde ein automatisierter Ansatz gewählt, um die CTS des Jets für jeden Tag für drei verschiedene Temperaturen, 75 °C, 85 °C und 95 °C, zu bestimmen. Da die CTS abhängig von den physikalischen Eigenschaften der Schmelze ist, gibt die CTS Aufschluss über chemischen Änderungen, sofern diese die physikalischen Eigenschaften beeinflussen. Die Ergebnisse zeigten, dass sich PCL bei 75 °C über 25 d hinweg außerordentlich stabil verdrucken ließ. Bei 85 °C und 95 °C konnte jedoch eine steigende CTS während den letzten zehn Tagen des Experiments beobachten werden, was ein Hinweis auf den thermischen Zerfall des Materials sein kann. Alle drei Temperaturen hatten jedoch eine Gemeinsamkeit: Während den ersten 5 d verringerte sich die CTS stetig. Dieses Verhalten konnte durch Inhomogenitäten der Schmelze erklärt werden, die möglicherweise durch fehlende Durchmischung entstanden sind und die erst im Verlauf der ersten 5 d langsam verschwanden. Obwohl eine steigende CTS während der letzten 10 d bei 85 °C und 95 °C beobachtet werden konnte, konnte durch physikalische Analyse der gedruckten Fasern mittels XRD und mechanischer Zugtests keine signifikanten Änderungen der Kristallinität, der Kristallgröße, des Elastizitätsmoduls und der Streckgrenze festgestellt werden. Möglicherweise sind die chemischen Änderungen des Materials zwar groß genug, um einen Effekt auf die CTS zu haben, jedoch zu klein, um diese physikalischen Größen zu beeinflussen. Insgesamt konnte die Studie zeigen, dass PCL außerordentlich widerstandsfähig gegenüber der thermischen Belastung für mindestens 15 d ist. Dieser Zeitraum kann auf 25 d und darüber hinaus ausgeweitet werden, falls das Polymer bei 75 °C verdruckt wird.

Um die Gründe für diese thermische Widerstandsfähigkeit von PCL auch chemisch zu erfassen, wurde eine detaillierte Analyse durchgeführt, die in **Kapitel 4** vorgestellt wurde. Dabei wurde PCL in einem Ofen bei 75 °C, 85 °C und 95 °C künstlich gelaltert. Für die Analyse wurden anschließend GPC- und GC-MS-Messungen durchgeführt, um mögliche

chemischen Änderungen zu untersuchen, und DSC- und Rheologiemessungen durchgeführt, um den Einfluss chemischer Änderungen auf die physikalischen Eigenschaften zu ermitteln. Die Daten der GPC- und Rheologiemessungen zeigten, dass PCL stetig über den gesamten Zeitrahmen bei allen drei Temperaturen zerfällt. Die Änderungen, die dieser Zerfall hervorgerufen hat, waren jedoch nicht groß genug, um einen Effekt auf die mit DSC gemessene Schmelztemperatur und Schmelzenthalpie zu haben. Zum Mechanismus des thermischen Zerfalls von PCL waren zwei verschiedene Wege in der Literatur bekannt: eine zufällige Spaltung der Polymerketten und ein reißverschlussartiger Zerfall von einem Kettenende her. Da der reißverschlussartige Zerfall zur Erzeugung von Monomer führt, wurden GC-MS-Messungen durchgeführt, um die Entwicklung des Gehalts an ε-Caprolacton im Polymer über die Zeitspanne von 25 d zu bestimmen. Dabei konnte bei 95 °C eine Freisetzung von Monomer beobachtet werden, was zu der Annahme führte, dass der reißverschlussartige Mechanismus zum Zerfall beiträgt. Im Gegensatz dazu konnte bei den Proben, die bei 75 °C gealtert wurden, beobachtet werden, dass der Monomergehalt über den gewählten Zeitraum kleiner wurde. Zusammen mit den oben genannten GPC-Daten konnte gezeigt werden, dass die genannten Mechanismen tatsächlich zum thermischen Zerfall von PCL beitragen. Zuletzt wurde ein zweites GPC-Experiment durchgeführt, für das PCL mit einem 3 kDa großem, fluoreszenzmarkiertem PCL gemischt und ebenfalls bei 85 °C für 25 d gealtert. Die gesammelten Daten zeigten, dass PCL mit dem markiertem PCL sogenannte Esteraustauschreaktionen einging. Diese Reaktionen sorgen im Fall von PCL dafür, dass Polymerketten, die durch den Zerfall kürzer geworden sind, sich in einem ständigen Austausch mit den restlichen Ketten befinden. Dadurch lassen sich die Auswirkungen durch den thermischen Zerfall verringern, da sich ein Gleichgewicht der mittleren Kettenlänge einstellt. Insgesamt konnte diese Studie die Ergebnisse von Kapitel 3 bestätigen und die Langzeitstabilität von PCL unter MEW-Bedingungen näher beleuchten.

Zuletzt wurde in **Kapitel 5** PLGA als neues Material für den MEW-Prozess etabliert. Da PLGA bei hohen Temperaturen sehr schnell zerfällt, wurde dafür zunächst die kleinstmögliche Prozesstemperatur ermittelt. Obwohl die Daten zu CTS und Faserdurchmesser eine unerwartete thermische Stabilität über 24 h zeigten, konnten GPC-Messungen deutlich machen, dass das Material bereits nach dem einstündigen Vorheizen stark degradiert war. Um diesen Zerfall abzumildern, wurde PLGA mit dem Weichmacher ATEC in den Verhältnissen 10 w-%, 20 w-% und 30 w-% gemischt, um die

Verarbeitungstemperatur und die damit einhergehende Degradation zu reduzieren. Die erhobenen GPC-Daten zeigten, dass der Zusatz des Weichmachers und damit die Erniedrigung der Prozesstemperatur den Degradationsprozess verlangsamen konnten. Jedoch wurde dadurch auch der initiale Degradationsprozess verlängert, was letztendlich dazu führte, dass während dem Druckprozess drastische Änderungen der CTS und des Faserdurchmessers auftraten. Deshalb konnte hier keine Empfehlung ausgesprochen werden, die Mischungen über einen Zeitraum von 24 h zu verdrucken. Stattdessen konnte ein Fenster von 6 h etabliert werden, in dem die Änderungen von CTS und Faserdurchmesser noch durch eine ausreichend hohe Kollektorgeschwindigkeit ausgeglichen werden kann. Da die Zugabe von Weichmacher auch die mechanischen Eigenschaften der erzeugten Fasern beeinflussen kann, wurden Zugexperimente mit PLGA und allen drei Mischungen durchgeführt. Während PLGA wie erwartet sehr spröde war, zeigten die Mischungen mit ATEC, insbesondere aber die 20 gew.-%igen und 30 gew.-%igen, ein elastisches Verhalten. Eine mögliche Erklärung könnten auch hier Esteraustauschreaktionen sein, bei denen die vier Estergruppen des ATEC mit den Akoholgruppen der Polymerketten reagieren können und damit ein loses Netzwerk ausbilden. Zusammengefasst kann festgehalten werden, dass PLGA erfolgreich als neues Material für den MEW-Prozess etabliert werden konnte, welches ein weit verbreitetes Material im Bereich TERM ist. Außerdem konnte gezeigt werden, dass die Zugabe von ATEC die Prozesstemperatur verringern konnte und zu einem elastischen Verhalten der erzeugten Fasern geführt hat.

Chapter 8

APPENDIX

8.1 G-Code for sample production (Chapter 3)

```
' This G-Code can only be used with x-y-axis from Aerotech Inc., Pittsburgh, USA

' Repetition of a long-term printing experiment

'define variables

DVAR $IX, $IY, $IZ, $IL, $ICTS, $SN, $IW, $FEEDF, $HIGHT, $LPITCH, $CSIZE, $FEEDR, $PI,
$PO, $PLINE $GAP, $START, $FINISH, $STAB

'set variables values

$IX = 0

$IY = 0

$IZ = 0

$IL = 0

$ICTS = 0

$IW = 0

$SN = 0

$LPITCH = 0.1

$PI = 0.05

$PO = 0.01

$PLINE = 0.01


$FEEDF = 1050

$FEEDR = 800

$CSIZE = 14


'Box spacing
```

```
$GAP = 0.5


'enable axes
ENABLE X Y Z


'Blending profile on
VELOCITY OFF


'Feedrates in mm/min
MINUTES


'starting position
ABSOLUTE
Linear X(-50+($IW*26)) Y-68 Z-17 F500
Dwell (28*60)
FOR $IW = 0 TO 4
        ABSOLUTE
        F1000
        WAIT MOVEDONE x y
        TIMER 0 CLEAR
        $START = TIMER (0)
        $AO[0].X = 2
        MSGCLEAR 1
        Linear X(-50+($IW*26)) Y-68 Z-17 F500
```

```
Dwell (3*60)
'Slide with boxes
Linear X(-60+$IW*26) Y-63 Z-17
INCREMENTAL
CALL XYLAYERC O500 P25
$STAB = TIMER (0)
MSGDISPLAY 1, ($STAB-$START)/60000, "Stab Time [min]"
'Slide with CTS
WAIT MOVEDONE x y
'MSGDISPLAY 1, [TIMER (0)]/60000, "one layer"
'CTS #1
ABSOLUTE
Linear X(-60+$IW*26) Y-33 Z-17
INCREMENTAL
CALL CTSY K20 S22.5 T0.5 U190
'CTS #2
ABSOLUTE
Linear X(-62+$IW*26) Y-33 Z-17
Linear X(-62+$IW*26) Y10 Z-17
Linear X(-60+$IW*26) Y10 Z-17
INCREMENTAL
CALL CTSY K20 S22.5 T0.5 U190
'CTS #3
ABSOLUTE
```

```
Linear X(-62+$IW*26) Y10 Z-17

Linear X(-62+$IW*26) Y40 Z-17

Linear X(-60+$IW*26) Y40 Z-17

INCREMENTAL

CALL CTSY K20 S22.5 T0.5 U190

ABSOLUTE

Linear X(-62+$IW*26) Y40 Z-17

Linear X(-62+$IW*26) Y-63 Z-17

'Wall #1

Linear X(-40+$IW*26) Y-63 Z-17

Linear X(-39+$IW*26) Y-63 Z-17

INCREMENTAL

CALL WALL S25 U310

ABSOLUTE

Linear X(-40+$IW*26) Y-38 Z-17

Linear X(-40+$IW*26) Y-63 Z-17

'Wall #2

Linear X(-38.2+$IW*26) Y-63 Z-17

INCREMENTAL

CALL WALL S25 U310

ABSOLUTE

Linear X(-40+$IW*26) Y-38 Z-17

Linear X(-40+$IW*26) Y-63 Z-17

'Wall #3
```

```
Linear X(-37.4+$IW*26) Y-63 Z-17
INCREMENTAL
CALL WALL S25 U310
ABSOLUTE
Linear X(-40+$IW*26) Y-38 Z-17
Linear X(-40+$IW*26) Y-63 Z-17
'Wall #4
Linear X(-36.6+$IW*26) Y-63 Z-17
INCREMENTAL
CALL WALL S25 U310
ABSOLUTE
Linear X(-40+$IW*26) Y-38 Z-17
Linear X(-40+$IW*26) Y-63 Z-17
$AO[0].X = 0
IF $IX<4
    Linear X(-50+($IW+1)*26) Y-68 Z-17
    Linear X(-50+($IW+1)*26) Y-68 Z-10
ELSE
    Linear X(-50+($IW*26)) Y-68 Z-10
ENDIF
WAIT MOVEDONE x y
MSGDISPLAY 1, TIMER (0), "2 slides"
$FINISH = TIMER (0)
MSGDISPLAY 1, ($FINISH-$START)/60000, "Printing Time [min]"
```

```
        DWELL (24*60*60-($FINISH-$START)/1000)
        NEXT $IW
M30



'SUBROUTINES
DFS XLAYER2
'S - construct Y size, L - construct X size, T - box size, U - feedrate
FOR $IX = 1 TO ($L/(2*$T))
        Linear X$S F$U
        Dwell $PI
        IF $T<1 THEN
                CCW X0 Y$T R-1 F$FEEDR
        ELSE
                CCW X0 Y$T R-$T F$FEEDR
        ENDIF
        Dwell $PO
        Linear X-$S F$U
        Dwell $PI
        IF $T<1 THEN
                CW X0 Y$T R-1 F$FEEDR
        ELSE
                CW X0 Y$T R-$T F$FEEDR
        ENDIF
```

```
        Dwell $PO
NEXT $IX
Linear Y-$L F$U
ENDDFS


DFS YLAYER2
FOR $IY = 1 TO ($S/(2*$T))
        Linear Y$L F$U
        Dwell $PI
        IF $T<1 THEN
                CCW Y0 X$T R-1 F$FEEDR
        ELSE
                CCW Y0 X$T R-$T F$FEEDR
        ENDIF
        Dwell $PO
        Linear Y-$L F$U
        Dwell $PI
        IF $T<1 THEN
                CW Y0 X$T R-1 F$FEEDR
        ELSE
                CW Y0 X$T R-$T F$FEEDR
        ENDIF
        Dwell $PO
NEXT $IY
```

```
Linear X-$S F$U
ENDDFS


DFS XYLAYERC
INCREMENTAL
'O - frame building feedrate, P-frame height, Q-construct size, L-gap
G4 F0.1
FOR $IZ = 1 TO $P
        CALL XLAYER2 S18 T$GAP L25 U$O
        CALL YLAYER2 S18 T$GAP L25 U$O
NEXT $IZ
G4 F0.1
ENDDFS


DFS CTSY
INCREMENTAL
'K - speed increment, S - construct size, T - line distance, U - starting feedrate
FOR $ICTS = 1 TO ($S/(5*$T))
        Linear Y25 F($U+($ICTS-1)*$K)
        Dwell $PI
        IF $T<1 THEN
                CW X$T Y0 R-1 F(($U+($ICTS-1)*$K)*0.9)
        ELSE
                CW X$T Y0 R-$T F(($U+($ICTS-1)*$K)*0.9)
```

```
ENDIF
Dwell $PO
Linear Y-25 F($U+($ICTS-1)*$K)
Dwell $PI
IF $T<1 THEN
    CCW X$T Y0 R-1 F(($U+($ICTS-1)*$K)*0.9)
ELSE
    CCW X$T Y0 R-$T F(($U+($ICTS-1)*$K)*0.9)
ENDIF
Dwell $PO
Linear Y25 F($U+($ICTS-1)*$K)
Dwell $PI
IF $T<1 THEN
    CW X$T Y0 R-1 F(($U+($ICTS-1)*$K)*0.9)
ELSE
    CW X$T Y0 R-$T F(($U+($ICTS-1)*$K)*0.9)
ENDIF
Dwell $PO
Linear Y-25 F($U+($ICTS-1)*$K)
Dwell $PI
IF $T<1 THEN
    CCW X($T*2) Y0 R-1 F(($U+($ICTS-1)*$K)*0.9)
ELSE
    CCW X($T*2) Y0 R(-$T*2) F(($U+($ICTS-1)*$K)*0.9)
```

```
        ENDIF
        Dwell $PO
NEXT $ICTS
Linear X-$S F$U
ENDDFS


DFS WALL
INCREMENTAL
'S - Wall height, U - Linear Speed
Linear Y5 F$U
FOR $IL = 1 TO (($S-1)/2)
        Linear Y15 F$U
        Dwell $PLINE
        Linear Y-15 F$U
        Dwell $PLINE
NEXT $IL
Linear Y20 F$U
ENDDFS
```

8.2 Appendix of Chapter 5

This is the supporting information of chapter 5 and the respective publication.

Supporting video 1 shows a comparison of the printing behavior of PLGA, PLGA10, PLGA20 and PLGA 30 and can be found at the following link:

https://onlinelibrary.wiley.com/action/downloadSupplement?doi=10.1002%2Fmacp.202100417&file=macp202100417-sup-0002-VideoS1.mp4

Supporting video 2 shows a comparison of stretching experiments of PLGA, PLGA10 and PLGA20 with PLGA10 showing partial and PLGA20 full strain recovery and can be found at the following link:

https://onlinelibrary.wiley.com/action/downloadSupplement?doi=10.1002%2Fmacp.202100417&file=macp202100417-sup-0003-VideoS2.mp4

The following G-Code was used to investigate the CTS development of different PLGA/ATEC mixtures with time:

;Automated CTS measurement with arrays in Y-Direction

;========== Parameters ==========

;Temperature, Pressure and wait for temperature in min

1 #T1=2200

1 #T2=2200

1 #P=20

1 #PS=100

1 #HV1=

1 #HVS1=500

1 #HV2=

1 #HVS2=500

1 #TWAIT=30

;Starting Position LEFT and RIGHT and Z-Position

1 #XSTL=9

1 #YST=158

1 #XSTR=152

1 #ZPOS=3

;Linear, Turn Speed, Speed up type check (0 for absolute, 1 for percentage) and Speed increase (absolute or percentage)

1 #LSPEED=250

1 #STYPE=0

1 #SPEEDUP=100

;Turn Radius

1 #RAD=1

;Stabilization and initiation pause in min

1 #SWAIT=2

1 #SSPEED=200

1 #SLAYERS=3

1 #SARRAYS=12

1 #SYDIST=18

1 #SFSPACE=0.5

```
;Slide Layout
1 #BLOCKS=26
1 #YDIST=20
1 #FSPACE=0.5
1 #BSPACE=1

;Number of slides and Slide pause (in min)
1 #SLIDES=6
1 #SLIDEP=30

;Pause
1 #TI=0
1 #TO=0

;Counter and Position Variable
1 COUNT=1
1 XSTV=#XSTL

;======================== Main Program ================================
G8 G17 G21

1 DIM CLOCKS$ (20)
```

```
1 DIM STABS$ (20)

1 DIM STABF$ (20)

1 DIM ARRAYS$ (20)

1 DIM ARRAYF$ (20)

1 DIM D$ (20)

1 DIM T$ (20)


1 D$ = DATE

1 T$ = TIME


G90

G1              X[#XSTL]        Y[#YST]         Z[#ZPOS+3.7]            F500


1 WAIT

1 TOTALS = CLOCK


T3=[#T3] T4=[#T4]

HV1=[#HV1] HVS1=[#HVS1]

HV2=[#HV2] HVS2=[#HVS2]


G4                                                                      F[#TWAIT*60]


1 OPENW (1, "Print Report.csv", , 1024)

1 OPENW (2, "Speed Map.csv")
```

```
1 FOR I%=1 TO #SLIDES
        1 WAIT
        1 CLOCKS$ = TIME
        1 TIMESTART = CLOCK
        G90
        G1              X[XSTV+(1*COUNT+((COUNT-1)*(#SARRAYS*2*#SFSPACE)))]
                        Y[#YST]                                         F[#SSPEED]
        P=[#P] PS=[#PS]
        G4                                                              F[#SWAIT*60]
        G91
        G1              X0              Y-1                             F[#SSPEED]

        ;==================Start of stabilization==================
        1 WAIT
        1 STABS$ = TIME
        1 STABSTART = CLOCK
        1 CALL SRStabY (#SLAYERS, #SARRAYS, #SYDIST, #SFSPACE, #SSPEED)
        1 WAIT
        1 STABFINISH = CLOCK
        1 STABF$ = TIME
        1 STABTIME = (STABFINISH - STABSTART)/60000
        G1              X[-1*COUNT-((COUNT-1)*(#SARRAYS*2*#SFSPACE))]
                        Y0                                              F[#SSPEED]
        G1              X0      Y[-(#SYDIST+COUNT*26+1)]                F[#SSPEED]
```

```
G1              X3              Y0                              F[#SSPEED]


;=========================Start of Arrays============================

1 WAIT

1 ARRAYSTART = CLOCK

1 ARRAYS$ = TIME

1 PRN# (2, "Slide #", I%)

1 CALL SRArraysY (#BLOCKS, #YDIST, #FSPACE, #BSPACE, #LSPEED, #SPEEDUP,
#STYPE)

1 PRN# (2, "-")

1 WAIT

1 ARRAYFINISH = CLOCK

1 ARRAYF$ = TIME

1 ARRAYTIME = (ARRAYFINISH - ARRAYSTART)/60000

P=0 PS=[#PS]

G1              X2              Y0                              F[#LSPEED]

G1              X0              Y[#YDIST+1]                     F[#LSPEED]

G1              X[-(#BLOCKS*(3*#FSPACE+#BSPACE))-1]     Y0      F[#LSPEED]

G1              X0              Y[(26*COUNT)-3]                 F[#LSPEED]

1 COUNT=COUNT+1

1 IF I%=3 THEN

        1 COUNT=1

        1 XSTV=#XSTL+76

1 ENDIF
```

```
        1 WAIT

        1 TIMEFINISH = CLOCK

        1 CLOCKF$ = TIME

        1 PRINTTIME = (TIMEFINISH - TIMESTART)/60000

        1 WAITTIME = (#SLIDEP - PRINTTIME)


        ;==Generation of a printing report containing start and finish time and durations==

        1 PRN# (1, "Slide #", I%)

        ;1 PRN# (1, "Printing started at ", CLOCKS$)

        ;1 PRN# (1, "Printing ended at ", CLOCKF$)

        1 PRN# (1, "Stab + Slide Printtime: ", PRINTTIME, " min")

        ;1 PRN# (1, "Stabilization started at ", STABS$)

        ;1 PRN# (1, "Stabilization ended at ", STABF$)

        1 PRN# (1, "Stabilization time: ", STABTIME, " min")

        ;1 PRN# (1, "Array printing started at ", ARRAYS$)

        ;1 PRN# (1, "Array printing ended at ", ARRAYF$)

        1 PRN# (1, "Array printing time: ", ARRAYTIME, " min")

        1 PRN# (1, "Actual waiting time: ", WAITTIME, " min")

        1 PRN# (1, "-")


        G4                                              F[WAITTIME*60]

1 NEXT I%


1 WAIT
```

```
1 TOTALF = CLOCK

1 TOTALT = (TOTALF - TOTALS)/60000

1 PRN# (1, "--")

1 PRN# (1, "Total Printingtime: ", TOTALT, " min")


1 CLOSE (1)

1 CLOSE (2)

T3=200 T4=200

M30
```

References

References

[1] WHO, The top 10 causes of death, 2020. https://www.who.int/news-room/fact-sheets/detail/the-top-10-causes-of-death. (Accessed March 18, 2021).
[2] A. Loupy, O. Aubert, P.P. Reese, O. Bastien, F. Bayer, C. Jacquelinet, *The Lancet* **2020**, *395*, e95-e96.
[3] T.M. Ramos, Lorenzo, *Tissue Engineering Part C: Methods* **2020**, *26*, 91-106.
[4] T.D. Brown, P.D. Dalton, D.W. Hutmacher, *Advanced Materials* **2011**, *23*, 5651-+.
[5] O. Abdulhameed, A. Al-Ahmari, W. Ameen, S.H. Mian, *Advances in Mechanical Engineering* **2019**, *11*, 1687814018822880.
[6] C.W. Hull, Apparatus for production of three-dimensional objects by stereolithography, 1986.
[7] J. Huang, Q. Qin, J. Wang, *Processes* **2020**, *8*, 1138.
[8] J.R. Tumbleston, D. Shirvanyants, N. Ermoshkin, R. Janusziewicz, A.R. Johnson, D. Kelly, K. Chen, R. Pinschmidt, J.P. Rolland, A. Ermoshkin, E.T. Samulski, J.M. DeSimone, *Science* **2015**, *347*, 1349-52.
[9] M. Shusteff, A.E.M. Browar, B.E. Kelly, J. Henriksson, T.H. Weisgraber, R.M. Panas, N.X. Fang, C.M. Spadaccini, *Science Advances* **2017**, *3*, eaao5496.
[10] History of Additive Manufacturing. Available online: http://www.wohlersassociates.com/history2014.pdf. (Accessed April 2 2021).
[11] S. Vyavahare, S. Teraiya, D. Panghal, S. Kumar, *Rapid Prototyping J* **2020**, *26*, 176-201.
[12] C. Bellehumeur, L. Li, Q. Sun, P. Gu, *Journal of Manufacturing Processes* **2004**, *6*, 170-178.
[13] Q. Sun, G. Rizvi, C.T. Bellehumeur, P. Gu, *Rapid Prototyping J* **2008**, *14*, 72-80.
[14] B. N. Turner, R. Strong, S. A. Gold, *Rapid Prototyping J* **2014**, *20*, 192-204.
[15] T.J. Coogan, D.O. Kazmer, *Rapid Prototyping J* **2017**, *23*, 551-561.
[16] D. Espalin, K. Arcaute, D. Rodriguez, F. Medina, M. Posner, R. Wicker, *Rapid Prototyping J* **2010**, *16*, 164-173.
[17] R. Ilardo, C.B. Williams, *Rapid Prototyping J* **2010**, *16*, 174-179.
[18] M.D. Monzon, N. Diaz, A.N. Benitez, M.D. Marrero, P.M. Hernandez, Advantages of Fused Deposition Modeling for Making Electrically Conductive Plastic Patterns, Proceedings of the 2010 International Conference on Manufacturing Automation, IEEE Computer Society, 2010, pp. 37–43.
[19] J. Korpela, A. Kokkari, H. Korhonen, M. Malin, T. Närhi, J. Seppälä, *Journal of Biomedical Materials Research Part B: Applied Biomaterials* **2013**, *101B*, 610-619.
[20] N. Xu, X. Ye, D. Wei, J. Zhong, Y. Chen, G. Xu, D. He, *ACS Appl Mater Inter* **2014**, *6*, 14952-14963.
[21] E. Pei, J. Shen, J. Watling, *Rapid Prototyping J* **2015**, *21*, 556-571.
[22] C.R. Decker, Method and apparatus for producing parts by selective sintering, U.S., 1989.
[23] W.W. Meiners, Konrad; Gasser, Andres, Verfahren zur Herstellung eines Formkörpers, DE, 1998.
[24] G.B.M. Cervera, G. Lombera, *Rapid Prototyping J* **1999**.
[25] C.Y. Yap, C.K. Chua, Z.L. Dong, Z.H. Liu, D.Q. Zhang, L.E. Loh, S.L. Sing, *Applied Physics Reviews* **2015**, *2*, 041101.
[26] Production Methods: What's the Difference Between Selective Laser Sintering, Direct Metal Laser Sintering, Laser Melting and LaserCusing? Available online: https://www.core77.com/posts/26457/production-methods-whats-the-difference-between-selective-laser-sintering-direct-metal-laser-sintering-laser-melting-and-lasercusing-26457. (Accessed April 29 2021).
[27] Z. Chen, Z. Li, J. Li, C. Liu, C. Lao, Y. Fu, C. Liu, Y. Li, P. Wang, Y. He, *Journal of the European Ceramic Society* **2019**, *39*, 661-687.
[28] M. Drexler, M. Lexow, D. Drummer, *Phys Procedia* **2015**, *78*, 328-336.
[29] D.M. Nieto, D.M. Sánchez, *Applied Sciences* **2021**, *11*, 1571.
[30] E.J. Parry, J.M. Best, C.E. Banks, *Materials Today Communications* **2020**, *25*, 101225.
[31] C. Mavroidis, R.G. Ranky, M.L. Sivak, B.L. Patritti, J. DiPisa, A. Caddle, K. Gilhooly, L. Govoni, S. Sivak, M. Lancia, R. Drillio, P. Bonato, *Journal of NeuroEngineering and Rehabilitation* **2011**, *8*, 1.
[32] T. Grimm, *User's guide to rapid prototyping*, Society of Manufacturing Engineers, **2004**.
[33] P. Jamshidi, M. Haddad, S. Mansour, A new database approach to improve STL files correction algorithms, 18th International Conference on Production Research, 2005.
[34] J.P. Kruth, *CIRP Annals* **1991**, *40*, 603-614.
[35] K.V. Wong, A. Hernandez, *ISRN Mechanical Engineering* **2012**, *2012*, 208760.
[36] T. Billiet, M. Vandenhaute, J. Schelfhout, S. Van Vlierberghe, P. Dubruel, *Biomaterials* **2012**, *33*, 6020-6041.
[37] ISO/ASTM52900-15, Standard Terminology for Additive Manufacturing – General Principles – Terminology, ASTM International, West Conshohocken, PA, 2015.

[38] T. Jungst, W. Smolan, K. Schacht, T. Scheibel, J. Groll, *Chemical Reviews* **2016**, *116*, 1496-1539.
[39] H. Ramanath, K. Chua, K.F. Leong, K. Shah, *J Mater Sci-Mater M* **2008**, *19*, 2541-50.
[40] M. Spoerk, C. Holzer, J. Gonzalez-Gutierrez, *J Appl Polym Sci* **2020**, *137*, 48545.
[41] W. Gilbert, *Price DJ, editor. London: The Chiswick Press* **1600**.
[42] J.F. Cooley, Improved methods of and apparatus for electrically separating the relatively volatile liquid component from the component of relatively fixed substances of composite fluids. , 1900.
[43] E.F. Burton, W.B. Wiegand, *The London, Edinburgh, and Dublin Philosophical Magazine and Journal of Science* **1912**, *23*, 148-165.
[44] J. Zeleny, *Physical Review* **1914**, *3*, 69-91.
[45] J. Zeleny, *Physical Review* **1917**, *10*, 1-6.
[46] J. Zeleny, *Physical Review* **1920**, *16*, 102-125.
[47] A. Formhals, Process and apparatus for preparing artificial threads, U.S., 1934.
[48] A. Formhals, Production of artificial fibers, U.S., 1937.
[49] A. Formhals, Method of producing artificial fibers, U.S., 1939.
[50] A. Formhals, Method and apparatus for the production of artificial fibers, 1939.
[51] A. Formhals, Artificial thread and method of producing same, 1940.
[52] A. Formhals, Production of artificial fibers from fiber forming liquids, 1943.
[53] C.L. Norton, Method of and apparatus for producing fibrous or filamentary material, U.S., 1936.
[54] G.I. Taylor, *Proceedings of the Royal Society of London. Series A. Mathematical and Physical Sciences* **1964**, *280*, 383-397.
[55] J.R. Melcher, G.I. Taylor, *Annu Rev Fluid Mech* **1969**, *1*, 111-146.
[56] N. Tucker, J.J. Stanger, M.P. Staiger, H. Razzaq, K. Hofman, *Journal of engineered fibers and fabrics* **2012**, *7*, 155892501200702S10.
[57] D.H. Reneker, I. Chun, *Nanotechnology* **1996**, *7*, 216-223.
[58] L. Larrondo, R.S.J. Manley, *J Polym Sci Pol Phys* **1981**, *19*, 909-920.
[59] L. Larrondo, R.S.J. Manley, *J Polym Sci Pol Phys* **1981**, *19*, 921-932.
[60] R. Rangkupan, D. Reneker, *J. Met. Mater. Miner.* **2003**, *12*.
[61] P.D. Dalton, K. Klinkhammer, J. Salber, D. Klee, M. Möller, *Biomacromolecules* **2006**, *7*, 686-690.
[62] P.D. Dalton, D. Grafahrend, K. Klinkhammer, D. Klee, M. Möller, *Polymer* **2007**, *48*, 6823-6833.
[63] P.D. Dalton, N.T. Joergensen, J. Groll, M. Moeller, *Biomed Mater* **2008**, *3*.
[64] T.M. Robinson, D.W. Hutmacher, P.D. Dalton, *Adv Funct Mater* **2019**, *29*.
[65] C. Böhm, P. Stahlhut, J. Weichhold, A. Hrynevich, J. Teßmar, P.D. Dalton, *Small n/a*, 2104193.
[66] J. Pfitzner, *Anaesthesia* **1976**, *31*, 273-275.
[67] W. Ostwald, *Kolloid-Zeitschrift* **1925**, *36*, 99-117.
[68] A. De Waele, *Assoc. J* **1923**, *6*, 33.
[69] A. Hrynevich, B.Ş. Elçi, J.N. Haigh, R. McMaster, A. Youssef, C. Blum, T. Blunk, G. Hochleitner, J. Groll, P.D. Dalton, *Small* **2018**, *14*, 1800232.
[70] C. Blum, J. Weichhold, G. Hochleitner, V. Stepanenko, F. Würthner, J. Groll, T. Jungst, *3D Printing and Additive Manufacturing* **2021**.
[71] D. Tang, F.H. Marchesini, L. Cardon, D.R. D'hooge, *Macromolecular Materials and Engineering* **2020**, *305*, 2000340.
[72] G. Taylor, *Proc R Soc Lon Ser-A* **1969**, *313*, 453-475.
[73] D.T. Papageorgiou, *Journal of Fluid Mechanics* **1995**, *301*, 109-132.
[74] F.J. Higuera, *Physics of Fluids* **2002**, *14*, 423-426.
[75] Y. Pan, L. Zeng, *Micromachines (Basel)* **2019**, *10*, 94.
[76] S.K. Singh, A. Subramanian, *RSC Advances* **2020**, *10*, 25022-25028.
[77] L. Wang, A.J. Ryan, in *Electrospinning for Tissue Regeneration*, (Eds: L.A. Bosworth, S. Downes), Woodhead Publishing2011, Ch.
[78] T.A. Osswald, G. Menges, in *Materials Science of Polymers for Engineers*, (Eds: Ch.
[79] G. Hochleitner, A. Youssef, A. Hrynevich, J.N. Haigh, T. Jungst, J. Groll, P.D. Dalton, *BioNanoMat* **2016**, *17*, 159-171.
[80] F.M. Wunner, M.-L. Wille, T.G. Noonan, O. Bas, P.D. Dalton, E.M. De-Juan-Pardo, D.W. Hutmacher, *Advanced Materials* **2018**, *30*, 1706570.
[81] M. Castilho, D. Feyen, M. Flandes-Iparraguirre, G. Hochleitner, J. Groll, P.A.F. Doevendans, T. Vermonden, K. Ito, J.P.G. Sluijter, J. Malda, *Adv Healthc Mater* **2017**, *6*, 1700311.

[82] C. Blum, K. Schlegelmilch, T. Schilling, A. Shridhar, M. Rudert, F. Jakob, P.D. Dalton, T. Blunk, L.E. Flynn, J. Groll, *ACS Biomaterials Science & Engineering* **2019**, *5*, 6655-6666.
[83] T. Tylek, C. Blum, A. Hrynevich, K. Schlegelmilch, T. Schilling, P.D. Dalton, J. Groll, *Biofabrication* **2020**, *12*, 025007.
[84] J. Kim, E. Bakirci, K.L. O'Neill, A. Hrynevich, P.D. Dalton, *Macromolecular Materials and Engineering* **2021**, *306*, 2000685.
[85] A. Youssef, A. Hrynevich, L. Fladeland, A. Balles, J. Groll, P.D. Dalton, S. Zabler, *Tissue Eng Pt C-Meth* **2019**, *25*, 367-378.
[86] A. Hrynevich, P. Achenbach, T. Jungst, G.A. Brook, P.D. Dalton, *Macromolecular bioscience* **2021**, *n/a*, 2000439.
[87] A. Hrynevich, I. Liashenko, P.D. Dalton, *Advanced Materials Technologies* **2020**, *5*, 2000772.
[88] I. Liashenko, A. Hrynevich, P.D. Dalton, *Advanced Materials* **2020**, *32*, 2001874.
[89] W. Schuurman, V. Khristov, M.W. Pot, P.R. van Weeren, W.J. Dhert, J. Malda, *Biofabrication* **2011**, *3*, 021001.
[90] M. Schuster, C. Turecek, B. Kaiser, J. Stampfl, R. Liska, F. Varga, *Journal of Macromolecular Science, Part A* **2007**, *44*, 547-557.
[91] A.U. Daniels, M.K.O. Chang, K.P. Andriano, J. Heller, *Journal of Applied Biomaterials* **1990**, *1*, 57-78.
[92] Y. Tokiwa, B.P. Calabia, C.U. Ugwu, S. Aiba, *International Journal of Molecular Sciences* **2009**, *10*, 3722-3742.
[93] G. BaoLin, P.X. Ma, *Sci China Chem* **2014**, *57*, 490-500.
[94] D.W. Hutmacher, *Biomaterials* **2000**, *21*, 2529-43.
[95] F.M. Wunner, P. Mieszczanek, O. Bas, S. Eggert, J. Maartens, P.D. Dalton, E.M. De-Juan-Pardo, D.W. Hutmacher, *Biofabrication* **2019**, *11*, 025004.
[96] M. Labet, W. Thielemans, *Chemical Society Reviews* **2009**, *38*, 3484-3504.
[97] J.E. Mark, *Polymer Handbook*, Oxford University Press, University of Cincinnati, **1999**.
[98] K. Van de Velde, P. Kiekens, *Polymer Testing* **2002**, *21*, 433-442.
[99] V.R. Sinha, K. Bansal, R. Kaushik, R. Kumria, A. Trehan, *Int J Pharm* **2004**, *278*, 1-23.
[100] Y. Ikada, H. Tsuji, *Macromol Rapid Comm* **2000**, *21*, 117-132.
[101] D. Mondal, M. Griffith, S.S. Venkatraman, *International Journal of Polymeric Materials and Polymeric Biomaterials* **2016**, *65*, 255-265.
[102] J.C. Middleton, A.J. Tipton, *Biomaterials* **2000**, *21*, 2335-46.
[103] P.A. Gunatillake, R. Adhikari, *Eur Cell Mater* **2003**, *5*, 1-16; discussion 16.
[104] S.C. Woodward, P.S. Brewer, F. Moatamed, A. Schindler, C.G. Pitt, *J Biomed Mater Res* **1985**, *19*, 437-44.
[105] J.B. Lee, J.E. Kim, M.S. Bae, S.A. Park, D.A. Balikov, H.J. Sung, H.B. Jeon, H.K. Park, S.H. Um, K.S. Lee, I.K. Kwon, *Polymers (Basel)* **2016**, *8*.
[106] S. Shirian, S. Ebrahimi-Barough, H. Saberi, A. Norouzi-Javidan, S.M. Mousavi, M.A. Derakhshan, B. Arjmand, J. Ai, *Mol Neurobiol* **2016**, *53*, 5278-87.
[107] A. Abdal-hay, N. Abbasi, M. Gwiazda, S. Hamlet, S. Ivanovski, *European Polymer Journal* **2018**, *105*, 257-264.
[108] G. Hochleitner, E. Fursattel, R. Giesa, J. Groll, H.W. Schmidt, P.D. Dalton, *Macromol Rapid Comm* **2018**, *39*.
[109] D. Nahm, F. Weigl, N. Schaefer, A. Sancho, A. Frank, J. Groll, C. Villmann, H.-W. Schmidt, P.D. Dalton, R. Luxenhofer, *Materials Horizons* **2020**, *7*, 928-933.
[110] S. Florczak, T. Lorson, T. Zheng, M. Mrlik, D.W. Hutmacher, M.J. Higgins, R. Luxenhofer, P.D. Dalton, *Polymer International* **2019**, *68*, 735-745.
[111] J.C. Kade, P.D. Dalton, *Adv Healthc Mater* **2021**, *10*, 2001232.
[112] S. Matsumura, K. Mabuchi, K. Toshima, *Macromol Rapid Comm* **1997**, *18*, 477-482.
[113] O. Dechy-Cabaret, B. Martin-Vaca, D. Bourissou, *Chemical Reviews* **2004**, *104*, 6147-6176.
[114] S. Zhou, X. Deng, X. Li, W. Jia, L. Liu, *J Appl Polym Sci* **2004**, *91*, 1848-1856.
[115] M. Ajioka, H. Suizu, C. Higuchi, T. Kashima, *Polym Degrad Stabil* **1998**, *59*, 137-143.
[116] Z.-Y. Wang, Y.-M. Zhao, F. Wang, J. Wang, *J Appl Polym Sci* **2006**, *99*, 244-252.
[117] M.L. Houchin, E.M. Topp, *J Appl Polym Sci* **2009**, *114*, 2848-2854.
[118] M.A. Washington, S.C. Balmert, M.V. Fedorchak, S.R. Little, S.C. Watkins, T.Y. Meyer, *Acta Biomater* **2018**, *65*, 259-271.
[119] P. Zhang, H. Wu, H. Wu, Z. Lù, C. Deng, Z. Hong, X. Jing, X. Chen, *Biomacromolecules* **2011**, *12*, 2667-2680.
[120] S.M. Morgan, S. Tilley, S. Perera, M.J. Ellis, J. Kanczler, J.B. Chaudhuri, R.O.C. Oreffo, *Biomaterials* **2007**, *28*, 5332-5343.
[121] D.W. Chen, J.Y. Liao, S.J. Liu, E.C. Chan, *Int J Nanomedicine* **2012**, *7*, 763-71.
[122] B. Jiang, G. Zhang, E.M. Brey, *Acta Biomater* **2013**, *9*, 4976-4984.

[123] K.K. Chereddy, G. Vandermeulen, V. Préat, *Wound Repair and Regeneration* **2016**, *24*, 223-236.
[124] K. Park, S. Skidmore, J. Hadar, J. Garner, H. Park, A. Otte, B.K. Soh, G. Yoon, D. Yu, Y. Yun, B.K. Lee, X. Jiang, Y. Wang, *Journal of Controlled Release* **2019**, *304*, 125-134.
[125] K. Ochi, G. Chen, T. Ushida, S. Gojo, K. Segawa, H. Tai, K. Ueno, H. Ohkawa, T. Mori, A. Yamaguchi, Y. Toyama, J.-i. Hata, A. Umezawa, *Journal of Cellular Physiology* **2003**, *194*, 45-53.
[126] M. Borden, M. Attawia, Y. Khan, C.T. Laurencin, *Biomaterials* **2002**, *23*, 551-559.
[127] Z.X. Meng, Y.S. Wang, C. Ma, W. Zheng, L. Li, Y.F. Zheng, *Materials Science and Engineering: C* **2010**, *30*, 1204-1210.
[128] W. Ji, F. Yang, H. Seyednejad, Z. Chen, W.E. Hennink, J.M. Anderson, J.J.J.P. van den Beucken, J.A. Jansen, *Biomaterials* **2012**, *33*, 6604-6614.
[129] T. Ouhadi, C. Stevens, P. Teyssié, *J Appl Polym Sci* **1976**, *20*, 2963-2970.
[130] Y. Aoyagi, K. Yamashita, Y. Doi, *Polym Degrad Stabil* **2002**, *76*, 53-59.
[131] G. Sivalingam, R. Karthik, G. Madras, *J Anal Appl Pyrol* **2003**, *70*, 631-647.
[132] O. Persenaire, M. Alexandre, P. Degée, P. Dubois, *Biomacromolecules* **2001**, *2*, 288-294.
[133] I.C. McNeill, H.A. Leiper, *Polym Degrad Stabil* **1985**, *12*, 373-385.
[134] G. Sivalingam, G. Madras, *Polym Degrad Stabil* **2004**, *84*, 393-398.
[135] I.C. McNeill, H.A. Leiper, *Polym Degrad Stabil* **1985**, *11*, 267-285.
[136] I.C. McNeill, H.A. Leiper, *Polym Degrad Stabil* **1985**, *11*, 309-326.
[137] F.D. Kopinke, M. Remmler, K. Mackenzie, M. Möder, O. Wachsen, *Polym Degrad Stabil* **1996**, *53*, 329-342.
[138] H. Lim, S.W. Hoag, *AAPS PharmSciTech* **2013**, *14*, 903-910.
[139] in *Handbook of Plasticizers (Third Edition)*, (Eds: G. Wypych), ChemTec Publishing2017, Ch.
[140] P.H. Daniels, *Journal of Vinyl and Additive Technology* **2009**, *15*, 219-223.
[141] A. Earla, L. Li, P. Costanzo, R. Braslau, *Polymer* **2017**, *109*, 1-12.
[142] P. Jia, L. Hu, X. Yang, M. Zhang, Q. Shang, Y. Zhou, *RSC Advances* **2017**, *7*, 30101-30108.
[143] J. Jang, D.K. Lee, *Polymer* **2003**, *44*, 8139-8146.
[144] P. Bergo, P.J.A. Sobral, *Food Hydrocolloids* **2007**, *21*, 1285-1289.
[145] H. Xiao, W. Lu, J.-T. Yeh, *J Appl Polym Sci* **2009**, *113*, 112-121.
[146] A. Kirkpatrick, *J Appl Phys* **1940**, *11*, 255-261.
[147] F. Clark, *Chem. Ind* **1941**, *60*, 225-230.
[148] R. Houwink, London, **1947**.
[149] P. Walters, D.F. Cadogan, C.J. Howick, in *Ullmann's Encyclopedia of Industrial Chemistry*, (Eds: 2020, Ch.
[150] A.K. Doolittle, *J Polym Sci* **1947**, *2*, 121-141.
[151] D.J. Bonda, S. Manjila, W.R. Selman, D. Dean, *Neurosurgery* **2015**, *77*, 814-824.
[152] D.W. Hutmacher, T.B.F. Woodfield, P.D. Dalton, in *Tissue Engineering*, 2nd (Eds: C. van Blitterswijk, J. De Boer), Elsevier, Amsterdam, 2014, Ch. 10.
[153] L. Moroni, T. Boland, J.A. Burdick, C. De Maria, B. Derby, G. Forgacs, J. Groll, Q. Li, J. Malda, V.A. Mironov, C. Mota, M. Nakamura, W. Shu, S. Takeuchi, T.B.F. Woodfield, T. Xu, J.J. Yoo, G. Vozzi, *Trends Biotechnol* **2018**, *36*, 384-402.
[154] M.A. Woodruff, D.W. Hutmacher, *Prog Polym Sci* **2010**, *35*, 1217-1256.
[155] P.D. Dalton, T.B.F. Woodfield, V. Mironov, J. Groll, *Adv Sci* **2020**, *7*, 1902953.
[156] M.C. Allenby, M.A. Woodruff, *J Cyst Fibros* **2019**, *18*, 161-162.
[157] A. Youssef, S.J. Hollister, P.D. Dalton, *Biofabrication* **2017**, *9*, 012002.
[158] F.A. Probst, D.W. Hutmacher, D.F. Müller, H.G. Machens, J.T. Schantz, *Handchir Mikrochir Plast Chir* **2010**, *42*, 369-373.
[159] A. Hrynevich, B.S. Elci, J.N. Haigh, R. McMaster, A. Youssef, C. Blum, T. Blunk, G. Hochleitner, J. Groll, P.D. Dalton, *Small* **2018**, *14*, e1800232.
[160] Z. Qiao, M. Lian, Y. Han, B. Sun, X. Zhang, W. Jiang, H. Li, Y. Hao, K. Dai, *Biomaterials* **2021**, *266*, 120385.
[161] F. Wagner, B.M. Holzapfel, J.A. McGovern, A. Shafiee, J.G. Baldwin, L.C. Martine, C.A. Lahr, F.M. Wunner, T. Friis, O. Bas, M. Boxberg, P.M. Prodinger, A. Shokoohmand, D. Moi, R. Mazzieri, D. Loessner, D.W. Hutmacher, *Biomaterials* **2018**, *171*, 230-246.
[162] N.T. Saidy, F. Wolf, O. Bas, H. Keijdener, D.W. Hutmacher, P. Mela, E.M. De-Juan-Pardo, *Small* **2019**, *15*, 1900873.
[163] O. Bas, D. D'Angella, J.G. Baldwin, N.J. Castro, F.M. Wunner, N.T. Saidy, S. Kollmannsberger, A. Reali, E. Rank, E.M. De-Juan-Pardo, D.W. Hutmacher, *ACS Appl Mater Inter* **2017**, *9*, 29430-29437.
[164] T. Jungst, I. Pennings, M. Schmitz, A.J.W.P. Rosenberg, J. Groll, D. Gawlitta, *Adv Funct Mater* **2019**, *29*, 1905987.

[165] C. Grosshaus, E. Bakirci, M. Berthel, A. Hrynevich, J.C. Kade, G. Hochleitner, J. Groll, P.D. Dalton, *Small* **2020**, e2003471.
[166] A. Youssef, T. Jungst, N.T. Ziani, B. Tandon, P.D. Dalton, *J Polym Sci* **submitted**.
[167] F.M. Wunner, M.L. Wille, T.G. Noonan, O. Bas, P.D. Dalton, E.M. De-Juan-Pardo, D.W. Hutmacher, *Adv Mater* **2018**, *30*, e1706570.
[168] J.C. Kade, P.D. Dalton, *Adv Healthc Mater* **2021**, *10*, e2001232.
[169] G. Sivalingam, G. Madras, *Polym Degrad Stabil* **2003**, *80*, 11-16.
[170] E.T. Pashuck, M.M. Stevens, *Sci Transl Med* **2012**, *4*.
[171] P. Skoglund, Å. Fransson, *J Appl Polym Sci* **1996**, *61*, 2455-2465.
[172] F. Tuba, L. Olah, P. Nagy, *Express Polym Lett* **2014**, *8*.
[173] M.P. Grosvenor, J.N. Staniforth, *Int J Pharm* **1996**, *135*, 103-109.
[174] E. Bakirci, N. Schaefer, O. Dahri, A. Hrynevich, P. Strissel, R. Strick, P.D. Dalton, C. Villmann, *Adv Biosyst* **2020**, *4*.
[175] N.A. Hotaling, K. Bharti, H. Kriel, C.G. Simon, *Biomaterials* **2015**, *61*, 327-338.
[176] H. Bittiger, R.H. Marchessault, W.D. Niegisch, *Acta Crystallogr B* **1970**, *26*, 1923-1927.
[177] P. Scherrer, *Nachrichten von der Gesellschaft der Wissenschaften zu Göttingen, Mathematisch-Physikalische Klasse* **1918**, *1918*, 98-100.
[178] J.I. Langford, A.J.C. Wilson, *J Appl Crystallogr* **1978**, *11*, 102-113.
[179] D.J. Richards, Y. Tan, J. Jia, H. Yao, Y. Mei, *Isr J Chem* **2013**, *53*, 805-814.
[180] J. Groll, T. Boland, T. Blunk, J.A. Burdick, D.-W. Cho, P.D. Dalton, B. Derby, G. Forgacs, Q. Li, V.A. Mironov, L. Moroni, M. Nakamura, W. Shu, S. Takeuchi, G. Vozzi, T.B.F. Woodfield, T. Xu, J.J. Yoo, J. Malda, *Biofabrication* **2016**, *8*, 013001.
[181] S. Nemati, S.-j. Kim, Y.M. Shin, H. Shin, *Nano Convergence* **2019**, *6*, 36.
[182] T. Barrows, *Clinical Materials* **1986**, *1*, 233-257.
[183] L.P.d. Melo, G.V. Salmoria, E.A. Fancello, C.R.d.M. Roesler, *International Journal of Biomaterials* **2017**, *2017*, 1256537.
[184] J.-S. Yoon, I.-J. Chin, M.-N. Kim, C. Kim, *Macromolecules* **1996**, *29*, 3303-3307.
[185] A.M. Kotliar, *Journal of Polymer Science: Macromolecular Reviews* **1981**, *16*, 367-395.
[186] P.J. Flory, *Journal of the American Chemical Society* **1940**, *62*, 2255-2261.
[187] F.L. Hamb, *Journal of Polymer Science Part A-1: Polymer Chemistry* **1972**, *10*, 3217-3234.
[188] I. Goodman, B.F. Nesbitt, *Polymer* **1960**, *1*, 384-396.
[189] P.J. Flory, *Chem Rev* **1946**, *39*, 137-97.
[190] S. Tiptipakorn, N. Keungputpong, S. Phothiphiphit, S. Rimdusit, *J Appl Polym Sci* **2015**, *132*.
[191] T.M. Robinson, D.W. Hutmacher, P.D. Dalton, *Advanced Functional Materials* **2019**, *29*, 1904664.
[192] T.D. Brown, P.D. Dalton, D.W. Hutmacher, *Advanced Materials* **2011**, *23*, 5651-5657.
[193] C. Böhm, P. Stahlhut, J. Weichhold, A. Hrynevich, J. Teßmar, P.D. Dalton, *Small* **in press**.
[194] G. Hochleitner, T. Jungst, T.D. Brown, K. Hahn, C. Moseke, F. Jakob, P.D. Dalton, J. Groll, *Biofabrication* **2015**, *7*, 035002.
[195] C. Mota, D. Puppi, M. Gazzarri, P. Bártolo, F. Chiellini, *Polymer International* **2013**, *62*, 893-900.
[196] G. Hochleitner, T. Jungst, T.D. Brown, K. Hahn, C. Moseke, F. Jakob, P.D. Dalton, J. Groll, *Biofabrication* **2015**, *7*.
[197] R.S. Diaz, J.-R. Park, L.L. Rodrigues, D. P.D., E.M. De-Juan-Pardo, T.R. Dargaville, *Adv Mater Tech* **2021**, *in press*.
[198] G. Hochleitner, M. Kessler, M. Schmitz, A.R. Boccaccini, J. Tessmar, J. Groll, *Materials Letters* **2017**, *205*, 257-260.
[199] Z. Pan, J. Ding, *Interface Focus* **2012**, *2*, 366-377.
[200] C.E. Holy, C. Cheng, J.E. Davies, M.S. Shoichet, *Biomaterials* **2001**, *22*, 25-31.
[201] J.M. Anderson, M.S. Shive, *Advanced Drug Delivery Reviews* **1997**, *28*, 5-24.
[202] K.A. Athanasiou, G.G. Niederauer, C.M. Agrawal, *Biomaterials* **1996**, *17*, 93-102.
[203] I. Harte, C. Birkinshaw, E. Jones, J. Kennedy, E. DeBarra, *J Appl Polym Sci* **2013**, *127*, 1997-2003.
[204] D. Wei, J. Zhao, T. Liu, Z. Wang, *Journal of Thermoplastic Composite Materials* **2016**, *29*, 366-380.
[205] L.V. Labrecque, R.A. Kumar, V. Davé, R.A. Gross, S.P. McCarthy, *J Appl Polym Sci* **1997**, *66*, 1507-1513.
[206] V.P. Ghiya, V. Dave, R.A. Gross, S.P. McCarthy, *Journal of Macromolecular Science, Part A* **1996**, *33*, 627-638.

Acknowledgements / Danksagung

Acknowledgements / Danksagung

Zuerst würde ich mich gerne dafür bei Prof. Dr. Jürgen Groll bedanken, dass ich diese Dissertation an seinem Lehrstuhl anfertigen konnte. Ich möchte mich auch für die sehr guten Gespräche bedanken, die mich dem Ideal des Forschers nähergebracht haben. Auch bedanken möchte ich mir dafür bedanken, dass ich an vielen Konferenzen teilnehmen und meine Forschung präsentieren konnte. Außerdem möchte ich mich für die Möglichkeit bedanken, am PONTEA-Seminar teilzunehmen. Diese Erfahrung hatte nicht nur Einfluss auf meine Doktorarbeit, sondern wird mich auch mein restliches Leben begleiten, da es mir ermöglicht hat mich selbst besser zu verstehen.

Ich möchte mich bei Prof. Dr. Lutz Nuhn für die Begutachtung meiner Thesis bedanken. Außerdem danke ich Prof. Dr.-Ing. Martin Bastian, dass er die Rolle des Drittprüfers übernimmt.

Dr. Jörg Teßmar gilt ein besonderer Dank für seine Rolle als Betreuer, Ideengeber, Lehrer, Kummerkasten und besonders als Freund. Jörg, ohne dich wäre diese Arbeit nicht nur halb so gut geworden, sondern hätte auch nur halb so viel Spaß gemacht.

I would like to thank Prof. Dr. Paul D. Dalton not only for his supervision, but also for sharing his vision about the MEW technology wiht me and to allow me to work on interesting topics scratching the very foundations of this technology. I also would like to thank you for your input sharing your vast knowledge about MEW with me and helping to cast my thoughts into works to publish my work and write up this thesis.

Many thanks to Dr. Andrei Hrynevich, who taught me the high art of G-Code writing and for his support with any question around MEW. You always had an open door, whenever an issue arose, that needed fixing and helped me with setting up my printing endeavors on Machine Black.

Bei Philipp Stahlhut möchte ich mich für die riesige Zahl (über 10.000) SEM-Bilder bedanken, die er für mich gemacht hat. Seine Expertise für SEM hat die korrekte Aufnahme von Bildern und eine automatische Auswertung dieser erst möglich gemacht.

Vielen Dank auch bei Jan Weichhold, der mir der Röntgenbeugung nähergebracht hat und mich mit seiner Erfahrung auf diesem Gebiet unterstützt hat.

Additionally, I would like to thank Ali Nadernezhad for sharing his knowledge on rheology with me and helping with designing a suitable experimental setup to answer the scientific questions I had about the flow behavior of polymers.

Außerdem möchte ich mich bei unseren besten Feinmechanikern Anton Hofmann und Harald Hümpfer bedanken. Ich konnte stets mit den verrücktesten Ideen zu euch kommen und ihr habt sie entweder weiter verbessert oder mit eurem Wissen mir alternative, oft einfachere, Lösungswege aufgezeigt.

Vielen Dank an meinen Bacheloranten Christian Schlör, der viele der wichtigen Vorversuche für MEW von PLGA durchgeführt hat und mich mit seiner selbstständigen Arbeitsweise tatkräftig unterstützt hat.

Danken möchte ich auch den vielen Kollegen im MEW Labor Dr. Gernot Hochleitner, Dr. Almoataz Bellah Yussef, Dr. Andrei Hrynevich, Dr. Biranchi Tandon, Dr. Carina Blum, Dr. Matthias Ryma, Dr. Ezgi Bakirci, Michael Bartolf-Kopp und viele mehr. An eurer Seite habe ich viel gelernt und gelacht. Außerdem möchte ich mich bei allen noch ungenannten Mitarbeitern beim FMZ bedanken. Durch euch war jedes FMZ Event ein Highlight.

Ein besonderer Dank gilt meinen beiden Bürokollegen Johanna Lutz und Johannes Herbig. Vielen Dank für die vielen guten Gespräche in denen wir die Freuden und Leiden diskutieren konnten, die eine Doktorarbeit mit sich bringt. Ihr habt dazu beigetragen, dass meine Zeit am FMZ trotz all der Hürden in guter Erinnerung bleiben wird.

Zu guter Letzt möchte ich mich bei meiner Familie bedanken, die mich auf meinem gewählten Lebensweg stets unterstützt haben. Ein besonderer Dank gebührt hierbei meinen Eltern Judith und Klaus Böhm, die mir immer zur Seite standen und mich zu der Person gemacht haben, die ich heute bin. Die letzten Zeilen widme ich meiner Frau Junwen Shan: Jun, vielen Dank, dass du stets an mich glaubst und mir den Rücken stärkst. Danke auch, dass du mich mit all meinen Stärken und Schwäche so akzeptierst, wie ich bin und immer an meiner Seite bist.